



INTERNATIONAL SCHOOL FOR ADVANCED STUDIES

PHD COURSE IN STATISTICAL PHYSICS

ACADEMIC YEAR 2011/2012

**A journey into
localization, integrability and
thermalization**

THESIS SUBMITTED FOR THE DEGREE OF

Doctor Philosophiae

Advisors:
Prof. Antonello Scardicchio
Prof. Giuseppe Mussardo

Candidate:
Andrea De Luca

17th September 2012

Abstract

We present here the results obtained during my PhD work. Together with a broad introduction to the Anderson localization transition, the quantum adiabatic algorithm and the quench dynamics problem, we include our original achievements. We report the study of the many body localization transition in a spin chain and the breaking of ergodicity measured in terms of return probability in a state evolution. In the many-body localized phase an initial quantum state evolves in a much smaller fraction of the Hilbert space than would be allowed by conservation of energy only. By the anomalous scaling of the participation ratios with system size we are led to consider the eigenfunctions in configuration space by means of the distribution of the wave function coefficients, a canonical observable in modern studies of Anderson localization. We show how the delocalized phase is less ergodic than predicted by random-matrix theory and how in the localized phase some properties of such distribution are very close to those of the Anderson model on the Bethe lattice. We finally present a criterion for the identification of the many-body localization transition based on these distributions which is quite robust and perfectly suited for numerical investigations of a broad class of problems. Moreover, we introduce the Richardson model, an exactly solvable model, that turns out to be suitable for investigating the many-body localized phase. In this way, we show that this phase shares some properties common in glassy systems, such as slowing of the dynamics and fractality. Then we turn to the analysis of the quench problem in an ensemble of random matrices. We analyze the thermalization properties and the validity of the Eigenstate Thermalization Hypothesis for the typical case, where the quench parameter explicitly breaks a Z_2 symmetry. Our analysis examines both dense and

sparse random matrix ensembles. Sparse random matrices may be associated with local quantum Hamiltonians and they show a different spread of the observables on the energy eigenstates with respect to the dense ones. In particular, the numerical data seems to support the existence of rare states, i.e. states where the observables take expectation values which are different compared to the typical ones sampled by the micro-canonical distribution. In the case of sparse random matrices we also extract the finite size behavior of two different time scales associated with the thermalization process.

Contents

Contents	iii
List of Figures	v
Nomenclature	xi
1 The Anderson localization transition	5
1.1 Introduction	5
1.2 The Anderson model	6
1.3 The perturbative expansion	10
1.3.1 Second order	10
1.3.2 The multiple-scattering technique	14
1.3.3 An estimation for the transition point	18
1.4 The self-consistent approach: Bethe lattice	20
1.4.1 The pool method	23
1.5 Some rigorous results	24
1.6 Conclusions	26
2 Many-body localization	27
2.1 Introduction	27
2.2 The importance for adiabatic quantum computation	29
2.2.1 NP vs P	29
2.2.2 The exact cover problem	31
2.2.3 Adiabatic quantum computation	32
2.2.4 Anticrossing and small gaps	34

2.2.5	The role of localization	39
2.3	The structure of the eigenstates in a disordered many-body problem	40
2.3.1	The XXZ spin chain	40
2.3.1.1	Return probability.	43
2.3.1.2	Distribution of wave function amplitudes.	44
2.3.2	An integrable model for the localized phase	50
2.3.2.1	Integrability and localization	51
2.3.2.2	Solution of the model	52
2.3.2.3	A first check of the localized phase	55
2.3.2.4	Montecarlo dynamics inside a quantum state	58
2.4	Conclusions.	61
3	Thermalization in closed quantum systems	62
3.1	Introduction	62
3.2	Locality	66
3.3	Quantum quenches, thermalization, and the ETH	68
3.4	\mathbb{Z}_2 symmetry breaking quench protocol	70
3.5	Thermalization in Dense Random Matrices Ensemble	72
3.5.1	Numerical results	73
3.6	Thermalization in Sparse Random Matrices	78
3.6.1	Numerical results	81
3.7	Time Scales of Thermalization	89
3.8	Conclusions	91
4	Final remarks	93
	References	95

List of Figures

1	From [64], absence of thermalization in a $1d$ Bose gas with δ -like interaction. An explanation of this phenomenon has been searched in the integrability of the corresponding Hamiltonian (known as Lieb-Liniger model [72]) or in the dimensionality of the problem. But a full comprehension is still missing.	2
2	From [17], schematic temperature dependence of the dc conductivity (T) for electrons subject to a disorder potential localizing all single particle eigenstates, in the presence of weak short-range electron-electron interaction δ_ζ , $\ll 1$. Below the point of the many-body metal-insulator transition, $T < T_c$, no inelastic relaxation occurs and $\sigma(T) = 0$. At $T \gg \delta_\zeta/\lambda^2$, Drude theory is applicable. In the intermediate region, electron-electron interaction leads to electron transitions between localized states, and the conductivity depends on temperature as a power-law.	3
1.1	From [112], Anderson localized modes of light. The high intensity peaks show the random positions where the light emitted in a disordered photonic crystal waveguide becomes strongly localized. These are signatures of Anderson localization of light.	6
1.2	The contour integral to recover the time evoluter from the resolvent	8
1.3	Behavior of the pdf for Y : the finite most probable value is showed, together with the long $3/2$ power-law tail, inducing a divergent average value.	13
1.4	The scaling of the typical minimum gap with increasing lattice size N ; the dashed line is the power-law N^{-2}	15

LIST OF FIGURES

1.5	An example of a path in the perturbative expansion where the repeated hopping among two sites (4 and 5 in this example) can give an arbitrarily big contribution.	16
1.6	An example of a diagrammatic representation of one term of the perturbative series (1.25): repeated indexes manifest themselves as loops around g_i . Real processes (blue) are here indicated as opposed to virtual process (black) where the system coherently returns to the initial state and just renormalize the unperturbed energies.	17
1.7	The estimation of the critical ratio $\left(\frac{2V}{W}\right)_c$ for different values of the graph connectivity K given by the upper limit estimation (1.36).	21
1.8	A portion of the Bethe-lattice with connectivity $Z = K + 1 = 3$; from the plot it becomes evident that all the descendent self-energies are on the same ground.	22
1.9	From [24]. Phase diagram for the Bethe lattice with connectivity $K + 1 = 3$. The innermost solid line indicates the mobility edge between extended and localized states, the outermost solid line being the edge of the density of states $E = \pm(2\sqrt{k} + W/2)$. The dashed line is the numerically estimation for the density of states.	24
1.10	A cartoon of the density of states, separated into the localized spectrum, at low energies, and extended spectrum in the middle of the band. The two regions are separated by the mobility edge.	26
2.1	The Herschel graph, the smallest possible polyhedral graph that does not have a Hamiltonian cycle.	30
2.2	A typical example of level repulsion for the eigenvalues of the matrix depending on a parameter: an exact degeneracy would need an additional condition and is therefore generically very rare.	37
2.3	The behavior with M clauses for the evolution with λ of the two states σ_1 and σ_2 : the degeneracy is lifted by the off-diagonal elements (left); adding one more clause, there is a finite probability that the degeneracy at $\lambda = 0$ is lifted in an opposite way with respect to large λ , thus producing an avoided crossing at λ_c	38

LIST OF FIGURES

2.4	From [96], finite-size scaling of the parameter r vs h . The crossing of the different curves seems to indicate a transition in the spectral properties at a finite h	41
2.5	Average fraction of occupied Hilbert space vs h for different system sizes $N = 8$ to 16 using exact diagonalization. Notice how the limit for $h \rightarrow 0$ is different from $1/3$ which is the RMT prediction.	45
2.6	Average diagonal entropy vs disorder strength for different sizes $N = 8, 10, 12, 14, 16$. From the N -dependence the transition is identified at $h_c \simeq 2.7 \pm 0.3$	45
2.7	The distribution of scaled wave function amplitudes $x = \mathcal{N} \langle a e \rangle ^2$ for different values of h . Upper panel: $h = 1.2$ in the middle of the ergodic phase where the scaling is perfectly verified, lower panel $h = 4.2$ in the many-body localized phase. In each figure the different curves correspond to different values of N , from 8 to 16. Each curve is obtained by binning of not less than $3 \cdot 10^6$ squared amplitudes.	47
2.8	The value of the exponent α (blue squares) and β (pink circles) in Eq. (2.26) for $N = 16$ (these exponents are independent of N within the symbol size). The exponent α crosses the value 1 required by summability, which occurs at $h \simeq 2.55 \pm 0.05$, precisely where (within errors) β crosses the value 2, required for the existence of the first moment (normalization of the wave function).	48
2.9	The educated guess for $q(g)$ coming from (2.49) for \bar{q} (solid line) and the lower-bound coming from the conserved charges (dashed line): the Mazur inequality is satisfied but not saturated.	58
2.10	$\ln \mathcal{J}$ as a function of the average distance L . The points are (square, diamond, circle) $N = 28, 30, 32$ averaged over 100 realizations: the dashed straight line is the second order perturbation theory approximation Eq. (2.50).	59
2.11	The stretched exponential exponent β data as a function of g for $N = 28, 32, 36$ (square, circle, diamond) together with a fit of the form $(1 + a_1 g)/(b_0 + b_1 g + b_2 g^2)$	60
2.12	Connectivity fraction as a function of g . Different lines corresponds to $N = 18$ (dashed), 24 (dotted and dashed), 30 (solid).	60

LIST OF FIGURES

3.1	Dense random matrices (with $\mathcal{N} = 4000$). Overlaps for the quench process. Left: $ c_E ^2$ for the 'ground' state. Right: $ c_E ^2$ for the 2000 th state, in the middle of the energy band.	73
3.2	Dense random matrices (with $\mathcal{N} = 4000$). Typical PR_2 of the initial states.	74
3.3	Dense random matrices. PR_2 vs. matrix size. The red lines are linear fits $y = ax$. Left panel: average PR_2 on all initial states ($a = 0.3336$). Right panel: maximum PR_2 ($a = 0.3764$).	75
3.4	Dense random matrices. EEV $\langle E \mathcal{O} E\rangle$ vs E . Left: even observable. Right: odd observable.	75
3.5	Dense random matrices. EEV variance (averaged over the entire spectrum) vs. matrix size. The continuous line is the fit a/x^b with $b = 0.(9)$. The data points for the even and odd observables exactly overlap in this plot.	76
3.6	Dense random matrices. Max-min EEV vs. matrix size for the range of even observables. The continuous line is the fit $a\sqrt{\frac{\ln \mathcal{N}}{\mathcal{N}}}$	76
3.7	Dense random matrices. $\sigma = \sqrt{(\mathcal{O}_{\text{micro}} - \mathcal{O}_{\text{diag}})^2}$ vs. matrix size for initial states laying in the central part of the spectrum $\bar{e} \approx 0$. The continuous line is the fit a/x^b . Left: even observable $b = 1.(9)$; right: odd observable $b = 2.(1)$	77
3.8	Sparse random matrices (with $\mathcal{N}=4000$). Left: density of states, right: level spacing statistics, the continuous line is the Wigner surmise for GOE matrices.	78
3.9	Sparse random matrices. Behavior of the overlaps $ c_E ^2$ for a state mid-spectrum (left) and for one in the upper portion of the spectrum (right).	79
3.10	Sparse random matrices (with $\mathcal{N} = 4000$). The PR_2 for a specific realization. The ordering of the initial states in this plot is according to their energy relative to the post-quench Hamiltonian, $\langle \psi_0 H^> \psi_0\rangle$. . .	79
3.11	Sparse random matrices. PR_2 vs. matrix size. The continuous line is the $y = ax$ fit. Left, average PR_2 on the whole spectrum ($a = 0.0738$). Right, maximum PR_2 ($a = 0.2096$).	80

LIST OF FIGURES

3.12 Sparse random matrices (with $\mathcal{N} = 4000$). The PR_2 of the post-quench eigenstates w.r.t. the local basis for a specific realization. The ordering of the initial states in this plot is according to their energy eigenvalue.	80
3.13 Sparse random matrices. PR_2 w.r.t. local basis vs. matrix size. The continuous line is the $y = ax$ fit. Left, average PR_2 on the whole spectrum ($a = 0.0321$). Right, maximum PR_2 ($a = 0.1632$).	81
3.14 Sparse random matrices. $\text{EEV} \langle E \mathcal{O} E\rangle$ vs e_E . Left: even observable. Right: odd observable	82
3.15 Sparse random matrices. EEV variance vs. matrix size for the full spectrum. The continuous lines are the fit a/x^b . Left: even observable $b = 0.5(0)$ Right: odd observable $b = 0.7(5)$	83
3.16 Sparse random matrices. Max-min EEV vs matrix size for the full spectrum. Left: even observable. Right: odd observable.	83
3.17 Sparse random matrices. EEV variance vs. matrix size for a small energy window around $e = 0$. The continuous line is the fit a/x^b . Left: even observable $b = 1.2(9)$. Right: odd observable $b = 1.(2)$. . .	84
3.18 Sparse random matrices. Max-min EEV vs. matrix size for a small energy window around $e = 0$ in log-scale. The continuous line is the fit $a/x^b + c$. Left: even observable $e = 0$, $b = 0.6(5)$, $c = 0.06(7)$. Right: odd observable $e = 0$, $b = 0.5(0)$, $c = 0.0(1)$	84
3.19 Sparse random matrices. Max-min EEV vs. matrix size for a small energy window around $e = 1$. The continuous line is the fit $a/x^b + c$. Left: even observable $e = 1$, $b = 0.3(5)$, $c = 1.(7)$. Right: odd observable $e = 1$, $b = 0.3(3)$, $c = 0.1(4)$	85
3.20 Sparse random matrices. $\sigma = \sqrt{(\mathcal{O}_{\text{micro}} - \mathcal{O}_{\text{diag}})^2}$ vs. matrix size for initial states laying in the central part of the spectrum $\bar{e} \approx 0$. The continuous lines are the fits a/x^b . Left: even observable $b = 1.1(5)$. Right: odd observable $b = 1.3(0)$	86
3.21 Sparse random matrices. $\sigma = \sqrt{(\mathcal{O}_{\text{micro}} - \mathcal{O}_{\text{diag}})^2}$ vs. matrix size for initial states laying in a small window around $e = 1$. The continuous lines are the fits a/x^b . Left: even observable $b = 0.3(1)$. Right: odd observable $b = 0.4(4)$	86

LIST OF FIGURES

3.22	Sparse random matrices. Kullback-Leibler entropy vs matrix size for the center of the spectrum for the uniform (squares) and the Gaussian distribution (circles).	87
3.23	Left: time evolution of the observable \mathcal{O}_t versus time t . Right: time evolution of the fluctuations $\Delta_t^\mathcal{O}/\Delta_0^\mathcal{O}$ versus time t , log-scale on y axis. The straight line is the exponential fit whose slope defines τ_S	88
3.24	Scaling with the matrix size of the two time scale τ_S (left) with a linear fit $(-3.94 + 0.066\mathcal{N})$ and τ_F (right) with a logarithmic fit $(-28.61 + 8.60 \ln \mathcal{N})$	90

Nomenclature

Roman Symbols

\mathcal{N} unless specified in the text, it is the Hilbert space size, exponentially large in N

$|a\rangle$ it is an index for one state in the computational basis $|\uparrow, \downarrow, \dots, \uparrow\rangle$

N unless specified in the text, it is the number of sites in the system

ABA algebraic bethe ansatz

AL Anderson localization

ETH eigenstate thermalization hypothesis

GOE gaussian orthogonal ensemble

M.P. Most probable

MBL many-body localization

pdf probability distribution function

QAA quantum adiabatic algorithm

RMT random matrix theory

SME sparse matrix ensemble defined in [3](#)

w.p. with probability

Introduction

The study of quantum system in presence of disorder or far away from standard equilibrium condition can be considered as two of the most important strands among the current research in condensed-matter physics. This is true, not only for their hardness from the theoretical point of view, but also because recent development of experimental techniques allowed enormous progress in the control of the microscopic details of a quantum systems. So, problems that in the past could look as completely academic, as it could be the evolution of a closed quantum systems, have nowadays become crucial also experimentally thanks, for example, to the cold atoms community [25] (see Fig. 1 for an important example). Last years represented an important development also for the quantum disordered community, with experimental works able to test and verify the Anderson localization [21, 106]. We can be therefore optimistic on the possibility to study in a controlled way also a quantum systems in presence of disorder and interactions. From the theoretical point of view, the questions regarding thermalization of closed quantum systems, especially in low dimensions, attracted an extraordinary effort, in the attempt to find general prescription and to investigate the mechanism needed to reach thermal equilibrium. While for a finite size system we expect recurrence, it is conceivable that a large system could decay towards a stationary state. The thermodynamic characterization of this (eventual) stationary state is one of the most intriguing puzzles of this field. The concept of disordered quantum system intertwines with the work of Anderson [11]. The notion of localization was originally introduced for a single quantum particle in a random potential. This concept can also be extended to many-particle systems. Statistical physics of many-body systems is based on the microcanonical distribution, i. e., all states with a given energy are assumed to be realized with equal probabilities. This assumption means delocalization in the space of possible states of the system. It does not hold for non-interacting particles; however, it

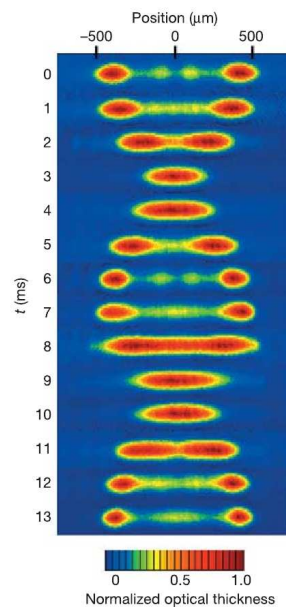


Figure 1: From [64], absence of thermalization in a $1d$ Bose gas with δ -like interaction. An explanation of this phenomenon has been searched in the integrability of the corresponding Hamiltonian (known as Lieb-Liniger model [72]) or in the dimensionality of the problem. But a full comprehension is still missing.

is commonly believed that an arbitrarily weak interaction between the particles eventually equilibrates the system and establishes the microcanonical distribution. However, in Fig. 2, we find the summary of the recent results from [16], showing that interacting disordered quantum systems can be characterized by a low-temperature phase where the system finds it hard to thermalize. This gave strength to the research of a many-body localized phase. It is interesting to notice how the low-temperature in this case, represents a new phase, where conductivity vanishes identically. So, we see

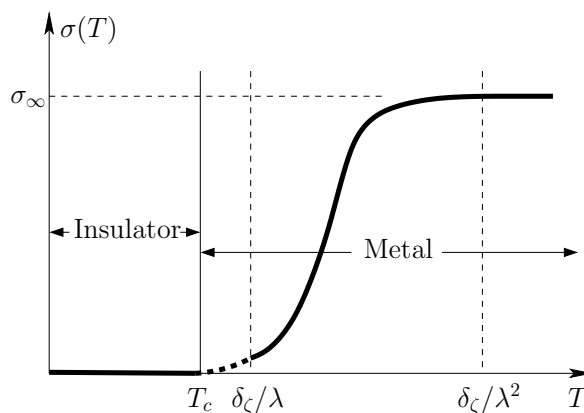


Figure 2: From [17], schematic temperature dependence of the dc conductivity (T) for electrons subject to a disorder potential localizing all single particle eigenstates, in the presence of weak short-range electron-electron interaction δ_ζ , $\ll 1$. Below the point of the many-body metal-insulator transition, $T < T_c$, no inelastic relaxation occurs and $\sigma(T) = 0$. At $T \gg \delta_\zeta/\lambda^2$, Drude theory is applicable. In the intermediate region, electron-electron interaction leads to electron transitions between localized states, and the conductivity depends on temperature as a power-law.

that these problems, though coming from different starting points and perspectives, end up interweaving with deep implications for the foundations itself of quantum statistical mechanics. The intriguing part is that for both of them, standard techniques as mean-field theory or renormalization theory do not work, or have at least to be reformulated properly. Therefore, beyond the possibility of an extensive perturbative analysis, that may be fruitful in some specific case, as in [15], one has to resort to: numerical methods or exactly solvable toy models. In this work of thesis, we indeed tried a combination of the two things. Together with exact diagonalization and an ac-

curate analysis of the finite-size corrections, we exploited exact results coming from integrable models, as the Richardson one, or the employment of the Bethe-lattice. We think that the fundamental issue is coming from the complicate behavior of the typical quantum wave-function, that in presence of many-body effects and disorder may acquire complicate shape. The Anderson localization framework, though derived for a much simpler context as the single-particle hopping problem, provided us, during the last fifty years, with a set of tools, terminology and concepts that can be applied fruitfully. Our focus was therefore on the breaking of ergodicity in the Hilbert space, an effect related both to the lack of thermalization and the lack of conductivity.

Finally, there is also a technological motivation for this research. We have already underlined how the perfectly insulating low temperature phase of a disordered many-body system already represents a novelty. Moreover, it is very plausible that the coherent quantum dynamics will play a major role in future experimental set up and technologies. An example could be provided by a quantum computer, that will definitely require the capability of manipulate interacting system in time. Therefore, a better understanding of out of equilibrium quantum physics could be crucial for the developing of new technologies.

This thesis is organized as follows. In chapter 1, we present the main ingredients of the Anderson localization transition, trying to follow the historical development of same aspects. This will be useful as a background in all the rest of the thesis. In chapter 2, we turn our attention to the many-body generalization of the localization transition. We will elaborate on its implication for the (quantum) complexity and we will explain our work on the subject coming from [29, 39]. In chapter 3, we present our work concerning non-equilibrium dynamics in closed quantum systems and in particular on the topic of quantum quenches. With a parallel use of random matrices, Anderson localization and exact diagonalization, we have been able to describe an ensemble of systems showing thermalization and characterize the mechanism behind. The results are published in [27].

During my PhD, I also worked on a different topic, i.e. the computation of the correction to critical entanglement entropy in a full class of $1d$ exactly solvable models, whose critical points coincide with the conformal minimal points; details can be found in [38].

Chapter 1

The Anderson localization transition

1.1 Introduction

In 1958, P. Anderson [11] came out with a paper where he put out the ideas at the origin of the nowadays incredibly famous phenomenon that goes under the name of Anderson localization (AL). The motivations behind that work were related to some experimental results from the George Feher's group at Bell Labs [50] in the fifties that were lacking a theoretical explanation. In particular, according to the classical Drude description of conductance in a metal, one imagines that electrons (or more generally the charge carriers) collide with the positive ions in the metal, thus following a diffusive motion. This theory is at the origin of the well known Ohm's law, where clearly the conductivity becomes proportional to the mean free path of the electron inside the metal. However, experimental observations made clear that the mean free path inside a metal is a couple of order of magnitude bigger than the lattice spacing and only with the development of the quantum theory it was possible to provide an explanation to this fact: in a regular lattice, electrons behave as waves and coherently diffract on the ions. The resistivity is therefore appearing only because of the impurities in the lattice. In this way the Drude theory becomes again reliable, but the electron is envisaged as zigzagging between impurities. It follows that the more are the impurities, the shorter will be the mean free path and the conductivity. With this picture in mind, Anderson tried to answer the question: what happens if the density of impurity is increased? Consistently with the known experimental results, he was able to provide

convincing arguments, showing that the increasing of lattice disorder would not only keep decreasing the mean free path and the conductance, but beyond a critical amount of impurity scattering the diffusive, zigzag motion of the electron is not just reduced, but can come to a complete halt. The electron becomes trapped and the conductivity vanishes. Since then, the concept of Anderson localization was shown to manifest itself in a broad variety of phenomena in quantum physics. Since then, the concept of

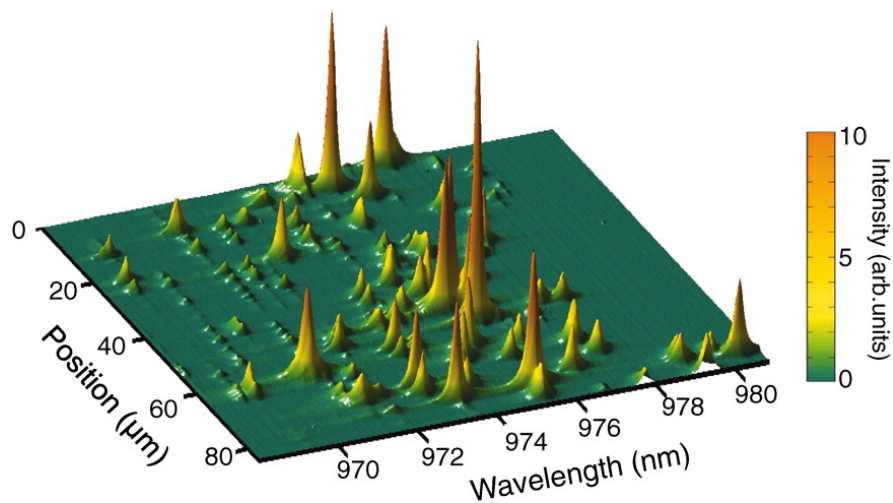


Figure 1.1: From [112], Anderson localized modes of light. The high intensity peaks show the random positions where the light emitted in a disordered photonic crystal waveguide becomes strongly localized. These are signatures of Anderson localization of light.

Anderson localization was shown to manifest itself in a broad variety of phenomena in quantum physics. As an important example we report in Fig. 1.1 the results from an experiment of localization of light.

1.2 The Anderson model

The simplest model involving (spin) transport and disorder showing this phenomenology is now known as Anderson model. To be more specific, the Hamiltonian, in its

simplest formulation, looks like:

$$H = \sum_i \epsilon_i |i\rangle \langle i| + V = H_0 + V \quad (1.1)$$

here ϵ_i are independent random variables distributed according to $P(\epsilon)$ and V is the hopping term, that can be short-range, i.e. the adjacency matrix of the lattice under consideration, or long-range with a potential of a specified form. For the moment we will consider the cases:

- $P(\epsilon) = \chi_{[-\frac{W}{2}, \frac{W}{2}]}(\epsilon)$, where χ_I is the characteristic function of the set I and W can be seen as a measure of the disorder strength;
- the lattice is the cubic lattice in d dimensions.

The Schrödinger equation takes the form

$$i\dot{a}_i = \epsilon_i a_i + \sum_j V_{ij} a_j \quad (1.2)$$

Then, the question that one would like to answer regards the long-time dynamics of an initially localized state: taking as initial condition $a_i = \delta_{i0}$, i.e. the wave function is completely concentrated at the origin, the typical long time dynamics is investigated perturbatively in the hopping. In order to formulate the perturbative expansion, it is useful to introduce the resolvent

$$G(z) \equiv (z - H)^{-1} \quad (1.3)$$

and the corresponding expression for $G_0(z)$ and H_0 . It is clear that in terms of this expression we can easily recover the time evolution operator by contour integral

$$U(t) = \int_{\mathcal{C}} G(z) e^{itz} dz \quad (1.4)$$

where $\mathcal{C} = C_+ \cup C_-$ is the contour depicted in the figure [1.2](#)

We use the following identity holding for two invertible operators A, B

$$A^{-1} + B^{-1} = A^{-1}(B - A)B^{-1} \quad (1.5)$$

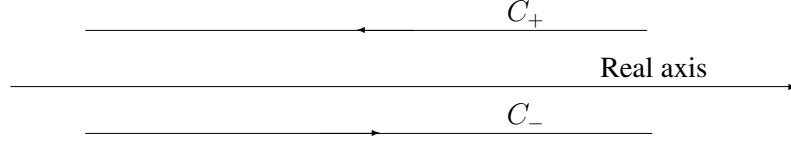


Figure 1.2: The contour integral to recover the time evolutor from the resolvent

to derive

$$G(z) = G_0(z) + G(z)V G_0(z) = G_0(z) + G_0(z)V G(z) = G_0(z) + G_0(z)T(z)G_0(z) \quad (1.6)$$

where we introduced the t -matrix with its perturbative expansion as

$$T(z) \equiv V G(z)(z - H_0) = V + V G_0(z)V + V G_0(z)V G_0(z)V + \dots \quad (1.7)$$

By setting

$$G_{ij}(z) \equiv \langle i | G(z) | j \rangle; \quad g(z) \equiv G_{00}(z). \quad (1.8)$$

we derive the expansion, where we assume the sum over repeated indexes

$$g(z) = \frac{1}{z - \epsilon_0} + \frac{1}{z - \epsilon_0} V_{0j} \frac{1}{z - \epsilon_j} V_{j0} \frac{1}{z - \epsilon_0} + \frac{1}{z - \epsilon_0} V_{0j} \frac{1}{z - \epsilon_j} V_{jl} \frac{1}{z - \epsilon_l} V_{l0} \frac{1}{z - \epsilon_0} + \dots \quad (1.9)$$

It is useful to introduce the self-energy $\Sigma(s)$, defined implicitly by the equation

$$g(z) \equiv \frac{1}{z - \epsilon_0 - \Sigma(z)} \quad (1.10)$$

and combining (1.10) and (1.6), one obtains the expression useful for the perturbative expansion

$$\Sigma(z) = (z - \epsilon_0) [1 - \langle 0 | (1 - G_0(z)V)^{-1} | 0 \rangle^{-1}] \quad (1.11)$$

that can be written as

$$\Sigma(z) = \sum_n \sum_{l_1, \dots, l_n \neq 0} \frac{V_{0l_1} V_{l_1 l_2} \dots V_{l_n 0}}{(z - l_1) \dots (z - l_n)} \quad (1.12)$$

The long-time dynamics corresponds to the behavior of $G(z)$ close to the real axis. The self-energy is also called *energy-shift operator* [36], because it moves the position of the poles of $g(z)$. In particular, if we suppose that for $z_0 = \omega - i\tau^{-1}$, we have

$$z_0 - \epsilon_0 - \Sigma(z_0) = 0$$

we derive by Laplace transform for large time t

$$g(z) \simeq \frac{A}{z - \omega + i\tau^{-1}} \Rightarrow a_0(t) \simeq Ae^{-i\omega t - \frac{t}{\tau}} \quad (1.13)$$

It is clear that if τ is finite, the wave function will spread from the origin, being delocalized. If instead τ is infinite, the wave function, or at least a finite fraction of it given by the constant A , will remain at the origin and no transport will take place. Two remarks are in order

- being mathematically rigorous, from the definition (1.3) of the resolvent, it is clear that, since H is an hermitian operator, each component of $G(z)$ can only have singularities on the real axis, corresponding to isolated poles or branch cuts in presence of a continuous spectrum: a finite τ would therefore be odd. However, the analytic continuation of $g(z)$ along the branch cuts goes on an other Riemann sheet, where the function can have new singularities [36];
- since the Hamiltonian H involves random variables, the question whether τ is finite or not, becomes a probability question that, as we will see in detail, is not simply answered considering average values.

To be more concrete, it is easy to see that the average of the Green function does not provide a quantity good to distinguish the localized from the delocalized phase. This was at the origin of the confusion during the first years after Anderson's one. In [74], it is considered the Anderson model, with a Cauchy distribution for the diagonal energies (Lloyd model):

$$P(\epsilon) = \frac{1}{\pi} \left[\frac{\gamma}{(\epsilon - \epsilon_0)^2 + \gamma^2} \right] \quad (1.14)$$

In this case the average of the Green function and therefore the average density of states, can be computed analytically. It turns out that in any dimension d , the average

of the Green function is given by the ordered one where the diagonal energies are all equal and given by $\epsilon_0 + i\gamma$. This result was used as a prove that no localization can occur in this model. However, it is clear that the long tails of the Cauchy distribution are practically irrelevant in high dimensions, where the wave function can always avoid values very far from the average. So, this result would have strong implication on the Anderson work too. However, the problem is that the average of the Green function is not a meaningful quantity for this transition. One can define an order parameter for the Anderson transition as the long time average of the return probability, i.e. the probability to find particle at the origin

$$\text{IPR}_2 \equiv \lim_{\tau \rightarrow \infty} \frac{1}{\tau} \int_0^\tau dt |a_0(t)|^2 = \sum_e |\psi_0(e)|^4 = \lim_{\epsilon \rightarrow 0} \frac{\epsilon}{\pi} \int_{-\infty}^{\infty} g(p + i\epsilon)g(p - i\epsilon)dp \quad (1.15)$$

where the sum is over the eigenstates $\psi(e)$ of H . Here $(\text{IPR}_2)^{-1}$ is a measure of the portion of explored Hilbert space during the quantum dynamics and it is usually dubbed *participation ratio* (PR). The average of this quantity, that involves the square of the Green function, can distinguish localized and extended states. Unfortunately, its analytic computation is not possible, even for the Lloyd model. We will come back on that in 2.3.1, where we will use a numerical approach to the problem. For now, we will use a different technique.

1.3 The perturbative expansion

1.3.1 Second order

The use of the self-energy introduced in (1.10) is particularly fruitful if one wants to consider an approximate perturbative expression. In fact, at the lowest non-zero order in V we obtain from (1.12), we get

$$\Sigma(z) = \sum_{j \neq 0} \frac{|V_{0j}|^2}{z - \epsilon_j} + O(V^3) \quad (1.16)$$

Inserting it in (1.10), we obtain

$$g(z) = \frac{1}{z - \epsilon_0 - \sum_{j \neq 0} \frac{|V_{0j}|^2}{z - \epsilon_j}}$$

To recover the same expression from (1.9), one already needs to re sum an infinite subset of terms. In fact, it is useful to notice that Eq. (1.9) at any finite order in V will still have poles corresponding to the spectrum of H_0 : it is only resumming an infinite subset of them that their positions can be shifted; this procedure is automatically encoded in the self-energy. Now, the expression appearing in (1.16) is a random variable due to the randomness of the energies ϵ_j . We are interested in investigating its behavior close to the unperturbed energy ϵ_0 and in presence of a small positive imaginary part: as we saw in (1.13), the imaginary part will be related to the decaying time τ . Therefore setting $z = s + ix$ where x is a small real quantity, and using the Sokhotski-Plemelj theorem, we get from the distributional limit of (1.16)

$$\lim_{x \rightarrow 0} \Sigma(s + ix) = \sum_{j \neq 0} \mathcal{P} \left(\frac{|V_{0j}|^2}{s - \epsilon_j} \right) - i\pi \sum_{j \neq 0} |V_{0j}|^2 \delta(s - \epsilon_j) \quad (1.17)$$

When $s \rightarrow \epsilon_0$, we notice that the first term, i.e. the real part of the self-energy, just reproduce the second order correction in V to the eigenvalue ϵ_0 of H_0 . The second term is just the Fermi's golden rule, directly related to the decaying time τ and the delta functions impose the energy conservation. It is clear that for any finite system, quantum mechanics predicts revivals, so the amplitude of the initial state can never really decay; indeed this term vanishes, with probability one the delta function are never satisfied and energy conservation forbids hopping unless one has a continuous spectrum. Here, the problem becomes even more subtle: it is a probability question to be settle already in the thermodynamic limit. Setting

$$\tau_x^{-1} \equiv -\Im \Sigma(\epsilon_0 + ix) = \sum_{j \neq 0} \frac{x |V_{0j}|^2}{x^2 + (\epsilon_0 - \epsilon_j)^2}$$

we can investigate this expression as a random variable, whose probability distribution can in principle be computed. Introducing

$$y_j = \frac{1}{x^2 + (\epsilon_0 - \epsilon_j)^2}; \quad Y = (x\tau_x)^{-1} = \sum_j |V_{0j}|^2 y_j$$

In order to simplify our computations without changing the substance of the results, we assume that energy at the origin falls in the middle of the band, $\epsilon_0 \ll W$. Then we have for the probability distribution function (pdf)

$$\rho(y) \equiv \begin{cases} \frac{1}{Wy\sqrt{y-x^2y^2}} & y \in [\frac{4}{4x^2+W^2}, x^{-2}] \\ 0 & \text{otherwise} \end{cases}$$

The Laplace transform of the pdf can be computed for small x

$$\phi(s) \equiv \int_0^\infty dy e^{-sy} \rho(y) = e^{-\frac{4s}{W^2}} + \frac{2\sqrt{\pi s}}{W} \left[\text{Erf} \left(\frac{2\sqrt{s}}{W} \right) - \text{Erf} \left(\frac{\sqrt{s}}{x} \right) \right] \quad (1.18)$$

Now, the Laplace transform of the pdf of Y is obtained by product:

$$\Phi(s) \equiv \int_0^\infty dY e^{-sY} \rho(Y) = \prod_i \phi(s|V_{0i}|^2) \quad (1.19)$$

Now since we are interested in both $s \rightarrow 0$ and $x \rightarrow 0$ limit, it is useful to consider the expansion

$$\phi(s) \stackrel{s \ll 1}{\simeq} \begin{cases} e^{-\frac{2\sqrt{\pi s}}{W}} & \sqrt{s} \gg x \\ 1 - \frac{2s}{Wx} & \sqrt{s} \ll x \end{cases} \quad (1.20)$$

It is illustrative of the mechanism involved to consider some concrete examples. Suppose that V_{ij} is V_0 times the adjacency matrix of the cubic lattice in d -dimensions. Being a finite product, the $x \rightarrow 0$ limit can be taken in (1.19) without troubles. For large d we can obtain an approximate result

$$\Phi(s) \simeq e^{-\frac{4d\sqrt{\pi s}V_0}{W}} \Rightarrow \rho(Y) \simeq \frac{e^{-\frac{4d^2\pi V_0^2}{tW^2}}}{t^{\frac{3}{2}}} \quad (1.21)$$

and the resulting distribution is plotted in Fig. 1.3. This example contains already

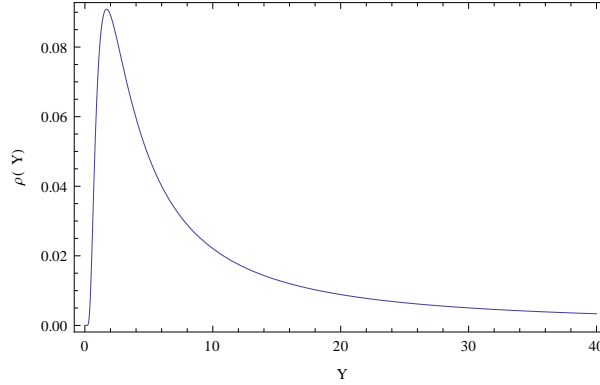


Figure 1.3: Behavior of the pdf for Y : the finite most probable value is showed, together with the long $3/2$ power-law tail, inducing a divergent average value.

some of the ingredients fundamental in Anderson localization: the derived distribution function has a long power-law tail and so the first momentum, i.e. the average value, is divergent. However, the most probable value is finite, and we obtain therefore

$$(\tau_x^{-1})_{\text{M.P.}} \simeq 16xd^2\pi \left(\frac{V_0^2}{W^2} \right) \quad (1.22)$$

showing that the decaying time diverges and the state never delocalizes. An interesting generalization is already contained in [11], i.e. a potential decaying as $V(r) = \frac{V_0}{r^{3+\epsilon}}$ for a 3 dimensional lattice. For $\epsilon > 0$, again the $x \rightarrow 0$ limit is harmless and it is enough to replace in (1.21) and (1.22)

$$d \rightarrow \frac{n}{2} \int_1^\infty V(r) 4\pi r^2 dr = \frac{4\pi n}{\epsilon} \quad (1.23)$$

For the limiting case $\epsilon = 0$, this integral becomes logarithmic divergent but a natural cut-off is obtained by (1.20), i.e. $r \ll \left(\frac{x}{V_0 \sqrt{s}} \right)^{\frac{1}{3}}$, from which we derive

$$\Im \Sigma(\epsilon_0 + ix) = (\tau_x^{-1})_{\text{M.P.}} \propto \frac{xV_0^2(\log x)^2}{W^2}$$

and once inserted in (1.10) and inverting the Laplace transform, turns out in a slower than exponential decay ($\simeq \exp(-\alpha(\log t)^2)$). In this example, therefore, transport

takes place even though in a particular way, where, due to the logarithmic divergence of the integral in (1.23), long-range hopping (for large value of r) are crucial. Here, we limited ourself to consider the first non-zero order in the perturbative expansion of the self-energy, i.e. the second order in the hopping term V : whenever $\epsilon > 0$ no delocalization, or transport occurs. In particular, for short range hopping (e.g. nearest-neighbor), from this approach, one should conclude that no transition would ever occur. However, as we will see in the following sections, this is due to the second order in the perturbative expansion. The AL transition, being inherently non-perturbative, requires the analysis of the full perturbative series: at any order, still finite, the decaying time will look infinite, and no delocalization, or transport, will ever occur. However, what can happen is that the full perturbative series is actually divergent, making meaningless all the finite order truncation. We will investigate therefore, the nature of the series in the following section.

1.3.2 The multiple-scattering technique

The perturbative series in the hopping term can be investigated considering the expansion (1.7) or (1.9), or more specifically the self-energy expansion appearing in (1.12). The main problem with this expansion is that it is affected by trivial divergences whenever the hopping term is big enough to induce a **level crossing**. For example, for a 2 sites system, we have

$$H = \begin{pmatrix} e_1 & V \\ V & e_2 \end{pmatrix}$$

and the spectrum is given by

$$e_{\pm} = \frac{\bar{e}}{2} \pm \frac{\Delta e}{2} \sqrt{1 + \frac{4V^2}{\Delta e^2}}$$

where $\bar{e} = \frac{1}{2}\text{Tr}H$ and $\Delta e = e_1 - e_2$; by comparison with 1.10, we see that the self-energy is given by the second term in this expression for the eigenvalues. Since the square root can be expanded perturbatively for small V only for

$$|V| \leq \frac{\Delta e}{2}$$

we can conclude that this has to be the radius of convergence for the perturbative expansion appearing in (1.12). Increasing the system size, the situation gets worse and worse, since such bound has to be replaced by the minimum level spacing, that for $N = L^d$ random variables e_1, \dots, e_N goes down as N^{-2} as showed in Fig. 1.4. It

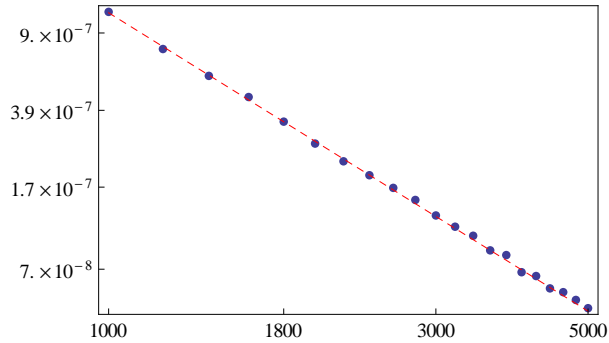


Figure 1.4: The scaling of the typical minimum gap with increasing lattice size N ; the dashed line is the power-law N^{-2}

means the radius of convergence of the perturbative expansion is vanishingly small, making the analysis of the full series completely meaningless. The strategy used by Anderson to face this issue follows the technique known as multiple-scattering [129]. In simple terms, the perturbation series appearing in 1.12, can be rewritten graphically as the sum over the paths (actually loops) starting from the origin and coming back to the origin itself, without never touching the origin but at the end. However, repetitions are allowed in these loops and therefore if we have a pair j, k such that

$$\left| \frac{1}{z - e_j} V_{jk} \frac{1}{z - e_k} V_{kj} \right| > 1$$

then we can get terms arbitrarily big in the perturbative expansion just taking paths that pass more and more times between j and k : this type of diagrams involves a “ladder” from j to k and an example is shown in Fig. 1.5.

One can see that all these divergent terms can be formally resummed, thus producing a perturbative expansion where the sum involves only self-avoiding loops where no repetition among the indexes are allowed. The problem with these procedure is that all the unperturbed energies ϵ_k , appearing in the denominators, have to be modified, defining as in (1.10), a hierarchical set of self-energy to be fixed self-consistently.

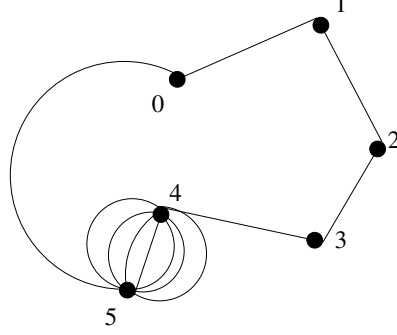


Figure 1.5: An example of a path in the perturbative expansion where the repeated hopping among two sites (4 and 5 in this example) can give an arbitrarily big contribution.

To be more explicit, we consider the expansion (1.9). It is useful to rewrite it in the following form

$$g(z) = \frac{1}{z - \epsilon_0} + \frac{1}{(z - \epsilon_0)^2} \sum_{\{k,j\} \neq 0} V_{0k} G_{k,j}(z) V_{j0} \quad (1.24)$$

and the last term can be written in terms of path connecting k and j

$$G_{k,j}(z) = \frac{\delta_{k,l}}{z - \epsilon_0} + \sum_n \sum_{l_1, \dots, l_n} \frac{V_{kl_1} V_{l_1 l_2} \dots V_{l_n j}}{(z - \epsilon_k)(z - \epsilon_{l_1}) \dots (z - \epsilon_{l_n})(z - \epsilon_l)} \quad (1.25)$$

and we will show how the terms in the sum can be rearranged. Let's fix a set of indexes representing a path connecting k to j with no repetitions: $g_0 = k, g_1, g_2, \dots, g_n = j$ ¹ and no repetitions occur. Among all the terms in the sum of (1.25), as shown in Fig. 1.6, we collect the subset of them where, except for the loops corresponding to the index repetitions and that we address as *virtual* processes, the system undergoes *real* transition along the path $g_0 \rightarrow g_1 \rightarrow \dots \rightarrow g_n$. The idea is to sum up step by step the virtual processes around g_0 , then g_1 , so on and so forth. To be more concrete, we analyze the first case $g_0 = k$. We notice that each term will start from k , will come back there in principle many times, and then will leave it definitely. If we put together all the terms that coincide after the last occurrence of k , we notice that the final part,

¹for simplicity we assume $k \neq j$; what has to be changed for the case $k = j$ will become clear.

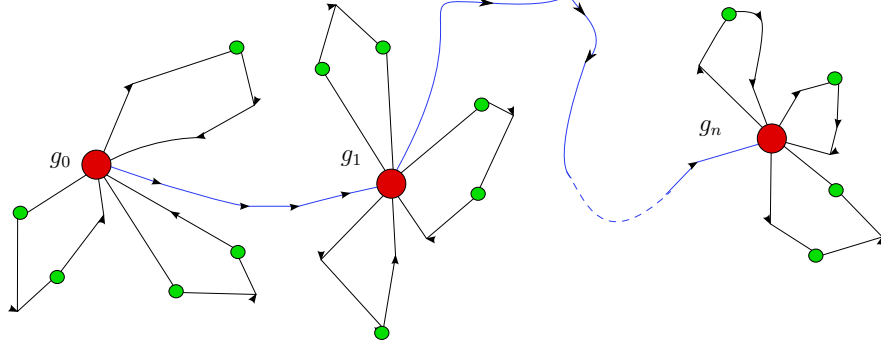


Figure 1.6: An example of a diagrammatic representation of one term of the perturbative series (1.25): repeated indexes manifest themselves as loops around g_i . Real processes (blue) are here indicated as opposed to virtual process (black) where the system coherently returns to the initial state and just renormalize the unperturbed energies.

non-containing k , being common among them, can be factorized. The remaining factor corresponds to the sum of all the possible loops around $g_0 = k$. Therefore we have

$$G_{kj}(z) = \frac{1}{z - \epsilon_k - \Sigma_k(z)} \sum_{k' \neq k} V_{kk'} G_{k'j}^{\neq k}(z) \quad (1.26)$$

where the first term, except for the replacement $k \leftrightarrow 0$ is analogous to (1.10) and appears therefore as a shift to the unperturbed energy. Instead, the last term is analogous to (1.25), but for the fact that k should not appear in any path. Therefore, repeating the previous argument, it can be rewritten as

$$G_{k',j}^{\neq k} = \frac{1}{z - \epsilon_{k'} - \Sigma_{k'}^{\neq k}(z)} \sum_{k'' \neq k'} V_{k'k''} G_{k''j}^{\neq k, k'}(z)$$

where now the self-energy in the denominator is computed using (1.12), but avoiding k in any path. Now it is clear how the procedure goes on taking $k' = g_1$ and iterating for the rest of the path g_2, g_3, \dots : (1.24) has been rewritten as a sum over just the loops without repetitions, but for any of these terms, the denominators have to be shifted with the appropriate set of path-dependent self-energies. Notice that in the same way, one can arrange the expansion (1.12) such that it will contain only path without repetitions, and the denominators will involve all the possible $\Sigma_{k_0}^{\neq k_1 k_2 \dots}(z)$, that have to

be determined self-consistently. However, one can wonder the usefulness of this rearrangement, since the resulting set of coupled equations, in general, does not allow for any explicit solution. We will see an explicit example, i.e. the Bethe-lattice in 1.4, where the locally tree-like structure of the lattice allows for a simplification of the self-energies equations. For scattering problem, it happens typically that from every site, it is possible to hop in a large number of new sites. and the condition of no-index repetition that characterizes self-avoiding loops, becomes actually irrelevant. Instead, for the disordered case we are considering, Anderson argued that the effect in the denominators due to the resummation is to increase the smallest of them, only slightly changing the nature of the series itself. Therefore, neglecting the self-energies in the denominators provide a larger value for the series. Since, we can estimate the position of the transition point as the value of the ration $\frac{W}{V}$ that makes the perturbative expansion divergent, it turns out that within this approximation we will be overestimating the transition point¹.

1.3.3 An estimation for the transition point

In the approximation suggested by Anderson, it is possible to derive an estimation for the critical point of the Anderson transition. As we explain in the previous section, it represents an over-estimation. We will follow [122] in the derivation. We will assume for simplicity that the hopping matrix will just be $\mathbb{V} = VA$ where A is the adjacency matrix of the cubic lattice and V is a measure of the hopping strength. As we did in 1.3.1, we will assume $\epsilon_0 \ll W$ and set $z = 0$, so that the general term at order L in the expansion we derived in the last section will look like

$$T_L = \frac{V^L}{\epsilon_{l_1} \epsilon_{l_2} \cdots \epsilon_{l_L}} \quad (1.27)$$

Here, all the indexes in the denominators have to be different, due to the multiple-scattering rearrangement we explained in the last section. Moreover, as we said, we neglect the self-energies that should shift the unperturbed energy. So the result is that the denominator will be the product of L independent random variables, uniformly

¹for this reason, Anderson addresses the result obtained in (84) of [11], in this approximation where the denominators are just considered as the unperturbed ones, an *upper limit*.

distributed in $[-\frac{W}{2}, \frac{W}{2}]$. Once set

$$a_i = -\ln \left| \frac{2\epsilon_{l_i}}{W} \right| \quad (1.28)$$

$$A = \sum_i a_i \quad (1.29)$$

we have that $|T_L| = (\frac{2V}{W})^L e^A = (\frac{2V}{W})^L \tau_L$. Computing the distribution functions, with the standard method of Laplace transform, we obtain

$$P_a(a) = e^{-a}\theta(a) \quad (1.30)$$

$$P_A(A) = \frac{e^{-A}A^{L-1}}{(L-1)!}\theta(A) \quad (1.31)$$

$$P_\tau(\tau_L) = \frac{(\ln \tau_L)^{L-1}}{(L-1)!\tau_L^2} \quad (1.32)$$

Now, at each order L , the number of terms like T_L in (1.27) will be exponentially large in L , K^L , being given by the number of path with no loops from the origin of length L .

$$O_L = \sum_{i \in \{\text{path}\}} \pm \tau_L^{(i)} \quad (1.33)$$

We are now interested to the distribution of $|O_L|$. If we were able to assume that all the terms involved are independent random variable, then the distribution of the sum would be computable with standard methods. This is clearly false, since the number of independent variable is polynomial in L , while the number of path, and so of variable T_L is exponential in L . However, assuming independence will overestimate O_L , therefore it is consistent with the previous approximation. Now, O_L , the sum of a large number of positive and negative random variables with a long-tailed distribution function, is dominated by the maximum of the variables. Therefore, instead that explicitly computing the distribution, for large value of O_L , it can be replaced with the distribution of the maximum of the K_L variables τ_L . The standard argument to obtain it is

$$\text{Prob}(|O_L| < O) \simeq \text{Prob}(\max\{\tau_L^{(1)}, \dots, \tau_L^{(K^L)}\} < O) = \left(1 - \int_O^\infty P(\tau_L)d\tau_L\right)^{K^L}$$

Differentiating, we get the pdf for O_L for large O

$$P_{|O_L|}(O) \simeq K^L P_\tau(O) \quad (1.34)$$

In order to compute the probability that the series

$$S = \sum_L \left(\frac{2V}{W} \right)^L O_L$$

is convergent, we compute the probability that it is dominated by a convergent geometric series, i.e.

$$\mathbb{P} = \text{Prob} \left(\exists x < 1, N \mid \forall L > N, |O_L| < \left(\frac{xW}{2V} \right)^L \right) = \lim_{x \rightarrow 1} \lim_{N \rightarrow \infty} \prod_{L=N}^{\infty} \int_0^{\left(\frac{xW}{2V} \right)^L} P_{|O_L|}(O) dO \quad (1.35)$$

To estimate the product of integrals, we notice that the extreme of integration will be big, therefore using (1.32) and (1.34)

$$\int_{\left(\frac{xW}{2V} \right)^L}^{\infty} P_{|O_L|}(O) dO = K^L \int_{\left(\frac{xW}{2V} \right)^L}^{\infty} P_\tau(O) \simeq \left(\frac{2VeK \ln \left(\frac{Wx}{2V} \right)}{xW} \right)^L O \left(L^{-\frac{1}{2}} \right)$$

Inserting this approximation in (1.35), we obtain

$$\frac{2VeK \ln \left(\frac{W}{2V} \right)}{W} < 1 \Rightarrow \mathbb{P} = 1 \quad (1.36)$$

So for big values of $\frac{W}{V}$ the series is almost surely convergent and as we said, this will imply localization. It is easy to show on the same ground that in the opposite regime, the series will be almost surely divergent.

1.4 The self-consistent approach: Bethe lattice

Along the derivation in 1.3.3, we pointed out some of the objections, due to Thouless in [122], to the derivation in Anderson original work. The analysis of the perturbative expansion is affected by a couple of weak points

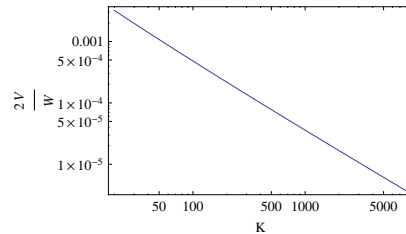


Figure 1.7: The estimation of the critical ratio $(\frac{2V}{W})_c$ for different values of the graph connectivity K given by the upper limit estimation (1.36).

- the complicate set of coupled equations that determine the energy shift in the denominators are neglected;
- the K^L terms of the same order obtained as different self-avoiding path are treated as probabilistically independent random variables, even though, as we already said, this assumption is clearly false.

A substantially different approach is the one first introduced in [1, 2]. The fundamental idea is to study the problem on a particular kind of lattice, the Bethe-lattice [19], where loops are long enough (or absent at all) to be neglected. This approach has become standard in the solution of classical statistical mechanics problems, as for example for spin glasses, where the cavity method [81] has provided a crucial tool of investigation. A similar technique has been developed recently also in the quantum case. [71]. It is nice to read an anecdote from D.J. Thouless in [4]:

“At the end of a dinner in the Andersons’ house in Cambridge, Anderson told me of a new approach to localization, and I left their house with a large envelope, on which a few suggestive equations were scribbled. I recognized these as being analogous to the Bethe-Peierls equations in statistical mechanics, which were known to be exact for a Bethe lattice, an infinite regular lattice with no loops. With the help of my student Ragi Abou-Chacra, we showed that these equations led to a set of nonlinear integral equations whose solutions could be found numerically, and which displayed a transition between extended and localized solutions. This result was mentioned in Anderson’s Nobel lecture.”

The fundamental equations for these results come from the expressions derived in 1.3.2, involving non-repeating paths: they dramatically simplify on the Bethe-lattice

$$\Sigma_i(z) = \sum_{j \neq i} V_{ij} \frac{1}{z - \epsilon_j - \Sigma_j^{\neq i}(z)} V_{ji} + \sum_{j \neq i} \sum_{k \neq i, j} V_{ij} \frac{1}{z - \epsilon_j - \Sigma_j^{\neq i}(z)} V_{jk} \frac{1}{z - \epsilon_k - \Sigma_k^{\neq i, j}(z)} V_{ki} + \dots \quad (1.37)$$

All the terms, but the first, vanish, since on the Bethe-lattice, in absence of loops, longer paths, starting and ending at the origin, must contain repeated indexes. This is true also for all the nested self-energies $\Sigma_i^{\neq j, k, \dots}(z)$ expansions. Moreover, it is crucial

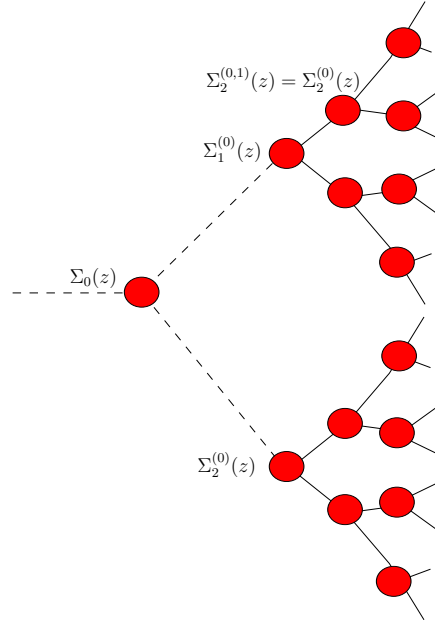


Figure 1.8: A portion of the Bethe-lattice with connectivity $Z = K + 1 = 3$; from the plot it becomes evident that all the descendent self-energies are on the same ground.

that the equations for the descendant self-energies appearing at the denominators, are completely analogous and do not involve different variables

$$\Sigma_j^{\neq i}(z) = \sum_{k \neq i, j} V_{jk} \frac{1}{z - \epsilon_k - \Sigma_k^{\neq j}(z)} V_{kj} \quad (1.38)$$

where we used the fact that on-the Bethe-lattice $\Sigma_i^{\neq i_1, i_2, \dots}(z) = \Sigma_i^{\neq i_1}(z)$, since when the site j has been removed, there is no link to the site i . This last equation is the central

point for the study of the localization phenomena. It is clear that $\Sigma_j^{\neq i}(z)$, $\Sigma_k^{\neq i}(j)$ and ϵ_k are random variables and therefore, if we assume that $\Sigma(z)$ on the lhs and rhs are equally distributed, Eq. (1.38) can be interpreted as an integral equation for the pdf. Unfortunately, this integral equation does not admit an explicit exact solution and one has to resort to some approximations. We will not go into the details of these computations that can be found in the original work [2]. It is however instructive to mention that, going toward the middle of the band ($\Re z \ll 1$) and neglecting the real part of the self-energy $\Sigma(z)$, one can recover the upper limit estimation (1.36). Even though derived with completely different methods, the coincidence of the two results shows that this estimation is quite robust and that a correct way to control the approximations made by Anderson is to go on the Bethe-lattice. Another important concept that can be derived from this approach is the *mobility edge*. We will comment more on it in the next subsection, where we will introduce a numerical method, known as *population dynamics* or *pool method*, to deal with equation involving random variables as (1.38).

1.4.1 The pool method

A numerical procedure to solve the distributional equations (1.38) was already proposed in [2], and revived more recently in the context of finite-connectivity mean-field disordered systems under the name of population dynamics [80] also called the pool method [86]. The idea is as follows: suppose we have an equation involving equally distributed and independent random variables on the two sides as (1.38). As we said, one can convert this equation into one for the pdf. Instead of trying to solve the integral equation determining analytically the pdf, one tries to approximate the distribution of a random variable by the empirical distribution of a sample of a large number M of representatives. Then one starts from an arbitrary initial conditions and it is produced a sequence of samples whose empirical distributions converges to a fixed point. Suppose we start from a sample of self-energies at a fixed value of z :

$$S_0 = \{\Sigma^{(1)}(z), \Sigma^{(2)}(z), \dots, \Sigma^{(M)}(z)\}$$

To obtain a new sample S_{i+1} , we replace one of its elements randomly chosen, say $\Sigma^{(j)}(z)$, with the rhs of (1.38), where the $\Sigma(z)$ -s are obtained selecting K elements uniformly at random from the current sample S_i and the energies ϵ_k are drawn uni-

formly in $[-W/2, W/2]$. Repeating these steps, if M is large enough, one reaches a sample \mathcal{S}_∞ approximating the fixed point solution of (1.38), and then the distribution, its moments and the typical values can be obtained by computing empirically the distribution over the representatives in \mathcal{S}_∞ . The numerical accuracy is controlled by the size M of the samples. In Fig. 1.9, we report the result obtained with this method

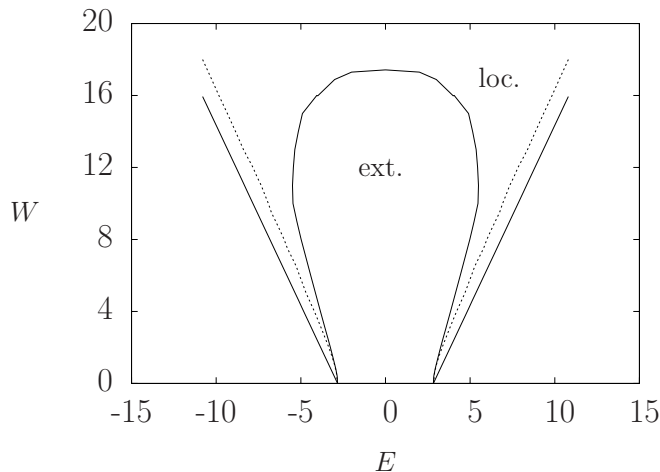


Figure 1.9: From [24]. Phase diagram for the Bethe lattice with connectivity $K+1 = 3$. The innermost solid line indicates the mobility edge between extended and localized states, the outermost solid line being the edge of the density of states $E = \pm(2\sqrt{k} + W/2)$. The dashed line is the numerically estimation for the density of states.

in [24]. By checking the behavior of the typical value of the imaginary part of the self-energy in the sample when $\Im z \rightarrow 0$ one knows whether the spectrum is localized or not. This can be done for different energies $E = \Re z$. The AL transition that we discussed corresponds to the localization of the full spectrum, but from this plot we deduce that for lower value of the disorder, the tails of the spectrum are already localized. The interface separating the middle of the band, which is delocalized, from the localized tails is known in the literature as mobility edge.

1.5 Some rigorous results

Being so simple to formulate, the Anderson model has attracted the interest of the mathematical community. Unfortunately, it must be stressed that even nowadays most

of the checks are based on numerical simulations and many relevant issues still remain open, as one can deduce from the Anderson's Nobel lecture (1977)

“Localization [..], very few believed it at the time, and even fewer saw its importance, among those who failed to fully understand it at first was certainly its author. It has yet to receive adequate mathematical treatment, and one has to resort to the indignity of numerical simulations to settle even the simplest questions about it.”

However, it may be useful to summarize what is already known, sometimes rigorously, sometimes not

1. The RAGE theorem [59] grants that under reasonable hypothesis, the spectrum of an Hamiltonian $s(H)$ can be split into two parts

$$s(H) = s_p(H) \cup s_c(H)$$

where $s_p(H)$ corresponds to the point spectrum, i.e. bound states, while $s_c(H)$ is the continuous part, giving transport. Point spectrum states will never leave a bounded region of space.

2. A random operator is *spectrally localized* if its spectrum H has with probability one an interval of pure point states:

$$s(H) \cap [a, b] \subset s_p(H) \quad w.p. 1$$

In the mathematical literature, the notion of Anderson localization is often identified with spectral localization. Nevertheless, counterexample exists, proving that spectral localization is not enough to prevent (sub-diffusive) transport.

3. In $d = 1$ an arbitrary amount of disorder is enough to localize the full spectrum. This result is already stated in the original Anderson paper and was proved subsequently by many authors [90], and more rigorously in [33].
4. In $d = 2$, in strict sense, again the spectrum is fully localized for arbitrary disorder. As shown in [5], this is the lower-critical dimensions for the Anderson transition and logarithmic scaling appears.

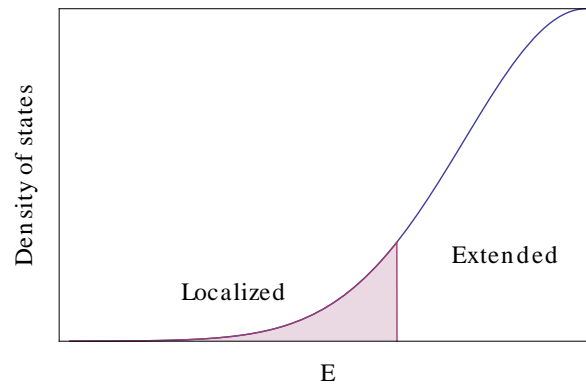


Figure 1.10: A cartoon of the density of states, separated into the localized spectrum, at low energies, and extended spectrum in the middle of the band. The two regions are separated by the mobility edge.

5. In $d \geq 3$, for low disorder, only the tails of the spectrum (Lifshits tails) are localized; the middle of the band is delocalized and the two regions are separated by the already introduced mobility edge (see Fig. 1.10).

1.6 Conclusions

In this chapter we presented some of the results coming from the original Anderson work. Many of the ideas and of the concepts will be useful in the rest of the next. In particular, the idea of distributions with long tails, whose average value is not significant, comes up often in the many-body case. Moreover, the Bethe-lattice approach allowed us to introduce important concepts as the mobility edge. Its particular “solvability” makes it useful as a comparison for more complicate example. We will deepen this in the next chapters.

Chapter 2

Many-body localization

2.1 Introduction

The result presented in the previous chapter have had a tremendous impact on the physics of condensed matter for the last fifty years [69]. We have already mentioned many applications for the AL transition and in particular, it must be stressed its fundamental role in reinterpreting the nature of metals and insulators. However, as Anderson already recognized in its original work, which was presented as a toy model, the absence of interactions makes every conclusion less robust and it is only in particular regimes that the standard AL paradigm is reliable. When interactions are negligible, the problem can be faced as a single-particle one. It means a great simplification of the problem complexity, that therefore admits, among all the other analytical treatments, a successful numerical approach. In the general situation, instead, it becomes necessary to take into account interactions among charge carriers and the problem must be treated as a many-body one. The Hilbert-space size is now exponentially large in the volume of the system and as usual, every numerical technique becomes rapidly inadequate. Moreover, as we already underlined in the previous chapter, when quantumness and disorder come together it is not possible to investigate at any finite perturbative order. For all these reasons, all these questions have remained substantially unsolved. One first step in this direction, is related to the study of the Anderson model in a bath of phonon at finite temperature. Even though all the single-particle eigenstates are localized, electrons can scatter with phonons and reach long distances: as a result, transport

is restored and conductivity is finite, though small. This class of phenomena have been dubbed *variable-range hopping* [88, 89]. Even in presence of a fully localized spectrum, the conductivity is small but finite and goes like

$$\sigma \propto e^{-\left(\frac{A}{T}\right)^{\frac{1}{d+1}}} \quad (2.1)$$

where d is the space dimensionality of the problem. A similar question is, whether in absence of phonons, transport can be restored when the interactions between electrons are turned on. Is a sufficient amount of interactions capable of overturning AL, without the help of an external bath? An answer has come recently in the positive [15, 16]. The mechanism, which underpins this effect (dubbed many-body localization or MBL transition) requires the interaction to act in a substantially non-perturbative way, therefore providing an example of how disorder and strong interactions interplay in a quantum theory.

The natural setup to study the MBL transition is the dynamics (these were also the terms of the question posed in [11]) and in this perspective it is a question about the foundations of statistical mechanics, namely, on the validity of the ergodic hypothesis. MBL also presents the terms in which a quantum glass can be defined and from there it is only a small leap to conjecturing that MBL is a natural ingredient for hard computational *quantum* problems [8, 131] (as Ising spin glasses are a natural scenario to discuss the Physics of hard combinatorial optimization problems [57, 94]).

It is useful to stress that the MBL is not only hard to treat but also difficult to define. One reason is that two complementary but somehow opposite approach are possible: 1) as we already said, it can be seen as the persistence or less of an Anderson localized phase, when interactions are turned on; 2) when the full many-body Hilbert space is taken into account, it can be seen as the standard Anderson model, but where the lattice is substituted with the complex and exotic multi-dimensional hypercube corresponding to the unperturbed many-body states. We will come back on both these points in the following sections.

MBL should be responsible, among other things, of the exact vanishing of the DC conductivity of metals below a critical temperature [15] and of the failure [10, 66] of the simplest version (and possibly of all versions) of the quantum adiabatic algorithm (QAA) [47] for the solutions of NP-complete problems.

In particular, in order to show the relevance for the quantum computation point of view, we will introduce the QAA; then we will follow [10] and show how the existence of a localized phase prevents the possibility of a successful adiabatic quantum computation, inducing (at least) exponentially small gaps in the system size.

Then, we will focus on the properties of typical eigenstates of many-body disordered systems, characterizing the phase transition as a dynamical one. Our investigation will be mainly based on one dimensional systems: they are particularly suited for studying MBL because, as we said in 1.5, the single particle spectrum is completely localized for arbitrarily small disorder, and therefore any observation of delocalization must be attributed to the interaction.

Finally, we will discuss the strong-disordered regime and we will characterize some of its features with a particularly suited integrable model that we propose as toy model for the many-body localized phase: the Richardson model. It corresponds to the XX model with random z fields and a fully-connected hopping term. Being integrable through *Algebraic-Bethe-ansatz* (ABA), it permits to access to matrix elements, correlation functions and overlaps of eigenstates in the middle of the band for quite large systems, that would be completely out of range for any exact diagonalization approach. This method allowed us to obtain quite accurate predictions for the thermodynamic limit: the integrable nature of the model completely prevents the system to delocalize even for very small (but finite) value of the disorder strength, thus defining the model as a good toy model for the localized phase.

2.2 The importance for adiabatic quantum computation

2.2.1 NP vs P

The existence of an algorithm to perform a specific computational task is usually not enough to really determine its concrete applicability: a central concept becomes that of complexity, usually related to the number of operations (therefore the computational time) needed for a task of given length n . This approach, formally founded on the Turing machine itself, allowed to classify algorithms in different classes. Among them,

one of the most important is for sure the **NP** (Nondeterministic Polynomial time) completeness. A computational problem belongs to the class **NP** if its solution can be verified in a time at most polynomial in the input size n . In other words, less than cn^k computational steps are required to check whether the given solution solves the problem or not. It is clear, already at the intuitive level, that checking if a solution is correct is much faster than really finding it. Indeed, the class **P** is defined by the problems whose solution can be found in a time at most polynomial in the input length. A classical example is the *Hamiltonian path problem*, that is, given a graph G , determining whether it exists a path visiting all its sites once and exactly once. It is clear that in this case, given a solution, checking that it satisfies the requirement is an easy task. An example of graph that does not admit an Hamiltonian cycle, i.e. one of these paths, is shown in Fig. 2.1. However, if the definition of the computational classes was

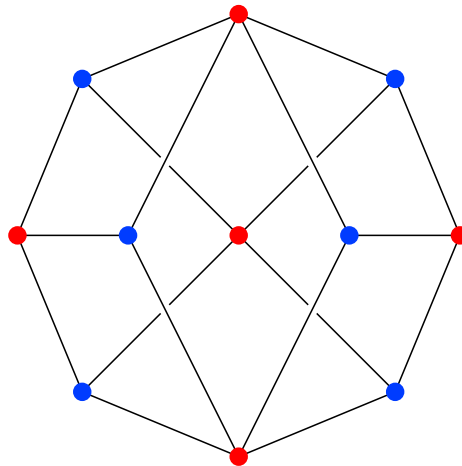


Figure 2.1: The Herschel graph, the smallest possible polyhedral graph that does not have a Hamiltonian cycle.

possible and provided a set of powerful ideas for the study of computational complexity, the relations among them are very difficult to investigate: for this reason, if it is obvious that $\mathbf{P} \subset \mathbf{NP}$, it is still unknown whether $\mathbf{P} = \mathbf{NP}$. Even though no formal proof is known either of the equality or of its opposite, it is commonly believed that they are distinct and that inside the **NP** class, there are problems that do not admit any polynomial algorithm for their solution. An useful class goes under the name of **NP-complete** problems: a problem is **NP-complete** if any other **NP** problem can be

reduced to it in a time at most polynomial in the input size. In some sense, they can be considered as the real core of NP-complexity, and therefore if $P \neq NP$, we can be sure that no polynomial algorithm will exist for any of them. Many examples of NP-complete problems are known: the already cited Hamiltonian path, 3-sat, Travelling salesman problem, Clique problem, Graph coloring problem, Exact Cover. We will see in detail this last example.

2.2.2 The exact cover problem

In mathematics, given a collection \mathcal{S} of subsets of a set X , an exact cover is a sub-collection $\hat{\mathcal{S}}$ of \mathcal{S} such that each element in X is contained in exactly one subset in $\hat{\mathcal{S}}$. In computer science, the exact cover problem is a decision problem to find an exact cover or else determine none exists. The exact cover problem is NP-complete [61] and is one of Karp's 21 NP-complete problems [63]. The exact cover problem is a kind of constraint satisfaction problem.

An exact cover problem can be represented by an incidence matrix or a bipartite graph. The Knuth algorithm X, together with its implementation known as Dancing Links (DLX), can be used to find all the solutions to an exact cover problem. Finding Pentomino tilings and solving Sudoku are noteworthy examples of exact cover problems. A particular instance can be presented as a matrix, e.g. with $X = \{1, 2, 3, 4, 5, 6, 7\}$ and $\mathcal{S} = \{A, B, C, D, E, F\}$ with

$$\begin{aligned} A &= \{1, 4, 7\} \\ B &= \{1, 4\} \\ C &= \{4, 5, 7\} \\ D &= \{3, 5, 6\} \\ E &= \{2, 3, 6, 7\} \\ F &= \{2, 7\} \end{aligned}$$

we have the matrix

$$\begin{array}{c|ccccccc}
 & 1 & 2 & 3 & 4 & 5 & 6 & 7 \\
 \hline
 A & 1 & 0 & 0 & 1 & 0 & 0 & 1 \\
 B & 1 & 0 & 0 & 1 & 0 & 0 & 0 \\
 C & 0 & 0 & 0 & 1 & 0 & 0 & 1 \\
 D & 0 & 0 & 1 & 0 & 1 & 1 & 0 \\
 E & 0 & 1 & 1 & 0 & 0 & 1 & 1 \\
 F & 0 & 1 & 0 & 0 & 0 & 0 & 1
 \end{array} \tag{2.2}$$

An other way to formulate the problem is in terms of boolean variables. If we associate to every subset S in \mathcal{S} a boolean variable x_S , a solution corresponds to a configuration of the variables satisfying $E[x] = 0$, where

$$E[x] = \sum_{x \in X} \left(1 - \sum_{S \in \mathcal{S}, x \in S} x_S \right)^2 \tag{2.3}$$

If we reinterpret this expression as an energy, the decision problem corresponds to the determination, if any, of the configurations, giving zero energy. It is easy to convert the boolean variables to spins by simply setting $\sigma_i^z = 1 - 2x_i$ and therefore, from now on, we will consider standard spin variables. The solution of the computational task coincide with finding the ground states. From now on, we will restrict to the problem known as *Exact cover - 3* (EC3), where each elements of x is contained in exactly 3 sets of \mathcal{S} (in other words each column of the matrix representation contains exactly 3 non-zero values). This restriction does not change the nature of the problem since EC3 still belongs to the NP-complete class.

2.2.3 Adiabatic quantum computation

As we saw in the previous section, any instance of EC3 can be recast in a classical spin Hamiltonian and we want to determine its ground state. Since the problem is known to be NP-complete, unless $\mathbf{P} = \mathbf{NP}$, which is hard to believe, no fast solution can be ever found for a classical computer. However, the possibility that with a quantum computer, it is possible to improve the efficiency of the algorithm is still open and under debate. We will not go into the details of the wide topic of quantum computation, usually introduced in terms of a discrete succession of unitary transformations (quan-

tum circuit). Instead, we will focus on a different implementation known as *quantum adiabatic algorithm* (QAA), that however, has been proved [6, 46, 123], to be general enough and equivalent in terms of computational cost to the quantum circuit formulation.¹

To understand better the mechanism, we start from one of its forerunner, known as *simulated annealing* [65]. The idea is to perform the computation through a classical statistical system, whose temperature we slowly decrease. In fact, once the energy function for each configuration of spin variables, as in (2.3), has been introduced, the Gibbs-Boltzmann probability law at inverse temperature β reads

$$\mu(\sigma) = \frac{e^{-\beta E(\sigma)}}{Z(\beta)} \quad (2.4)$$

where σ represents the global configuration of all the spin variables, and Z is the usual partition function, acting as normalization factor. If we perform a random walk in the configuration space, with transition probabilities respecting the detailed balance condition with the Gibbs-Boltzmann distribution, we will ensure thermal equilibrium. At small temperatures (or large β), the probability distribution in (2.4) will be more and more concentrated around the minima of $E(\sigma)$. Therefore, if we decrease the temperature slowly enough, at every time we will be at thermal equilibrium and at the end we will end up in one of the minima of $E(\sigma)$. In this case, the thermal fluctuations are used to overcome the barriers between local minima. The idea behind the QAA is to use quantum fluctuations [12, 28, 47, 51, 62] instead of the thermal ones. For the thermal case, at high temperature, the problem trivializes. Analogously, we introduce another Hamiltonian H_i , whose ground-state is easy to find (or in other terms it is easy to prepare the system in it). Then we define

$$H[\lambda] = (1 - \lambda)H_i + \lambda H_f \quad (2.5)$$

where the final Hamiltonian is the diagonal operator given by the energy function

$$H_f = \sum_{\sigma} E(\sigma) |\sigma\rangle \langle \sigma| \quad (2.6)$$

¹in [7] it was even showed that an Hamiltonian with 11-dimensional qudits and nearest-neighbor interactions is enough to encode any quantum circuit.

We suppose that at the initial time the system is in the ground-state of H_i and we perform a quantum evolution with a time dependent Hamiltonian $H[\lambda]$, where $\lambda = t/\mathcal{T} \in [0, 1]$ and \mathcal{T} will be the simulation time. If \mathcal{T} is so large that the hypothesis of the adiabatic theorem are holding [70, 79], then it is granted that the system will be at each time in the instantaneous ground-state of $H[\lambda]$ and therefore at the end it will be in a configuration corresponding to a minima of $E(\sigma)$. So a solution to the computational problem is found by simply measuring the state of each spin.

After this discussion, some remarks are in order

1. many possible choices for the initial Hamiltonian H_i are possible: the only requirement is that its ground state must be easy to prepare;
2. estimating the complexity of the algorithm is now converted into the estimation of the time \mathcal{T} that guarantees an adiabatic evolution.

The configurational space is chosen to be the product space, for each site i , of the common eigenvectors of the σ_i^z

$$\{|\uparrow\uparrow \dots \uparrow\rangle, |\uparrow\uparrow \dots \downarrow\rangle, \dots\} \quad (2.7)$$

One possible, and typical, choice for H_i is

$$H_i = - \sum_i \sigma_i^x \quad (2.8)$$

For a discussion of the experimental realization of the QAA, we remind to [20, 28, 119].

2.2.4 Anticrossing and small gaps

The standard results of the quantum adiabatic theorem allow to relate the computational time \mathcal{T} with the minimum gap between the ground-state and the first excited state

$$\mathcal{T} \gg O(N\Delta_{min}^{-2}) \quad (2.9)$$

where, given the two lowest eigenvalues $E_{gs}(\lambda), E_{es}(\lambda)$ of $H[\lambda]$, the minimum gap is defined as

$$\Delta_{min} = \min_{\lambda \in [0,1]} E_{es}(\lambda) - E_{gs}(\lambda)$$

Therefore, the estimation of the time \mathcal{T} is now related to the computation Δ_{min} . We will assume that $\Delta_{min} \neq 0$, since in absence of particular symmetries the "No crossing rule" should hold [126]. What happens typically is that the two Hamiltonians H_i and H_f have very different low-energy behavior, so that there will be a critical value λ_c where $H[\lambda_c]$ undergoes a phase transition. The common belief is that the order of the phase transition determines the scaling of the gap with the system size:

$$\Delta_{min} \simeq \begin{cases} N^{-\alpha} & \text{second order} \\ e^{-\gamma N} & \text{first order} \end{cases} \quad (2.10)$$

So generally we can assume that whenever a first order phase transition is encountered in the evolution of λ , the algorithm will need a time exponentially long in the input length. One may wonder whether it is possible to obtain any improvement to the relation (2.9), if instead of choosing the linear interpolation, we would have chosen a different interpolation scheme. It can be shown that the bound (2.9) is obtained if one suppose that $\Delta(s) = \Delta_{min}$ for all s . If we take into account that the gap is not always as small as its minimum value, we can obtain a better scaling $\mathcal{T} \simeq \Delta_{min}^{-1}$, that however, according to (2.10), does not change the nature of the algorithm (polynomial or exponential).

An important remark is that the complexity time is usually estimated considering the worst case: it means that we consider, for the given algorithm, the time needed for the worst instance. It happens often however that the worst-case is not the typical one, and so it is not so easy to be generated. This is meaningful if a probability distribution among the instances has been defined. To understand better the situation, we come back on the EC3 problem. We fix the scaling with the system size assuming that the set X will contain $M = \alpha N$ elements, where N is the number of sets in \mathcal{S} . Then we investigate the large N limit at fixed α . The energy function becomes

$$f(x) = \sum_c (x_{i_c} + x_{j_c} + x_{k_c} - 1)^2 \quad (2.11)$$

2. Many-body localization

Each term in the sum is called a clause, that involves 3 boolean variables and is satisfied if and only if only one among them is true. We consider a standard distribution of random instances, where we pick the M clauses independently, each clause being obtained by picking three boolean variables with uniform distribution. We will give now some ideas from [10], showing that for the typical instance, the gap closes (at least) exponentially. There are two characteristic values of α : the clustering threshold α_{cl} and the satisfiability threshold α_s [22]:

1. for $\alpha < \alpha_{cl}$ the density of the solution is high and essentially uniform
2. for $\alpha > \alpha_{cl}$ the solutions start to organize in clusters, each of them very far from the other (the distance between them measured by the Hamming distance)
3. for $\alpha > \alpha_s$ the probability that the problem is satisfiable vanishes when $N, M \rightarrow \infty$;

An estimation has been provided in [98] for the value is $\alpha_s \simeq 0.6263$. Now, the mechanism involved here is the so called *avoided crossing* or *anticrossing* and it is the same mechanism involved in the already cited “No crossing rule”. Let’s suppose that two diagonal elements in the Hamiltonian $H[\lambda]$, for a given value of λ , are particularly close. An arbitrary small off-diagonal element is already enough to prevent crossing. This is true already if we limit to the 2×2 matrix

$$H_{12} = \begin{pmatrix} e_1(\lambda) & V_{12} \\ V_{12} & e_2(\lambda) \end{pmatrix}$$

The gap between the two levels is then

$$\Delta[\lambda] = \sqrt{(e_1 - e_2)^2 + |V_{12}|^2} \tag{2.12}$$

and reaches its minimum value when the two diagonal elements meet, with $\Delta_{min} = |V_{12}|$: this is called *avoided crossing*, because the two lines would cross only if $V_{12} = 0$. The idea is to construct two states forming one of these anti-crossings, thus giving a small gap. We set $\alpha \lesssim \alpha_s$, so that we are in a region where solutions are few and far one from the other. Now, we suppose σ_1 and σ_2 are two spin configurations giving a

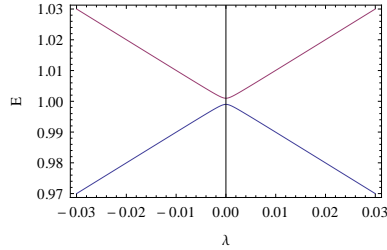


Figure 2.2: A typical example of level repulsion for the eigenvalues of the matrix depending on a parameter: an exact degeneracy would need an additional condition and is therefore generically very rare.

solutions, $f(x_{\sigma_1}) = f(x_{\sigma_2}) = 0$ (where x_{σ} is the configuration of the boolean variables corresponding to the spin configuration σ), and so they are degenerate ground-states of $H[\lambda = 0]$ ¹. When $\lambda \neq 0$, the two eigenvalues $E_1(\lambda), E_2(\lambda)$, corresponding at $\lambda = 0$ to σ_1, σ_2 , will move separately, the degeneracy will be lifted and it can be shown that it exists $\lambda^* \ll 1$ such that

$$\forall \lambda > \lambda^* \quad |E_1(\lambda) - E_2(\lambda)| > 4 \quad (2.13)$$

Without losing generality we can assume $E_1(\lambda) < E_2(\lambda)$. If we now add randomly a new clause, going to $M + 1$, there is a finite probability that σ_1 is still a solution, while σ_2 is not. It means that $f_{M+1}(x_{\sigma_2}) = 1$ or 4 and comparing with Eq. (2.13), the order of the eigenstates for large λ will remain the same. The resulting behavior is shown in Fig. 2.3 and it follows that at $\lambda = \lambda_c$ we will have an anticrossing. It remains to estimate the gap at λ_c and we can use Eq. (2.12); therefore we need to compute the matrix element between the two unperturbed states σ_1, σ_2 . For the given value of α , with high probability, the Hamming distance between them will be quite high: $d_H(\sigma_1, \sigma_2) \simeq \nu(\alpha)N = n$. It follows that the two states are connected only going to order n perturbation theory

$$V_{12} = \sum_{path} \frac{\lambda^n}{E_{p_1} \dots E_{p_n}} \simeq \frac{n!}{[(n/2)!]^2} \lambda^n \simeq \left(\frac{\lambda}{2}\right)^n \quad (2.14)$$

where the sum is over all the possible path connecting σ_1 and σ_2 . Here we used that for

¹this does not contradict the *No crossing rule*, due to the symmetry $[H[\lambda = 0], \sigma_z^i] = 0$.

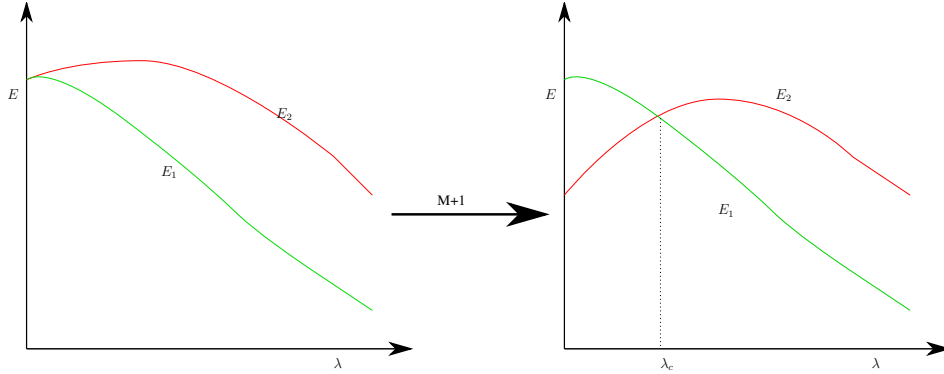


Figure 2.3: The behavior with M clauses for the evolution with λ of the two states σ_1 and σ_2 : the degeneracy is lifted by the off-diagonal elements (left); adding one more clause, there is a finite probability that the degeneracy at $\lambda = 0$ is lifted in an opposite way with respect to large λ , thus producing an avoided crossing at λ_c .

most of these paths, since solutions are very rare, every time we change a spin value, we break some clauses, therefore the energy increase linearly from the solution σ_1 , reaches a maximum in the middle, and start decreasing again toward σ_2 . In this way, the denominator produces a $(n/2)!^2$ that cancels out with the $n!$ coming from the sum over paths. Instead, the value of λ can be estimated imposing the condition (2.13) at the first non-zero order in perturbation theory

$$|E_1(\lambda) - E_2(\lambda)| = A\sqrt{N}\lambda^4 + O(\lambda^6) \Rightarrow \lambda^* = O\left(N^{-\frac{1}{8}}\right) \quad (2.15)$$

where we used that at each order, the perturbative correction having zero-mean, will scale as \sqrt{N} . Finally we get

$$\Delta_{min} \simeq \exp\left[-\frac{\nu(\alpha)N}{8} \log \frac{N}{N_0}\right]$$

where N_0 is a constant of $O(1)$. This shows that the gap for this situation is exponentially small.

Actually, we said that this situation happens with a finite probability. Is it possible that if we are lucky no anticrossing occurs and the adiabatic computation can perform without problems? Unfortunately, this is not the case, because we took into account only two degenerate states at the beginning σ_1 and σ_2 . By considering all the possi-

ble states that can in principle have the same role as σ_2 , it is easy to show that the probability to have at least one avoided crossing with the ground states, is practically 1.

2.2.5 The role of localization

From the discussion in the previous subsection, it may appear obscure what is the role of localization. However if we consider the Hamiltonian in Eq.(2.5), it is easy to recognize that it has the same form as the Hamiltonian (1.1) of the Anderson model. Here the randomness in the diagonal elements is coming from the random choice in the instance of the problem. The main difference is coming from the off-diagonal part: for Eq.(1.1), the hopping term coincided with the adjacency matrix of a finite-dimensional graph, e.g. the d -dimensional cubic lattice, therefore $K \simeq 2d$ and the number of sites is L^d . Here instead the connectivity is N and the number of sites is given by the number of possible configurations 2^N . It is crucial in the previous derivation that perturbation theory holds. If so, as we saw, one can prove that with high probability an avoided crossing with exponentially small gap will appear. The perturbation term appearing in Eq. (2.14) is meaningful only if the full series is convergent. This, by turn, was the criteria used in 1.3.3 to find the transition point. It follows that the perturbation theory is convergent in we are in the discrete region of the spectrum, or in the Anderson localized phase 1.5. In this case, due to the exponential scaling of the Hilbert space size, we are considering the many-body version of the Anderson problem, *the MBL transition*. If we naïvely set $K \simeq N$ in Eq. (1.36) to estimate the critical value of λ_{MBL} for the localization transition, we find that $\lambda^* \ll \lambda_{MBL}$; so this procedure becomes meaningful, thanks to the existence of the many-body localized phase.

In the following sections, we will investigate more on the structure of the eigenstates on the two sides of the MBL transition.

2.3 The structure of the eigenstates in a disordered many-body problem

We move now to the specific analysis of some features characterizing and distinguishing the two phases.

2.3.1 The XXZ spin chain

We will analyze in detail the ergodicity properties of an XXZ chain with random fields. The Hamiltonian is

$$H = -J \sum_{i=1}^N (s_i^x s_{i+1}^x + s_i^y s_{i+1}^y) - \Delta \sum_{i=1}^N s_i^z s_{i+1}^z - \sum_{i=1}^N h_i s_i^z, \quad (2.16)$$

with periodic boundary conditions. This particular example has already provided different indications of the MBL transition for sufficiently large disorder: in [96] correlation functions and spectral properties were studied, while in [13, 128] tDMRG was used to investigate the different saturation properties of the entanglement entropy in the two phases. In Fig. 2.4, we report the finite-size scaling for the parameter r defined as:

$$r_N = \left\langle \frac{\min(\delta_n, \delta_{n+1})}{\max(\delta_n, \delta_{n+1})} \right\rangle_{n,h} \quad (2.17)$$

where $\delta_n = E_{n+1} - E_n$ is the spectral distance between two subsequent eigenvalues and the average is taken over n and disorder realization. This parameter is known to have different limits according to the level-space statistics

$$r_{N \rightarrow \infty} \simeq \begin{cases} 0.39 & \text{Poisson statistics} \\ 0.54 & \text{Wigner-Dyson statistics} \end{cases} \quad (2.18)$$

and in the figure the finite-size scaling gives strong indication of the different thermodynamic limit for this quantity in the weak and strong disorder regions. Therefore, while the existence of a transition in the dynamics of this model is now almost certain, its precise location, the possible existence of a critical phase and the nature of the phases that it separates are subject of debate. This should not be regarded as a debate about a particular spin chain but rather as an attempt at characterizing as much

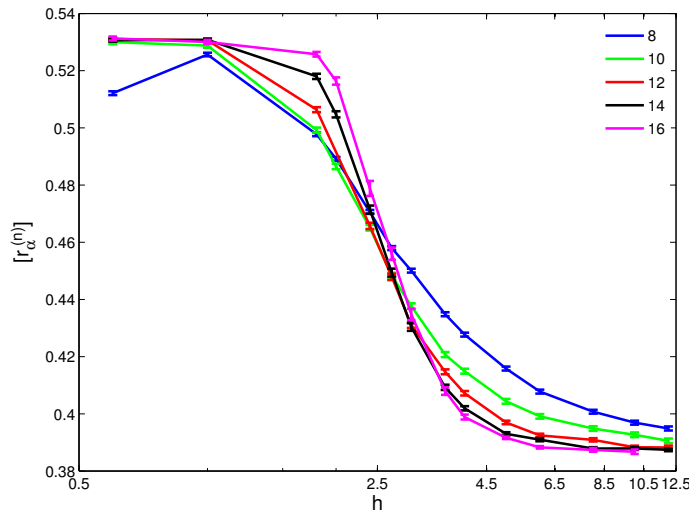


Figure 2.4: From [96], finite-size scaling of the parameter r vs h . The crossing of the different curves seems to indicate a transition in the spectral properties at a finite h .

as possible the differences between MBL and AL.

Consider the real time evolution of a state $|\psi_0\rangle$ as it is encoded into the Green's function

$$G(t) \equiv \langle \psi_0 | e^{-itH} | \psi_0 \rangle . \quad (2.19)$$

Generalizing what we did in (1.15), we introduce

$$\text{IPR}_q = \sum_E |\langle E | \psi_0 \rangle|^{2q} . \quad (2.20)$$

where the sum runs over the full set of eigenstates $|E\rangle$. Therefore, we already know that the long time average of the return probability is given by

$$\bar{P} \equiv \lim_{\tau \rightarrow \infty} \frac{1}{\tau} \int_0^\tau dt |G(t)|^2 = \text{IPR}_2 . \quad (2.21)$$

As we said, IPR_2^{-1} can be seen as a measure of the explored volume of Hilbert space during the dynamics. Higher order IPR_q 's describe finer details of the dynamics.

Let us now comment on the choice of a suitable initial state for a *gedankenexper-*

iment aimed at testing the breaking of ergodicity. First of all, consider what happens if we take a random state in the Hilbert space (therefore not an eigenstate) conditioned just to have an expectation value of the energy E and standard deviation δ (with high probability, for a random state and a local Hamiltonian $\delta = O(N^{1/2}) \ll E = O(N)$). In fact, in the phase dominated by a strong disorder there are states very close in energy ($\Delta E = O(e^{-S})$, where S is the microcanonical entropy at energy E) which are macroscopically different and the expectation value of a local operator will be the average of its values in these localized eigenstates, concealing the effect of disorder (as expected from the ergodic theorem [93]). If we want to observe the effect of disorder on the dynamics, a reasonable prescription consists in choosing an eigenstate of the part of the Hamiltonian which dominates in the strong disorder limit. Starting the dynamics coincides then with *turning on* the rest of the Hamiltonian. In the delocalized phase, during the quantum dynamics, the motion covers a finite fraction of the full Hilbert space (each eigenstate being individually thermal, the so-called “eigenstate thermalization hypothesis” (ETH) [105, 117, 118]). Instead, in presence of strong disorder, ergodicity breaks down and the many-body wave function motion is constrained on a small section of the full Hilbert space.

We also believe that this point of view on MBL is what better brings forward its implications for quantum computation (or at least for the performance of the Adiabatic Algorithm [47]). In the localized phase the system gets trapped, the dynamics unable to efficiently explore the Hilbert space, so the algorithm is not efficient in finding the ground state [8, 47, 131].

This view on the MBL transition will be the focus of this paper. We will show how the usual criteria for detecting AL need to be tweaked to capture the MBL transition; we will study the IPR’s and will show how, although much information is contained in them, it is actually necessary to study the distribution of wave-function coefficients $\langle \psi_0 | e \rangle$, which is heavily tailed both in the localized and delocalized regions.

As the Hamiltonian commutes with the total z spin $S^z = \sum_i s_i^z$, we focus on the subspace with $S^z = 0$. The random fields are chosen from a box distribution $h_i \in [-h, h]$. The model can be cast into a theory of fermions ($S^z = 0$ corresponds to half-filling), with on-site disorder h_i .

The $\Delta s^z s^z$ term can be written as a two-body, point-like interaction for the fermions and for zero temperature it can be included perturbatively or non-perturbatively [53]

leading to an interesting phase diagram. When $\Delta = 0$ the fermions are free, an arbitrarily small disorder localizes the entire spectrum and therefore ergodicity is broken for any $h > h_c = 0$. As Δ is increased the MBL conjecture implies that a peculiar phase transition exists (possibly even at infinite temperature) at a critical h_c increasing away from zero. On the other hand, for $\Delta \gg J$ the disorder necessary to break ergodicity should *decrease* again. In fact, for large Δ the relevant degrees of freedom are the domain walls of the classical Ising chain obtained by setting $J = 0$ in (2.16). Longer domain walls have smaller and smaller hopping matrix elements and therefore they are more prone to localization than the fermions at $J \gg \Delta$. Once a few of these large domain walls have frozen, ergodicity can be considered broken and this occurs for smaller h , since both the effective hopping and interaction are smaller (effective randomness is always h). Here we present results of exact diagonalization for $\Delta = J = 1$, where the delocalized phase is largest.

2.3.1.1 Return probability.

According to the discussion of the previous section, we should test ergodicity by taking an initial state ψ_0 as one of the $\mathcal{N} = \binom{N}{N/2}$ configuration of spins $|a\rangle$ polarized along the z or $-z$ direction, (e.g. $|a\rangle = |\uparrow\downarrow \dots\rangle$). We need to stress a major difference in the behavior of IPR_2 in the localized and delocalized phases between MBL and AL. While in the latter one can distinguish the two phases by the participation ratio being $O(1)$ or not in the thermodynamic limit, this is not a sufficient criterion in MBL. For a many-body state, even in absence of interaction, IPR_2 will be exponentially small in N also in presence of strong disorder, simply because each degree of freedom will have a localization length small but finite, corresponding to an individual *participation ratio* smaller than < 1 : multiplication of $O(N)$ of these factors leads to an exponentially small IPR_2 . We need to correct the previous criterion by requiring that the delocalized and localized phase are distinguished by whether the ratio $\text{IPR}_2/\mathcal{N}^{-1}$ is $O(1)$ or not. The other IPR_q 's, properly rescaled with powers of the Hilbert space dimension \mathcal{N} , also represent indicators of ergodicity breaking.

However, as far as averages over the initial states are involved we have found that

IPR's have better finite-size behaviors (more on this later), so we considered:

$$I_q^{(N)}(h) \equiv \left\langle \frac{\text{IPR}_q^{-1}}{\mathcal{N}^{q-1}} \right\rangle_{\{h\}, a} . \quad (2.22)$$

where the subscripts in the average correspond to disorder realizations (indicated with h) and initial spin configuration $|a\rangle$ ¹. In particular the data for I_2 , shown in Fig. 2.5, are consistent with the $\lim_{N \rightarrow \infty} I_2^{(N)}(h) = i_2(h)$ where $i_2(h) = 0$, for $h > h_c = 2.7 \pm 0.3$, although the finite-size corrections are strong already at $h \gtrsim 1.5$. A similar information is obtained by the diagonal entropy

$$S^{(N)} = \lim_{q \rightarrow 1} \frac{\langle \text{IPR}_{q-1} \rangle}{(q-1) \ln \mathcal{N}}, \quad (2.23)$$

which is plotted for varying h in Figure 2.6 and also this quantity is clearly far from its thermodynamic limit of $S = 1$ in the delocalized phase. If we identify the critical point as the place where the N dependence sets in (for I_2) or drops out (for S) then both quantities identify a critical point consistent with $h_c = 2.7 \pm 0.3$ consistently with the findings of [96].

The diagonal entropy and the IPR's testify that even in the localized region, the covered phase space is growing with the system size, even though it is an exponentially small fraction of the full Hilbert-space. This suggests that in a many-body system, the localized phase is necessarily characterized by the breaking of ergodicity, but not necessarily by a concrete localization ($\text{IPR}_2 \simeq O(1)$). However, to pinpoint the transition and understand the reasons of the scalings we should analyze the full probability distribution of $|\langle a|e\rangle|^2$.

2.3.1.2 Distribution of wave function amplitudes.

If one considers the various IPR_q averaged over $|a\rangle$, one observes a peculiar scaling with N of each of them, which can be considered as due to large fractal dimensions. In this scenario, the safest observable to consider is the distribution of the properly rescaled wave function coefficients. As we are interested in typical states (infinite

¹The number of realizations goes from 10000 for small sizes till about 100 for the maximum size $N = 16$

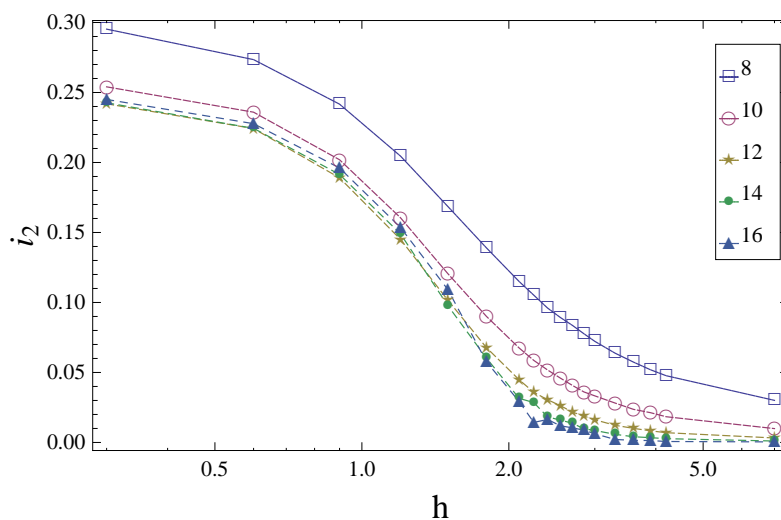


Figure 2.5: Average fraction of occupied Hilbert space vs h for different system sizes $N = 8$ to 16 using exact diagonalization. Notice how the limit for $h \rightarrow 0$ is different from $1/3$ which is the RMT prediction.

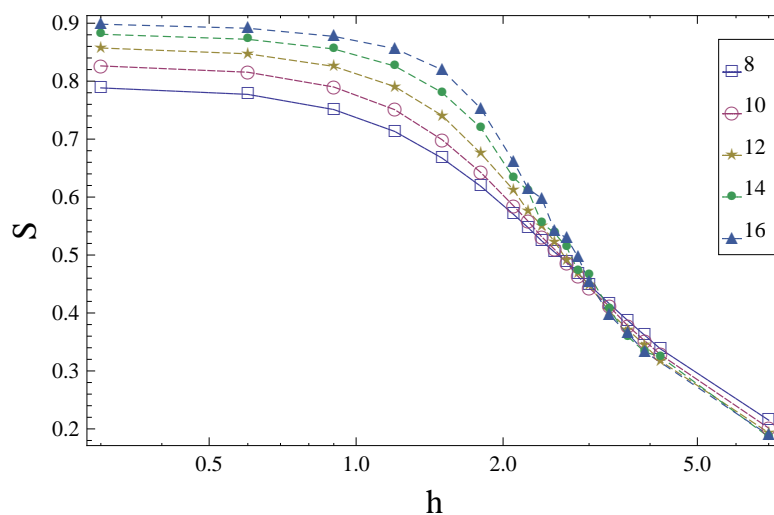


Figure 2.6: Average diagonal entropy vs disorder strength for different sizes $N = 8, 10, 12, 14, 16$. From the N -dependence the transition is identified at $h_c \simeq 2.7 \pm 0.3$.

2. Many-body localization

temperature) we will not follow the usual route of fixing the energy of the state but we will rather integrate over the whole spectrum. In the thermodynamic limit this corresponds to energy density $E/N = 0$.¹

We will consider therefore the average over eigenstates, initial states and disorder realizations:

$$\phi(x, N) = \langle \delta(x - \mathcal{N} | \langle a|e \rangle|^2) \rangle_{a,e,\{h\}}. \quad (2.24)$$

In the following we will drop the subscripts in the averages. This function depends both on x and N in general but in the delocalized phase, as \mathcal{N} plays the role of the space volume, we see that the dependence on N drops out [83, 84, 85].

We can then write the various IPR's as

$$\langle \text{IPR}_q \rangle = \mathcal{N}^{1-q} \int_0^\infty dx x^q \phi(x). \quad (2.25)$$

Illustrative plots are shown for different regimes in Fig. 2.7. As we said, even though in the ergodic phase, with this scaling the curves for different sizes collapse (similarly to AL), the distribution has an elbow at $x \sim 1$ and we find

$$\phi(x) \propto \begin{cases} x^{-\alpha} & \text{if } x \lesssim 1 \\ x^{-\beta} & \text{if } x \gtrsim 10, \end{cases} \quad (2.26)$$

where α, β depend on h . We have $\alpha < 1 < \beta$ ensuring the normalization of the distribution function in the delocalized phase and their values are almost independent of N for the largest sizes explored.² This is an uncommon distribution for the quantity x : usually $\alpha = 1/2$ and the large x behavior is exponential [82] as in the Porter-Thomas distribution of RMT [97]. As the tail is power-law, we see that the delocalized region is less so than one would expect on general grounds. The almost perfect collapse of the curves in the upper panel of Fig. 2.7 allow a much better finite size scaling analysis than any of its moments or IPR's.

As h approaches $h_c \simeq 2.6$ the elbow smoothens and $\alpha \rightarrow 1$ so that we can identify

¹The MBL mobility edge is not much of an issue here since the states at energy $E < E'$ for any $E'/N < 0$ are an exponentially small fraction of the total spectrum, unlike in single particle AL problem.

²A residual N dependence is found in the left tails, at $x \ll 10^{-3}$, that part of the distribution reaching its asymptotic form for larger N ($N \geq 14$).

2. Many-body localization

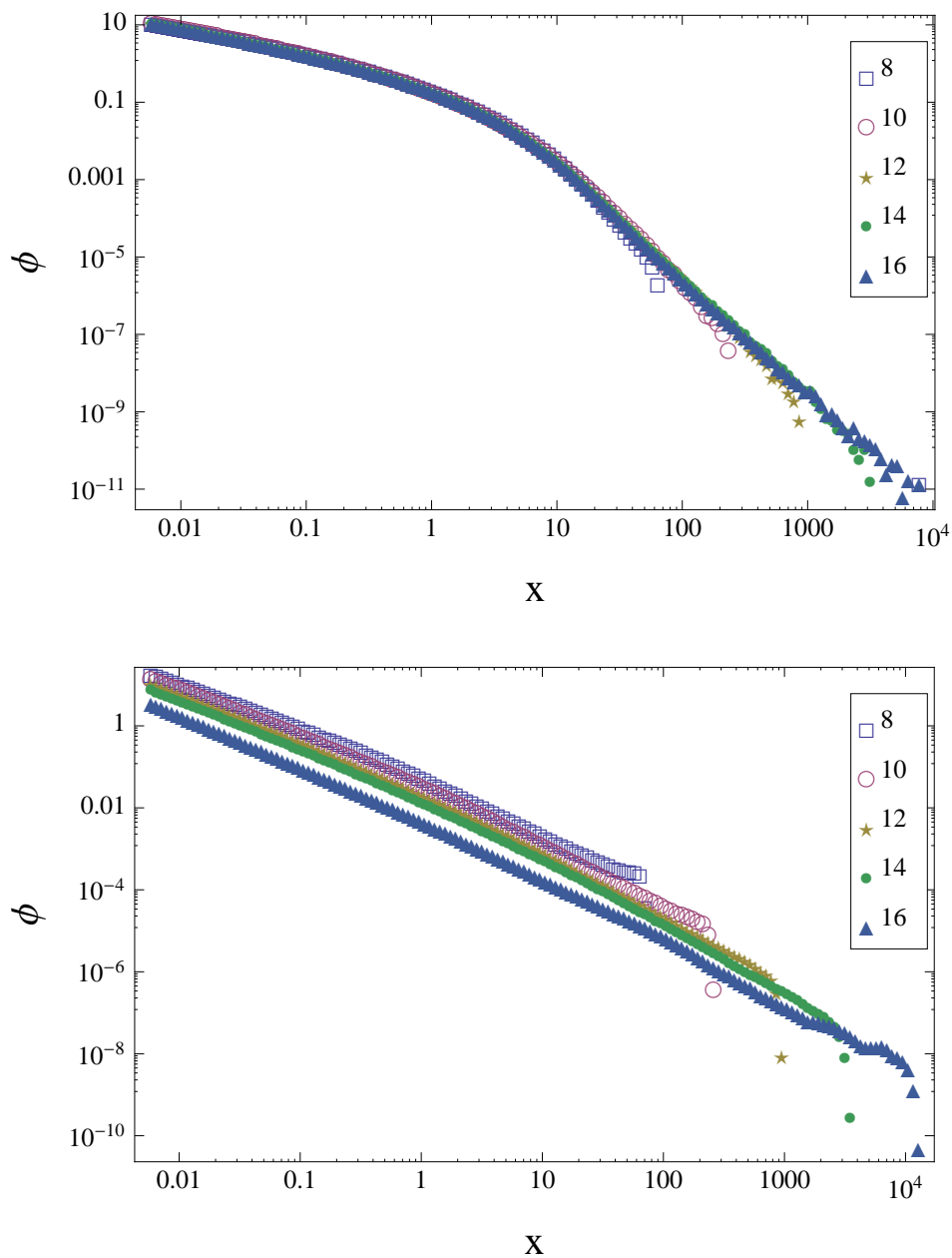


Figure 2.7: The distribution of scaled wave function amplitudes $x = \mathcal{N} |\langle a|e\rangle|^2$ for different values of h . Upper panel: $h = 1.2$ in the middle of the ergodic phase where the scaling is perfectly verified, lower panel $h = 4.2$ in the many-body localized phase. In each figure the different curves correspond to different values of N , from 8 to 16. Each curve is obtained by binning of not less than $3 \cdot 10^6$ squared amplitudes.

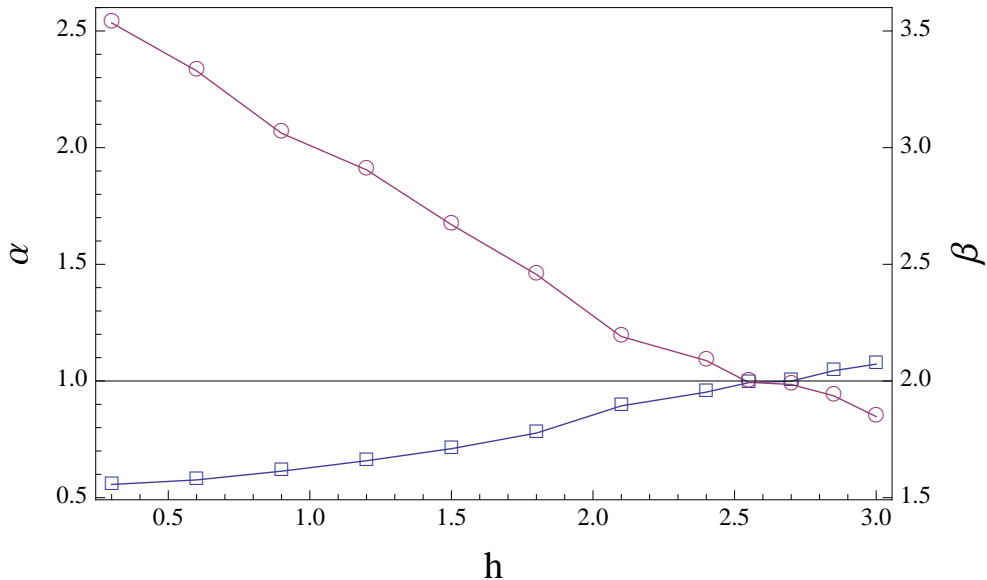


Figure 2.8: The value of the exponent α (blue squares) and β (pink circles) in Eq. (2.26) for $N = 16$ (these exponents are independent of N within the symbol size). The exponent α crosses the value 1 required by summability, which occurs at $h \simeq 2.55 \pm 0.05$, precisely where (within errors) β crosses the value 2, required for the existence of the first moment (normalization of the wave function).

h_c as the point at which $\alpha = 1$, the distribution stops being summable and necessarily the independence on N ceases.¹ This occurs at $h_c = 2.55 \pm 0.05$ as it can be seen in Fig. 2.8. An explicit N -dependence of ϕ means that the scaling of all the IPR's and of the diagonal entropy with N change abruptly and ergodicity is broken.

The exponent β governs the scaling of the various IPR_q 's. For $0 < q < \beta - 1$ the integral in (2.25) is finite and $\text{IPR}_q \sim \mathcal{N}^{1-q}$. If instead $\beta - 1 < q$, since the integral in (2.25) is divergent the average of the participation ratio IPR_q over the initial states $|a\rangle$ does not exist, but the typical value for a state should be found by looking of the sum \mathcal{N} i.i.d. variables x_a^q . One then finds the probability density for $\sum_{a \leq \mathcal{N}} x_a^q \equiv Y$ (by

¹As $\langle x \rangle = 1$ is fixed by normalization the divergence of $\langle 1 \rangle$ implies a divergence of the first moment as well. In fact, $\beta = 2$ occurs at the same value of h_c .

computing and then inverting its Laplace transform) as

$$P(Y) \propto Y^{-\frac{3-\gamma}{4-2\gamma}} \exp\left(-C \left(\frac{\mathcal{N}^{\frac{1}{\gamma-1}}}{Y}\right)^{\frac{\gamma-1}{2-\gamma}}\right), \quad (2.27)$$

where $\gamma = 1 + (\beta - 1)/q$, ($1 < \gamma < 2$) and C is a constant of $O(1)$. This distribution has a power law tail but the typical value of the sum is set by the exponential as $Y \sim \mathcal{N}^{1/(\gamma-1)} \gg \mathcal{N}$. This implies typical values of the IPR_q of a state, when $q > \beta - 1$:

$$\text{IPR}_q^{(N)} \sim \mathcal{N}^{-q + \frac{q}{\beta-1}}. \quad (2.28)$$

The different participation ratios define therefore different ‘‘critical points’’ h_q solutions of $\beta(h_q) = q + 1$. The real transition, signaled by an explicit N -dependence of full distribution ϕ can then be identified by the diagonal entropy (2.23).

As we said, the non-summable divergence of $\phi(x)$ at small x signals the beginning of the localized region. This implies an accumulation of wave-function amplitudes towards small values typical of localized states[85]. Approaching the transition from the delocalized region, in fact, and assuming the form $\phi(x) \propto x^{-\alpha}$ is preserved to arbitrarily small x , we see that the minimum of the eigenfunctions amplitudes is the minimum of \mathcal{N} i.i.d. random variables x_i , which is found to scale like $x_{\min} \sim \mathcal{N}^{-1/(1-\alpha)}$. The values of α in Fig.2.8 predict a scaling exponent which compares well with that obtained *explicitly* from the numerics, supporting this hypothesis. And as this exponent diverges when $h \rightarrow h_c$, we expect that the scaling becomes faster than a power-law in \mathcal{N} at the transition and stays so in the whole localized region. This observation is again verified in the numerics.

This suggests a description of the localized phase in which a typical eigenstate is described by a faster than exponential decay on ample regions of the Hilbert space, which is reminiscent of the ‘‘small branching number’’ Bethe lattice picture of [9, 16] and of the eigenstates of a disordered but integrable model [29].

This bring us again to discuss the similarities and differences with AL on the Bethe lattice (or regular random graph) [3, 85]. Our case however brings three differences from this classic topic: 1) our lattice has connectivity $O(N) \gg O(1)$ (but still $\ll O(N)$, the volume of the system), 2) the on-site disorder potentials of neighboring

configurations a and b are strongly correlated ($E_a - E_b = h_{i+1} - h_i \ll E_a, E_b$) and 3) our lattice is not random at all. In order to identify which of these three ingredients are necessary to preserve this phenomenology of the distribution functions we have investigated numerically a random graph with \mathcal{N} nodes and fixed connectivity $N/2$ and *independent* random energies ϵ_i on each node. We observe the same qualitative features in the distribution of the coefficients and the same distance from the Porter-Thomas distribution, even for small h . On the contrary, for the Anderson model on a Bethe lattice with connectivity $O(1)$ in the ergodic region we observe an exponential tail at large x as predicted by the theory. Therefore we conjecture that the necessary requirement for the large x power-law tail is the growing connectivity, and that one can get rid of the correlation of the energies and the specific topology of the hypercube.

This confirms that we have the right to look at MBL as a localization phenomenon on a Bethe lattice with asymptotically large connectivity, a problem amenable of analytic treatment, beyond the locator expansion [3].

2.3.2 An integrable model for the localized phase

We saw in the previous section which results can be obtained with the use of exact diagonalization technique. The exponential nature of the problem hardly constrains the possibility to go to big system sizes, that would be actually necessary for the estimation of the thermodynamic limit. If on one side we saw how particular quantities are less sensitive to the finite size corrections, on the other side, the other possibility is to limit ourselves to a particular class of models that are exactly solvable. These models have offered an important set of tools, with exact analytical results in many field of theoretical physics, including, in particular, low dimensional systems in condensed matter and statistical mechanics [91]. They spread from lattice models, based on the Bethe-ansatz approach, to the analytic S-matrix useful for integrable field theories. In spite of their success, their range of applicability seldom had any overlap with disordered systems. In fact, the mechanism involved in the exact solution of integrable models, is typically based on an infinite set of symmetries constraining their dynamics and thus providing a set of equations, whose solution produces eigenstates or correlation functions. For disordered systems, many evident symmetries are trivially broken, such as translational and rotational invariance and the standard approach to integrable systems are therefore

prohibitive. Specific examples have been built [40] but they usually lack of a concrete physical relevance.

In order to find a partial compromise, we focused on the Richardson model, the most famous member of a more general class of integrable models, known as Gaudin magnets [95]. It was first introduced as a model of nuclear matter and has been studied in connection with the finite-size scaling of the BCS theory of superconductivity. The Richardson model [43, 99, 100] is an XX-model (i.e. with no $s^z s^z$ coupling) of pairwise interacting spins with arbitrary longitudinal fields

$$H = -\frac{g}{N} \sum_{\alpha, \beta=1}^N s_{\alpha}^{+} s_{\beta}^{-} + \sum_{\alpha=1}^N h_{\alpha} s_{\alpha}^z, \quad (2.29)$$

where $s^{x,y,z}$ are spin- $\frac{1}{2}$ representation of $SU(2)$ algebra. The fields h_i appears as parameter in the Hamiltonian, that remains integrable for any choice of them, allowing therefore to study the model in presence of quenched disorder in the z fields. The price to pay to accommodate disorder together with integrability is that the hopping term connects all the sites, in other terms, it is a fully connected graph. As we already recall, the analogue of this model in 1-d, where the hopping g -term just connects nearest-neighbor sites on a chain, reduces to non-interacting fermions by Jordan-Wigner map and hence localizes for arbitrarily small disorder. So, if on one hand the fully-connectivity represents an unphysical aspects of this model, on the other hand, it is a crucial ingredient in order to make its dynamics non-trivial. The Hamiltonian (2.29) is exactly solvable: it means that each eigenstate and eigenvalue can be, in principle, obtained by the solution of a set of algebraic equations. We will add more on this point in the following sections.

2.3.2.1 Integrability and localization

We have already pointed out that integrable models represent rare examples in the sea of the possible quantum Hamiltonians. It may appear therefore weird that the Hamiltonian (2.29) is instead integrable for arbitrary value of each parameter involved: the hopping strength g and each local field h_i . It is interesting to investigate more on this issue. One of the main features of integrable Hamiltonians is the existence of local conserved quantities. It means a set of linear independent hermitian operators

Q_1, \dots, Q_n ¹ commuting among themselves and with the Hamiltonian

$$\forall i \quad [Q_i, Q_j] = 0; \quad [Q_i, H] = 0 .$$

For any Hamiltonian, a trivial set of charges is clearly provided by the set of eigenstates

$$P_E = |E\rangle \langle E| . \tag{2.30}$$

However, these operators are in most of the cases extremely complicate when expressed in terms of the local variables (e.g. the spins $s_i^{x,y,z}$ or local creation and annihilation operators for fermions or bosons); in other terms, they are non-local. One would like to say that an exception to this general framework is indeed provided by disordered Hamiltonians in the Anderson localized phase: as we saw, every wave-function will be localized in the real space and also the projectors in (2.30) will be local operators. However, attempts to explicitly write those projectors showed that, even in the localized phase, the expression would require an infinite perturbative series [127]. The Richardson model being both disordered and integrable, somehow, provides a simple example of this. In fact a set of conserved charges can be written as

$$\tau_\alpha = s_\alpha^z - \frac{2g}{N} \sum_{\beta \neq \alpha} \frac{1}{h_\alpha - h_\beta} \vec{s}_\alpha \cdot \vec{s}_\beta \tag{2.31}$$

Here, we see the leading term is $O(1)$ and is given by the local magnetization along the z direction, with a correction due to all the other sites. Therefore since we have that $\tau_\alpha \simeq s_\alpha^z$ are exactly conserved, this model can provide a good toy model for the description of the many-body localized phase.

2.3.2.2 Solution of the model

The model belongs to the class of models that are integrable through Algebraic Bethe Ansatz. It implies that all the states in the sector $S^z = (2M - N)/2$ can be found using

¹There is a lot of confusion in the literature due to the rigorous definition of the conserved charges. This is due to the fact that the naïve application of the correspondence principle to the classical definition of integrable systems, produces a trivial quantum case. In particular, it is not even easy to fix the number of charges needed to call a finite system, integrable. We will not comment more on this point and by purpose we leave the parameter n undefined here. A thorough discussion of these issues can be found in [34].

an ansatz of the form

$$|E[w]\rangle = \prod_{j=1}^M B(w_j) |\downarrow \dots \downarrow\rangle, \quad (2.32)$$

where the generalized raising operators are

$$B(w) = \sum_{\alpha=1}^N \frac{s_{\alpha}^{+}}{w - h_{\alpha}}. \quad (2.33)$$

Requiring that they are eigenstates, one obtains the set of M coupled Richardson equations for the roots w_j :

$$\forall j = 1, \dots, M : \quad \frac{N}{g} + \sum_{\alpha=1}^N \frac{1}{w_j - h_{\alpha}} - \sum_{k=1, k \neq j}^M \frac{2}{w_j - w_k} = 0 \quad (2.34)$$

and the energy of the state is then given by

$$E[w] = \sum_{j=1}^M w_j - \sum_{\alpha=1}^N \frac{h_{\alpha}}{2}. \quad (2.35)$$

We address the reader to reference [73] for an extensive review of the algebraic aspects of the model and its solution. As we said, we will focus on $S_z = 0$ so $M = N/2$, which means that we have to solve $N/2$ coupled nonlinear equations, which is numerically viable only provided one has a reasonably good initial condition for root-finding algorithms. A widely used technique is that of considering that when $g \rightarrow 0$ the roots tend to some of the fields h_{α} , and from (2.33) it is clear that such root configuration correspond to the different choices of sets of M spins which are flipped with respect to the ground state according to (2.32); the choice of the set can be used to label the state at any g .

When one adiabatically increases g , by moving it of some small amount and solving (2.34) at each step, the roots start departing from their initial h 's values towards the negative direction. The ensuing evolution depends on the initial configuration of roots, but generally, two of them may collide and form a pair of complex conjugate solutions, then they may also recombine and return real. When $g \rightarrow \infty$, roots either diverge in the negative direction or stay trapped within a couple of levels. The number

of roots that eventually diverge is equal to the total spin S of the state (which is a conserved quantum number at infinite g). An algorithm which can follow the evolution of the roots with g has to take into account these changes in the nature of the solution, where the roots become complex conjugate. These critical points, for random choices of the h 's can occur at particularly close values of g and this can create troubles for the algorithm. ¹

The reader may refer to [48] and [115] and references therein for further details on the solutions. Extensive study on critical points has been performed in [42].

When more than a pair of roots collide in a too small interval of g this change of variables may not be sufficiently accurate and one should think of something else (if one does not want to reduce the step in the increment of g indefinitely). The most general change of variables which smooths out the evolution across critical points is that which goes from the roots w_j to the coefficients c_i of the characteristic polynomial $p(w)$ –i.e. the polynomial whose all and only roots are the w_j 's

$$p(w) = \prod_{i=1}^M (w - w_i) = w^M + \sum_{i=0}^{M-1} c_i w^i \quad (2.36)$$

This polynomial is quite interesting in itself as it satisfies a second order differential equation whose polynomial solutions have been classified by Heines and Stjelties [121]

$$-h(x)p''(x) + \left(\frac{h(x)}{g} + h'(x) \right) p'(x) - V(x)p(x) = 0$$

where

$$h(x) = \prod_{\alpha=1}^N (x - h_\alpha) \quad (2.37)$$

$$V(x) = \sum_{\alpha=1}^N \frac{h(x)A_\alpha}{x - h_\alpha} \quad (2.38)$$

Similarly to an eigenvalue problem, one has to find a set of A_α 's such that there exists a polynomial solution of this equation. A similar approach has also been investigated

¹This problem is not so serious for the ground state and first excited states so one can go to much higher values of N without losing accuracy.

in the recent work [49].

Following the evolution of the coefficients $c_i(g)$ is a viable alternative to following the roots but we found out that the best strategy is a combination of both evolutions. Therefore we follow the evolution of the roots, extrapolating the coefficients and using them to correct the position of the roots at the next step in the evolution. In this way we do not implement any change of variables explicitly and we do not have to track the position of critical points. This algorithm¹ can be used on a desktop computer to find the roots of typical states with about 50 spins, although in order to collect extensive statistics we have limited ourselves to $N = 40$.

2.3.2.3 A first check of the localized phase

We have already introduced in 2.3.1 a good indicator for the MBL problem: the return probability and the higher momenta of the probability distribution function of the wave-function defined in (2.21) and (2.20). Similarly, when the roots of an eigenstate have been determine, one can compute

$$\text{PR}_q(e) = \sum_a |\langle a|e\rangle|^{2q} \quad (2.39)$$

which is slightly different from (2.20), since the sum here involves the states of $|a\rangle = |\uparrow\uparrow\downarrow\dots\rangle$ of the computational basis. The scalar product can be computed using

$$\langle a|e\rangle = \frac{\det\left(\frac{1}{w_i - h_{\alpha_j}}\right)^2}{\det\left(\frac{1}{w_i - h_{\alpha_j}}\right)} \quad (2.40)$$

where α_j corresponds to the indexes of the $M = N/2$ among N up spins in the state $|a\rangle$. However, when exact diagonalization is used, most of the computational effort goes in the diagonalization of the Hamiltonian matrix, that with the best known algorithms requires $O(\mathcal{N}^3)$ operations for an $\mathcal{N} \times \mathcal{N}$ matrix and $\mathcal{N} = \binom{N}{N/2} \simeq \frac{2^N}{\sqrt{N}}$. In the Richardson case, instead, the determination of a single eigenstate can be done much more efficiently and the computation of the sum in (2.39), involving \mathcal{N} terms,

¹Python code is available on the webpage:
<http://www.sissa.it/statistical/PapersCode/Richardson/>

2. Many-body localization

becomes the hardest part, making for example $N = 40$ completely prohibitive. To overcome this difficulty, we looked for other possible order parameters that exploit the integrable structure of the model, providing a fast way to compute them. Since the average values $\langle E | s_\alpha^z | E \rangle$ has an expression similar to (2.40), they can be calculated efficiently (in $O(N^3)$ time): therefore one is led to consider a *microcanonical* version the Edwards-Anderson (EA) order parameter associated to a single eigenstate

$$q(E) = \frac{4}{N} \sum_{\alpha=1}^N \langle E | s_\alpha^z | E \rangle^2, \quad (2.41)$$

with this normalization $q \in [0, 1]$. The average over eigenstates is

$$q = \frac{1}{2^N} \sum_E q(E). \quad (2.42)$$

To get the physical significance of this quantity, following [96] we start with a slightly magnetized spin α in an infinite temperature state:

$$\rho_0 = (\mathbb{I} + \epsilon s_\alpha^z) / 2^N \quad (2.43)$$

with magnetization $\langle s_\alpha^z \rangle_0 = \text{Tr} \rho_0 s_\alpha^z = \epsilon/4$ (as $s_z^2 = 1/4$). The same magnetization at large time t in the diagonal approximation reads

$$\langle s_\alpha^z \rangle_\infty = \lim_{t \rightarrow \infty} \text{Tr} e^{-iHt} \rho_0 e^{iHt} s_\alpha^z = \frac{\epsilon}{2^N} \sum_E \langle E | s_\alpha^z | E \rangle^2. \quad (2.44)$$

Therefore, averaging over α we obtain the equality with eq. (2.42):

$$q = \frac{1}{N} \sum_\alpha \frac{\langle s_\alpha^z \rangle_\infty}{\langle s_\alpha^z \rangle_0}, \quad (2.45)$$

namely the previously defined EA order parameter is the average survival fraction of the initial magnetization after very long times.

We notice two more things: *one* [125], that $q(E)$ is related to the average purity of

the state (here we use the total $S^z = 0$):

$$q(E) = \frac{2}{N} \sum_{\alpha} \text{Tr} \rho_{\alpha}^2 - 1 \quad (2.46)$$

and *two*, that $q(E)$ is related to the average Hamming distance of the points in configuration space when sampled with the probability distribution p_a relative to state $|E\rangle$:

$$\begin{aligned} d(a, b) &= \sum_{\alpha=1}^N (\langle a | s_{\alpha}^z | a \rangle - \langle b | s_{\alpha}^z | b \rangle)^2 \\ &= \sum_{\alpha=1}^N \frac{1 - 4 \langle a | s_{\alpha}^z | a \rangle \langle b | s_{\alpha}^z | b \rangle}{2}, \end{aligned} \quad (2.47)$$

and multiplying by p_a , p_b and summing over a, b we find:

$$L \equiv \langle d \rangle = \frac{N}{2} (1 - q). \quad (2.48)$$

So q is computationally easy and it captures both some geometric properties of the covering of the configuration space by an eigenstate and the long-time correlation function for s^z . We averaged q over the spectrum (sample over typical states) and then over realizations (the number of which depends on the size of the system but it will never be less than 100).

We found this average $\langle q \rangle$ as a function of g for $g \in [0, 40]$ and $N = 16, \dots, 38$ and studied the point-wise finite-size scaling (in the form $q_N(g) = q(g) + c_1(g)/N + c_3(g)/N^3$) to obtain the thermodynamic limit of q (see Figure 2.9). We fit the data using a ratio of polynomials with the condition that $q(0) = 1$ and we found that averaging over the state and the realization of disorder

$$\langle q \rangle = \frac{1 + 3 \times 10^{-8} g}{1 + 1.003 g + 0.009 g^2} \simeq \frac{1}{1 + g} \quad (2.49)$$

works in the whole range of data to an error of at most 0.5%. We therefore conjecture this to be the correct functional form of the EA order parameter at infinite temperature. Since $q(g) > 0$, no transport occurs in this model for arbitrary value of the hopping term g , as we expected being it integrable. Moreover, it is possible to obtain

a lower limit for $q(g)$ employing the expression of the conserved charges (2.31) and the Mazur's inequalities [34, 77, 120]. The two curves are shown in Fig. 2.9. One can

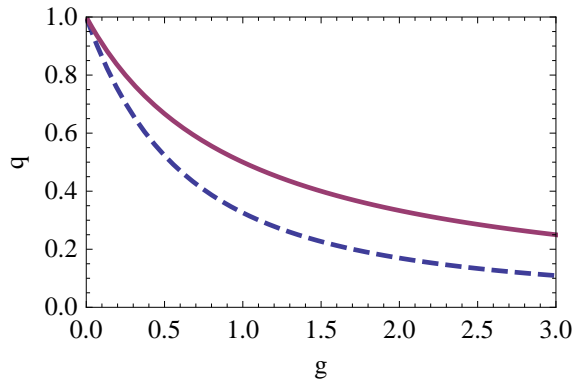


Figure 2.9: The educated guess for $q(g)$ coming from (2.49) for \bar{q} (solid line) and the lower-bound coming from the conserved charges (dashed line): the Mazur inequality is satisfied but not saturated.

wonder whether this parameter q is related to the participation ratio. From perturbation theory for small g one gets

$$\ln \mathcal{J} \simeq \frac{L}{2}. \quad (2.50)$$

where L is defined in (2.48). The relation is linear for small g and for higher value, the relation is plotted numerically in Fig. 2.10, showing that a relation exists.

2.3.2.4 Montecarlo dynamics inside a quantum state

Using the components of each eigenstate on the computational basis, that are easily computed, we devised a Montecarlo algorithm to explore the structure of the eigenstates. Fixed an eigenstate $|E\rangle$, define the probabilities $p_a = |\langle a|E\rangle|^2$ where $a \in \mathcal{C}$ stands for one of the $\binom{N}{N/2}$ allowed classical configurations of spins which constitute the configuration space \mathcal{C} . We perform a random walk with the probabilities p_a 's, namely start from a random configuration a . The neighboring configurations are those living within the same subspace $S^z = 0$ and differing from a by the exchange of a pair of opposite spins. We move to a random one of the $(N/2)^2$ neighboring states, say b , by accepting the move with probability $\min(1, p_b/p_a)$. The random walk proceeds in this way, generating a history of configurations a . The resulting dynamics can be com-

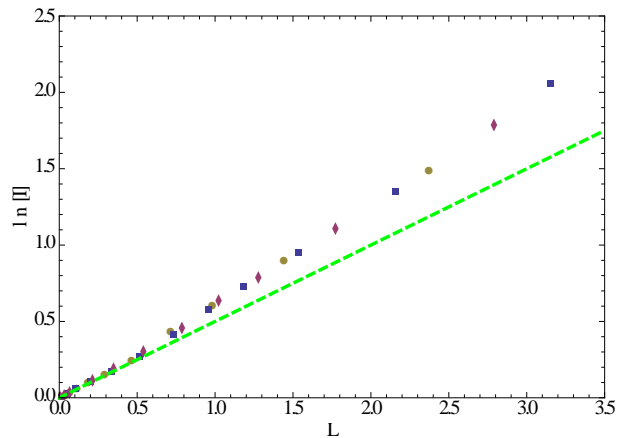


Figure 2.10: $\ln J$ as a function of the average distance L . The points are (square, diamond, circle) $N = 28, 30, 32$ averaged over 100 realizations: the dashed straight line is the second order perturbation theory approximation Eq. (2.50).

pared with that of random percolation on the hypercube, which has been proposed as a model of relaxation in a glassy system [32]. We will find that in both cases, a stretched exponential is the best fit and that the exponent depends on the coupling constant g . This, we believe, is a remarkable similarity.

An important quantity in this sense is the time dependence of the average distance from the starting point. Consider the Hamming distance $H(t)$ from the starting point $H(t) \equiv d(a(t), a(0))$, where $a(0)$ represents a classical configuration of spins and $a(t)$ the one reached after t Montecarlo steps. For $t \gg 1$, after averaging over many starting points $a(0)$, $H(t)$ is fit quite accurately by a stretched exponential ansatz of the form:

$$H(t) = L \left(1 - e^{-\left(\frac{t}{\tau}\right)^\beta} \right), \quad (2.51)$$

where L is the average distance introduced before and β is a new characteristic exponent. Let us consider the behavior of the exponent β with respect to g , as plotted in Fig. 2.11. Even if the results become quite noisy for small g , we can still see that starting from 1 for small values of g , β decreases as g increases, although quite slowly. The small time behavior of $H(t)$ can be used to obtain some information about the local

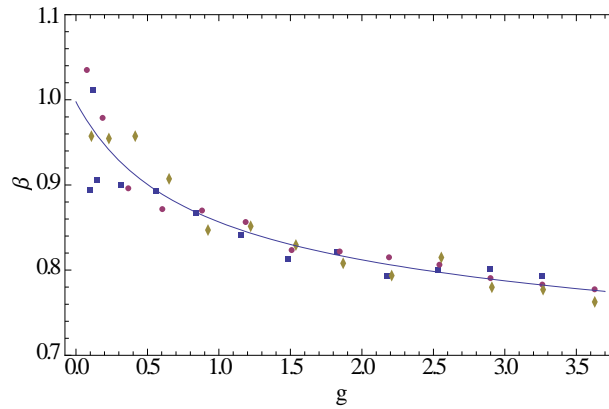


Figure 2.11: The stretched exponential exponent β data as a function of g for $N = 28, 32, 36$ (square, circle, diamond) together with a fit of the form $(1 + a_1g)/(b_0 + b_1g + b_2g^2)$.

structure of the state. In particular we can set

$$k \equiv \frac{H(1)}{2} = \frac{4}{N^2} \sum_{\langle a,b \rangle} \min(p_a, p_b) \quad (2.52)$$

where the last equality follows from the Montecarlo rate and the sum is over nearest-neighbor states. This connectivity fraction k can be considered as a measure of the average fraction of active links. From Fig. 2.12, we may deduce two things: one is that

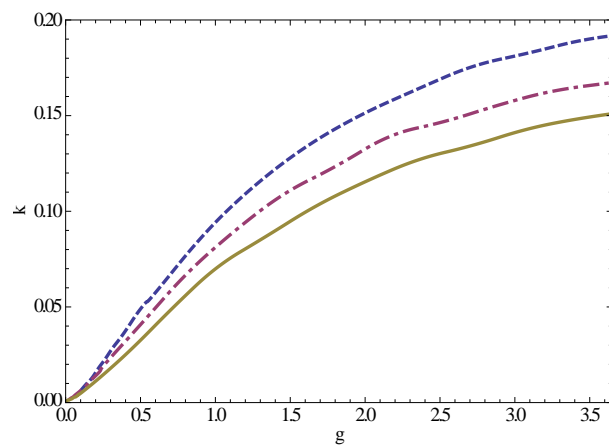


Figure 2.12: Connectivity fraction as a function of g . Different lines corresponds to $N = 18$ (dashed), 24 (dotted and dashed), 30 (solid).

k stays well below 1 even for large g , confirming, as we claimed before, that the typical state is never uniformly spread over the hypercube; the second is that the connectivity scales with N as N^{-1} for small g and with $N^{-1/2}$ for large g (a fit $k = A/N^\alpha$ shows a continuously decreasing α from 1 to $1/2$). This second property seems to be related to the specific details of the Richardson model and in particular of its large g limit. Instead, we conjecture that the first is a typical fingerprint of the localized phase in the MBL transition.

2.4 Conclusions.

In this chapter, we presented the MBL transition. We showed its relevance for both the study of transport in disordered metals and for quantum computation. We reported an argument for the failure of the QAA due to the existence of a many-body localized phase. Then we focused on a specific example, the XXZ spin chain in disordered z -fields; we have investigated the behavior of the return (or survival) probability as a possible detector of the MBL transition. We have shown how this question leads to the necessity of a thorough study of the distribution of the wave-function amplitudes of the eigenstates. We then identified the major changes which occur to said distribution at the MBL transition point. The delocalized, ergodic phase is more “localized” than the corresponding single-particle AL and RMT does not seem to be a good approximation for the eigenstates, not even deep in the delocalized region. The localized region seems very akin to the case of single particle AL on the Bethe lattice with connectivity $O(1)$, in particular the distribution functions of the amplitudes show a small- x accumulation which points towards localized wave function on configuration space. To further investigate this phase, we presented the results coming from the Richardson model, an exactly solvable model for arbitrary value of disordered fields. This gave us indication that the localized phase looks like a spin glass. The similarities and differences with the Bethe-lattice case suggested what are the necessary ingredients for a viable analytical study of MBL.

Chapter 3

Thermalization in closed quantum systems

3.1 Introduction

Largely triggered by recent experiments on cold atoms [55, 58, 64, 109, 130], there has been in the past few years intense theoretical activity aimed at understanding the non-equilibrium dynamics in closed and isolated quantum systems following a change in one of the system parameters. The simplest example is provided by the limit known as *quantum quench*: namely, the system is prepared in an energy eigenstate $|\psi_0\rangle$ of an initial pre-quench Hamiltonian, H_{pre} , and then is allowed to evolve according to a new post-quench Hamiltonian, H_{post} , which differs from H_{pre} by some variation of a parameter. Sure enough, there will be some transient effect, but after that does the system reach a stationary state? Given that such a time evolution is purely unitary, it is clear that for finite dimensional system, quantum recurrence will always occur. However for very large systems, in the thermodynamic limit, we can expect that focusing on finite portions of the system, the remaining (infinite) part of it will act as a thermal bath. It is not difficult to prove, even rigorously, that under these conditions a stationary states will be reached [124]. The question becomes how to characterize it and more specifically if thermalization occurs, i.e. if the system can be described with the standard approach of statistical mechanics in terms of Gibbs ensembles.

Recent progress in understanding thermalization of an extended quantum system

following a quench has involved both analytical and numerical studies. To be more concrete, imagine, as it typically happens, the pair $H_{\text{pre}}, H_{\text{post}}$ is such that the initial state will have an almost definite energy, meaning that it can be written as a linear superposition of $|E\rangle$, eigenstates of H_{post} , all in a shell of energies, $|E - \bar{E}| < \Delta$, centered at \bar{E} :

$$|\psi\rangle = \sum_{|E-\bar{E}|<\Delta} c_E |E\rangle . \quad (3.1)$$

The time average of the density matrix based on this state, given by

$$\rho_{\text{diag}}(\bar{E}) = \overline{|\psi_t\rangle\langle\psi_t|} = \sum_{|E-\bar{E}|<\Delta} |c_E|^2 |E\rangle\langle E| , \quad (3.2)$$

defines the so-called *diagonal ensemble* which is, in general, different from the micro-canonical density matrix defined by

$$\rho_{\text{mc}}(\bar{E}) = \frac{1}{\mathcal{N}_{\bar{E}}} \sum_{|E-\bar{E}|<\Delta} |E\rangle\langle E| . \quad (3.3)$$

where $\mathcal{N}_{\bar{E}}$ is the number of eigenstates inside the shell. Now, ergodicity in its classical sense, means that the time averages coincide with the phase space averages. So, unless it happens that $|c_E|^2 = 1/\mathcal{N}_{\bar{E}}$, a quantum analogous of the classical notion of ergodicity does not hold in most of the cases. In the attempt to define it, Von Neumann [92] (see also [54]) gave rise to a slightly different notion, still known as quantum ergodicity or, to avoid confusions *normal typicality*. The ideas of his work are as follows. Suppose we take a quantum system. Basic quantum mechanics tells us that, due to the possible non-commuting nature of the quantum observables, it is not always possible to fully characterize its state in terms of measurements. However, even though microscopic quantities are affected by quantum effects and the uncertainty principle, there must exist coarse-grained versions, that he dubbed *macroscopic observables*, that are commuting. Then he was able to prove that, under reasonable hypothesis for the Hamiltonian H_{post} , for all possible initial states in a given energy window, for most of the possible choices of the macroscopic observables O_{macro} and for most of the times t ,

thermalization occurs i.e.

$$\langle \psi_t | O_{\text{macro}} | \psi_t \rangle \simeq \text{Tr}(\rho_{mc}(\bar{E}) O_{\text{macro}}) \quad (3.4)$$

At first glance, this result could look as much more than we required, since no time average is involved. However, the requirement for the observable of being macroscopic is catchy and hard to check for a given operator. Therefore, the question whether for a given observable \mathcal{O} , long-time averages of expectation values coincide with the microcanonical average remains open. Defining $\langle \mathcal{O} \rangle_{\text{diag}} = \text{Tr}(\mathcal{O} \rho_{\text{diag}}(\bar{E}))$ and $\langle \mathcal{O} \rangle_{mc} = \text{Tr}(\mathcal{O} \rho_{mc}(\bar{E}))$, it may be true that the identity

$$\overline{\langle \psi_t | \mathcal{O} | \psi_t \rangle} = \langle \mathcal{O} \rangle_{\text{diag}} = \langle \mathcal{O} \rangle_{mc} \quad , \quad (3.5)$$

indeed holds. Eq. (3.4) may appear particularly weird if one takes into account that it holds for every initial state $|\psi_0\rangle$ including, for example, an eigenstate of H_{post} . In this case, no dynamics goes on and the statement can be interpreted as asking that the expectation values $\mathcal{O}_{EE} = \langle E | \mathcal{O} | E \rangle$ of the (macroscopic) observable do not fluctuate between the Hamiltonian eigenstates which are close in energy. This is, in a nutshell, the scenario known in the literature as the *Eigenstate Thermalization Hypothesis* (ETH) which was put forward by Deutsch and Srednicki [41, 116, 117], based on previous work by Berry [18], and which has been recently advocated by Rigol et al. [104] as the mechanism behind the thermalization processes in quantum extended systems. In fact, for such an observable, the identity (3.5) holds for all those initial states which are sufficiently narrow in energy.

Recently this hypothesis has been put under intense scrutiny by different groups. The main emphasis heretofore has been given to the numerical analysis of specific models¹, such as hard-core bosons [101, 104], the Bose-Hubbard model [68], strongly

¹Analytic results for quantum quenches have been obtained only for a restricted class of exactly solvable lattice models, such as the XY chain, the Ising model or the XXZ quantum spin chain [14, 31, 87, 107, 108, 113]. Analytic results have been also obtained for systems nearby the critical point [37] or for continuous exactly solvable systems, especially in the regime of conformal symmetry [30, 35, 60]. However it has been argued that the relaxation phenomena of these models, ruled by an infinite number of conserved quantities, may be different from the thermalization of a generic model and may require the introduction of a generalized Gibbs ensemble, as proposed in [103] (see also [52] for a derivation in integrable field theories). In this chapter, however, we will not deal with such systems, but rather address these issues in a separate publication.

correlated interacting fermions [75], the Hubbard model [44, 45, 67], etc. In this chapter, instead of analyzing a particular system, we take a different approach. We will not try to answer the question whether a specific observable for a given model and quench protocol will look thermal. Instead, we will study what happens *typically* and if thermalization occurs, what is the involved mechanism. *Typically*, here, means that Hamiltonian and observables will be drawn at random from an ensemble of random matrices [78], which in the following will parameterize both the Hamiltonians and the observables¹. In particular we have chosen to study the quantum quenches and the relative thermalization in a class of Hamiltonians given by

$$H(h) = H_0 + hV \quad , \quad (3.6)$$

where the quench parameter h is meant to explicitly break a Z_2 symmetry of the *unperturbed* Hamiltonian H_0 . Such Hamiltonians, which are arguably among the simplest examples of quantum systems, may model spin chains in the presence of an external magnetic field but, as we shall see later, they may also encode the familiar quantum Ising chain in a transverse magnetic field. Given the relative simplicity of this class of Hamiltonians, studying their quench dynamics may be a useful path to extract interesting information on generic properties of non-equilibrium systems, thus disregarding, in doing so, all additional complications coming from a richer structure of states of a specific model.

The natural choice when dealing with (real) random matrix is the *Gaussian orthogonal ensemble* (GOE). However, even upon adopting the abstract language of random matrices, an important issue governing thermalization properties and of which to be mindful is the locality. In fact, as we saw comparing (3.2) and (3.3), in general we do not expect that all the possible observables, meaning with that all the possible hermitian operator, will look thermal. But we have to focus on a subclass of them, that can be considered local, and for which we can expect, as we said, the mechanism works. Nevertheless, it is not easy to generate *local* random operators, even because the notion of locality is intuitive but not always rigorous. We decided therefore to focus on the structure of the hypercube corresponding to the Hilbert space: as we saw for (2.16) and (2.29), the connectivity scales as a power of the real-space volume $N^k \ll \mathcal{N}$, the

¹For simplicity we consider hereafter real symmetric matrices.

Hilbert space size, i.e. the number of points in the graph. This will result, when written in the computational basis, in a sparse matrix ensemble (SME), i.e. matrices with a small proportion of non-zero entries. The two kinds of matrices, GOE and SME, have two different properties, going from the densities of states to the localization of the wave-functions. For these reasons one observes a different behavior under a quench of the parameter h .

Important features of quantum quench processes in local systems were discussed in a paper by Biroli et al. [23], in particular the role played by rare fluctuations in the thermalization of local observables. These authors considered the existence of certain rare eigenstates – rare compared to the typical ones sampled by the micro-canonical distribution – but which may be responsible, if properly weighted, for the absence of thermalization observed in certain systems. As discussed in more detail later, the presence of such states can be detected by studying the spread of the expectation values of the observables on the energy eigenstates, in particular by the finite size dependence of the distribution of expectation values. The numerical analysis that we have performed seems indeed to indicate the existence of these rare states in the case of sparse random matrices, while they are absent in the case of dense random matrices. However, in our numerics, thermalization is observed nonetheless in SME, simply because our averaging procedure on the different sampling of observables and Hamiltonians does not place a natural exponentially large weight upon the rare states, thus enabling them to break thermalization.

It should be underlined that the existence of rare states in the thermodynamic limit has been debated in the literature and in particular in a series of papers by Santos and Rigol [102, 110, 111]. They have argued that in a portion of the phase diagram of an extended t-J model with next-nearest-neighbor interactions, rare states are absent. We will come back to this conclusion in our presentation of results.

3.2 Locality

In this section we discuss the nature of Hamiltonian matrices associated with *local* models. In order to consider finite-size matrices, we will focus on lattice models, keeping in mind that continuous ones can always be discretized adding proper cut-offs. The main idea of this section is the following: in most of the basis of the Hilbert

3. Quantum quenches

space, the matrix representation of a local Hamiltonian corresponds to a *dense* matrix, i.e. a matrix which has all entries different from zero (an explicit example will be given below). However, if the theory is local, there will exist a basis (in the following called the *local basis*), in which the Hamiltonian will be represented by a *sparse* matrix, i.e. a matrix where the great majority of its entries are zero. We have already seen that the computational basis does the job in the previous chapters. An other example is the 1d quantum Ising model in a longitudinal field (generically a non-integrable model). In this case the quantum Hamiltonian for N sites is given in terms of Pauli matrices and takes the form:

$$H \equiv \sum_{i=1}^N \sigma_i^z \sigma_{i+1}^z + h \sigma_i^x + \sigma_i^z = \sum_{i=1}^N H_i. \quad (3.7)$$

The last equality makes evident the local nature of this model: the Hamiltonian has been written as a sum of operators involving only two lattice sites. So an operator is local if it can be written as a sum over the volume of operators involving only few body terms. In the computational basis, given as usual by the common eigenstates of the σ_α^z operators, the matrix elements are

$$H_i^{a,b} = \langle a_1 \dots a_N | H_i | b_1 \dots b_N \rangle = ((a_i a_{i+1} + a_i) \delta_{a_i, b_i} + h \delta_{a_i, -b_i}) \prod_{k \neq i} \delta_{a_k, b'_k}, \quad (3.8)$$

where a, b are labels for the computational basis and each $a_i, b_i \in \{\uparrow, \downarrow\}$ corresponds to the two possible eigenstates of σ_i^z . From this expression it is easy to deduce that on each row of the matrix there are $N + 1$ non-zero entries and therefore the total number of non-zero elements of the $\mathcal{N} \times \mathcal{N}$ matrix H is $n_{nz} = (N + 1)\mathcal{N}$, where $\mathcal{N} = 2^N$ is the Hilbert space size. Since the total number of matrix elements is \mathcal{N}^2 , the density of non-zero elements is given by

$$\rho = \frac{n_{nz}}{\mathcal{N}^2} \propto \frac{\ln \mathcal{N}}{\mathcal{N}}, \quad (3.9)$$

In general the density of zeros will look like

$$\rho_0 = 1 - \rho \simeq 1 - \frac{k(\ln \mathcal{N})^\epsilon}{\mathcal{N}}. \quad (3.10)$$

The constant k and ϵ are related to specific properties of the model, such as dimensionality and conserved quantities. The Richardson Hamiltonian in (2.29), being fully-connected, can not be written as sum over the volume of density operators. Nevertheless, Eq. (3.10) holds with $\epsilon = 2$. Therefore for large values of \mathcal{N} , the Hamiltonian matrix H_N is a *sparse* matrix, i.e. a matrix with a large number of zeros and few non-zero entries. This statement holds in general for any quantum Hamiltonian involving few body terms and can be shown to be true also for the discretization of quantum field theories.

3.3 Quantum quenches, thermalization, and the ETH

Let us consider an initial state $|\psi_0\rangle$ which is an eigenstate of an initial Hamiltonian, $H(h^<)$, governed by the parameter $h^<$. At $t = 0$ we abruptly change the value of the parameter to $h^>$. The evolution of the initial state will be then governed by the dynamics given by $H(h^>)$. Our interest is in the long time behavior of expectation values of some one-point observable, $\langle\psi_0(t)|\mathcal{O}|\psi_0(t)\rangle$. An observable has a thermal behavior if its long time expectation values coincides with the micro-canonical prediction, i.e.

$$\langle\psi_0(t)|\mathcal{O}|\psi_0(t)\rangle \xrightarrow{t \rightarrow \infty} \text{Tr}\mathcal{O}\rho_{\text{mc}} = \langle\mathcal{O}\rangle_{\text{mc}} . \quad (3.11)$$

Dealing with finite-size matrices, it is natural to take a notion of convergence, similar to classical ergodicity, where time-averages are meant

$$\overline{\langle\psi_0(t)|\mathcal{O}|\psi_0(t)\rangle} \equiv \frac{1}{T} \int_0^T \langle\psi_0(t)|\mathcal{O}|\psi_0(t)\rangle = \sum_E |c_E|^2 \mathcal{O} = \langle\mathcal{O}\rangle_{\text{mc}} , \quad (3.12)$$

where $c_E = \langle\psi_0|E\rangle$ are the overlap of the initial state on the eigenstate $|E\rangle$ of $H(h^>)$, and $\mathcal{O}_{EE} = \langle E|\mathcal{O}|E\rangle$ are the expectation values of the observable, \mathcal{O} , on the post-quench eigenstates. Eq. (3.12) defines the diagonal ensemble prediction, with the corresponding density matrix defined as

$$\rho_{\text{diag}} = \overline{|\psi_0(t)\rangle\langle\psi_0(t)|} = \sum_E |c_E|^2 |E\rangle\langle E| , \quad (3.13)$$

supposing the eigenstates of $H(h^>)$ are non-degenerate.

3. Quantum quenches

A possible mechanism for the thermal behavior of physical observables is based on the so called *Eigenstate Thermalization Hypothesis* (ETH) [41, 116, 117]. It states that the expectation value of a physical observable, $\mathcal{O}_{EE} = \langle E | \mathcal{O} | E \rangle$, on an eigenstate, $|E\rangle$, of the Hamiltonian is a smooth function of its energy, E , with its value essentially constant on each micro-canonical energy shell. In such a scenario, thermalization in the asymptotic limit follows for every initial condition sufficiently narrow in energy. ETH implies that thermalization can occur in a closed quantum system, different from the classical case where thermalization occurs through the interactions with a bath. As pointed out by Biroli et al. [23] there are two possible interpretation of ETH: a weak one, which can be shown to be verified even for integrable models, which states that the fraction of non-thermal states vanishes in the thermodynamic limit, and a strong one which states that non-thermal states completely disappear in the thermodynamic limit. In the weak version of the ETH, not every initial condition will thermalize.

We briefly remind the reader of the origin of these two interpretations as it will be salient later. Firstly, for thermalization to occur one needs a distribution of the overlaps peaked around the energy $E = \langle \psi_0 | H | \psi_0 \rangle$. As shown in Ref. [104], the energy density e has vanishing fluctuations in the thermodynamic limit

$$\Delta e = \frac{\sqrt{\langle E^2 \rangle_{\text{diag}} - \langle E \rangle_{\text{diag}}^2}}{N} \propto \frac{1}{N^{1-\sigma/2}} \rightarrow 0 \text{ for } N \rightarrow \infty \quad (3.14)$$

where N is the system size and σ is the dimension of the space over which the coupling h is adjusted in the quench. In our case $\sigma = 1$ for SME. We will, however, see that σ is effectively larger when we consider quenches in dense matrices, and consequently Δe does not vanish in the thermodynamic limit. Correspondingly this property means that the distribution of intensive eigenenergies (eigenenergies scaled by $1/N$) with weights $|c_E|^2$ is peaked for large system sizes. If the ETH is true, an immediate consequence of property Eq. (3.14) would be that averages in the diagonal ensemble coincide with averages in the micro-canonical ensemble. However, for a finite system, there will always be finite fluctuations of \mathcal{O}_{EE} . To characterize the ETH mechanism we need then to have some control on the evolution of the distribution of \mathcal{O}_{EE} in approaching the thermodynamic limit. As shown in [23] the width of the distribution \mathcal{O}_{EE} of an

intensive local observable¹ vanishes in the thermodynamic limit

$$(\Delta\mathcal{O}_e)^2 = \frac{\sum_e \mathcal{O}_{EE}^2}{\mathcal{N}_e} - \left(\frac{\sum_e \mathcal{O}_{EE}}{\mathcal{N}_e} \right)^2 \rightarrow 0 \text{ for } N \rightarrow \infty \quad (3.15)$$

where e is the intensive energy defining a micro-canonical shell including $|E\rangle$ such that $E/N \in [e - \epsilon, e + \epsilon]$ and \mathcal{N}_e is the number of states in the microcanonical shell. Eq. (3.15) implies that the fraction of states characterized by a value of \mathcal{O}_{EE} different from the micro-canonical average vanishes in the thermodynamic limit. Nevertheless, states with different values of \mathcal{O}_{EE} may exist. These states live in the tails of the shrinking \mathcal{O}_{EE} distribution and are expected to be small in number. This is why they are called "rare". These states, however, under proper conditions, can be relevant to the issue of thermalization. Indeed, if in the $|c_E|^2$ distribution they are weighted heavily, the diagonal ensemble average will be different from the micro-canonical and the system keeps a memory of the initial state. As emphasized in [23], it is clear that the weak interpretation of ETH does not imply thermalization in the thermodynamic limit for every initial condition, while, with the proviso that Eq. (3.14) holds, the strong interpretation does.

3.4 \mathbb{Z}_2 symmetry breaking quench protocol

The class of Hamiltonians we choose to study can be thought as akin to the quantum Ising model in the presence of an additional longitudinal field. The quench protocol involves, for the sake of specificity, taking h to $-h$. This quench reflects that the Ising Hamiltonian is not invariant under the Z_2 operator, $\mathcal{P} = e^{i\pi(N/2+S_z)}$:

$$\mathcal{P}H(h)\mathcal{P}^\dagger = H(-h).$$

In order to mimic this in the context of random matrices, we suppose we have divided the canonical basis of Ising states into two groupings, even and odd under \mathcal{P} , and to then have sorted them by ordering all even states before any odd states. In Ising, the transverse field term couples states with different parity, such that the dependence of

¹ \mathcal{O} is an intensive local observables if it can be written as $\frac{1}{N} \sum_\alpha \mathcal{O}_\alpha$ where \mathcal{O}_α are finite ranged observables and the sum is over a local spatial region.

the Hamiltonian on the external field is seen in the off-diagonal blocks, i.e.

$$H(h) = \begin{pmatrix} A & hB \\ hB^T & C \end{pmatrix} . \quad (3.16)$$

It is this form then that we take for our random matrices.

Observables of the systems associated to the Hamiltonian (3.16) can be split into even and odd \mathbb{Z}_2 classes. This classification is again motivated by the case of the Ising-spin chain in a transverse magnetic field, where the natural observables σ_z and σ_x are respectively odd and even w.r.t. to the action of \mathcal{P} . The even observables have non-zero elements in the diagonal blocks alone, while the odd observables are non-zero only in the off-diagonal blocks:

$$E = \frac{1}{N} \begin{pmatrix} A & 0 \\ 0 & C \end{pmatrix}, \quad O = \frac{1}{N} \begin{pmatrix} 0 & B \\ B^T & 0 \end{pmatrix}, \quad (3.17)$$

where the volume factor N has been added to make these quantities intensive. Since we expect the Hilbert space to be exponentially large in the volume of the system we fix the system size corresponding to an $\mathcal{N} \times \mathcal{N}$ random matrix via

$$N = \ln \mathcal{N} .$$

After defining the Hamiltonian as above, we will analyze the quench dynamics under the quench $h \rightarrow -h$. We will study the long-time behavior of both odd and even observables. In our numerical analysis, we have examined different values of the initial and final value of the parameter h , and found that in the limits $h \ll 1$ and $h \gg 1$, the quench dynamics are essentially trivial because the initial and final Hamiltonian share the same eigenvectors. For this reason, we will discuss only the intermediate case

$$h^{\text{pre-quench}} = -1 \quad \rightarrow \quad h^{\text{post-quench}} = 1 . \quad (3.18)$$

Given these constraints we will still however consider two cases:

- In one case we will look at ensembles of sparse random matrices (SME), motivated by the previous considerations about the relationship between locality and sparseness. It should be stressed however that while a local observable will nec-

essarily be sparse the converse is not necessarily true. Nevertheless, the study of SME may provide some reliable insights into some of the questions of the thermalization in local Hamiltonians.

- In the second case we will look at matrices which are dense and follow the GOE.

In both cases the (non-zero) entries of the random matrices will be generated according to the normal distribution. We first consider quenches involving dense matrices.

3.5 Thermalization in Dense Random Matrices Ensemble

To define the Hamiltonian in the dense case, we generate three $\mathcal{N}/2 \times \mathcal{N}/2$ matrices A, B, C and then assemble them according to Eq. (3.16). The matrices A, C are symmetric and chosen according to the measure, $\mu(M)$, of a properly normalized GOE ensemble:

$$\mu(M) \equiv \exp\left(-\frac{\mathcal{N}\text{Tr}M^2}{4N^2}\right) ,$$

while the matrix B has all of its entries distributed according to a normal distribution with 0 mean and variance equal to $\frac{2N^2}{\mathcal{N}}$. For $h = \pm 1$ the Hamiltonian itself will also be distributed according to the GOE ensemble and therefore the eigenvalues obey the semicircle law:

$$\rho(E) = \frac{1}{2\pi N} \sqrt{4N^2 - E^2} . \quad (3.19)$$

The spectrum thus falls in the range $[-2N, 2N]$ and is therefore extensive as required. The observables are obtained with an analogous procedure, generating new matrices A, B, C and then using the expressions Eq. (3.17). The numerical results reported below are calculated according to the following procedure: five instances of the Hamiltonian are generated according to the prescriptions above and for each instance of the Hamiltonian forty instances of the observable are generated. The relevant quantities are calculated for each instance of the observables, then the results are averaged.

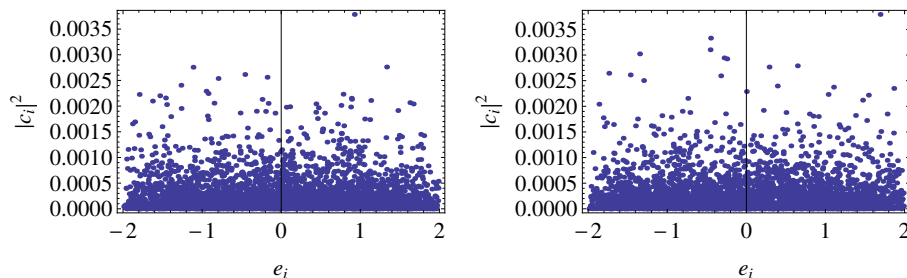


Figure 3.1: Dense random matrices (with $\mathcal{N} = 4000$). Overlaps for the quench process. Left: $|c_E|^2$ for the 'ground' state. Right: $|c_E|^2$ for the 2000th state, in the middle of the energy band.

3.5.1 Numerical results

One of the prerequisites for the ETH to operate is that given the initial state $|\psi_0\rangle$ with energy

$$\bar{e} \equiv \frac{1}{N} \langle \psi_0 | H_{\text{post}} | \psi_0 \rangle ,$$

the structure of its overlaps $|c_E|^2 = |\langle \psi_0 | E \rangle|^2$ with the post-quench eigenstates, as a function of the intensive energy $e = E/N$, is peaked around \bar{e} .

We find this to be not the case for dense matrices, as can be explicitly seen by the two sample states in Fig. 3.1 drawn from the bottom and middle of the spectrum. Moreover, calculating the standard deviation of the energy on the initial state, we find that it is always large (around 1/4 of the range of the total spectrum) for all initial states, showing that the relation Eq. (3.14) does not hold, i.e. the effective dimension σ satisfies $\sigma > 2$. The broad distribution of overlaps is confirmed by the analysis of the already introduced Participation Ratio (PR_2), defined as

$$\text{PR}_2 = \frac{1}{\sum_E c_E^4} . \quad (3.20)$$

We show in Fig. 3.2 the PR_2 for the eigenstates of a single realization of a dense matrix. The PR_2 in this case is sharply distributed around $\mathcal{N}/3$. This finding can be understood through a simple model of random vectors on a \mathcal{N} -sphere of unit radius (Porter-Thomas distribution). By a simple integration one finds [56]

$$\langle c_E^4 \rangle = 3/\mathcal{N}^2 , \quad (3.21)$$

and therefore the PR_2 scales as

$$\frac{1}{\sum_E c_E^4} \simeq \mathcal{N}/3 . \quad (3.22)$$

This scaling is confirmed by our data, as shown in Fig. 3.3. Moreover, the fact that the mean PR_2 and the maximum PR_2 almost coincide is confirmation that all initial states are equivalent. This means that the pre-quench and the post-quench bases of the energy eigenvectors are completely random with respect one another. Eigenstates therefore have no reason to be localized in energy.

Let us now turn our attention to the expectation values of observables since the main content of the ETH concerns the distribution of the eigenstate expectation values (EEVs), \mathcal{O}_{EE} , and their behavior when the system size is increased. We first report two sample EEV distributions, given in Fig. 3.4, which show no energy dependence. We can argue (and we have checked numerically) that the distribution of an intensive observable over the whole energy spectrum shrinks to zero for increasing system size. Moreover, it is not only the variance but even the support of the distribution of the observables that goes to zero inasmuch as the difference of the EEV maximum and minimum is going to zero as $\mathcal{N} \rightarrow \infty$ (see Fig. 3.26).

More precisely, we have:

$$\mathcal{O}_{EE} \equiv \langle E | \mathcal{O} | E \rangle = \sum_{\theta} A_{E,\theta} \mathcal{O}_{\theta} , \quad (3.23)$$

where θ indexes the eigenstates, $|\theta\rangle$, of the observable \mathcal{O} , while \mathcal{O}_{θ} is the corresponding eigenvalue, and $A_{E,\theta} = |\langle E | \theta \rangle|^2$. To estimate the r.h.s. we argue for an equivalence

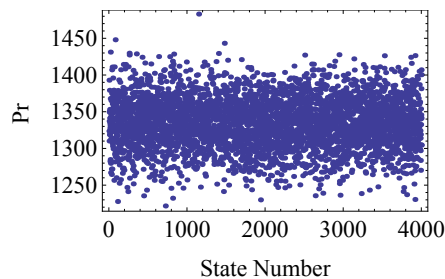


Figure 3.2: Dense random matrices (with $\mathcal{N} = 4000$). Typical PR_2 of the initial states.

3. Quantum quenches

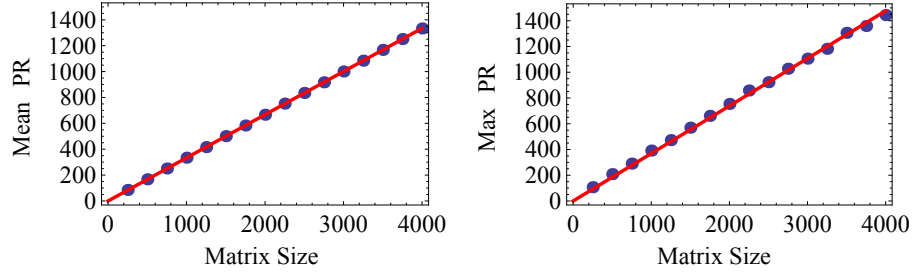


Figure 3.3: Dense random matrices. PR_2 vs. matrix size. The red lines are linear fits $y = ax$. Left panel: average PR_2 on all initial states ($a = 0.3336$). Right panel: maximum PR_2 ($a = 0.3764$).

of observables and hold that the PR_2 of an eigenvector $|E\rangle$ of the post-quench Hamiltonian relative to the basis of eigenvectors $|\theta\rangle$ equals the PR_2 of the initial state $|\psi_0\rangle$ in the basis $|E\rangle$. So we can suppose that \mathcal{O}_{EE} can be expanded in terms of a set of $\frac{N}{3}$ states, each of which is given by

$$A_{E,\theta} \simeq \frac{1}{\text{PR}_2(H \rightarrow \mathcal{O})} \simeq \frac{3}{N}. \quad (3.24)$$

Then, if we assume $A_{E,\theta}$ and $A_{E,\theta'}$ are independent and note that \mathcal{O}_{EE} has zero mean, we obtain

$$|\overline{\mathcal{O}_{EE}}|^2 \simeq \frac{N}{3} \left(\frac{3\sigma_{obs}}{N} \right)^2 \simeq \frac{3\sigma_0^2}{N},$$

where σ_0^2 is the variance of the spectrum of the observable \mathcal{O} . In Fig. 3.5, the numerical results are plotted together with a power-law fit and, as expected, the exponent is indeed close to one.

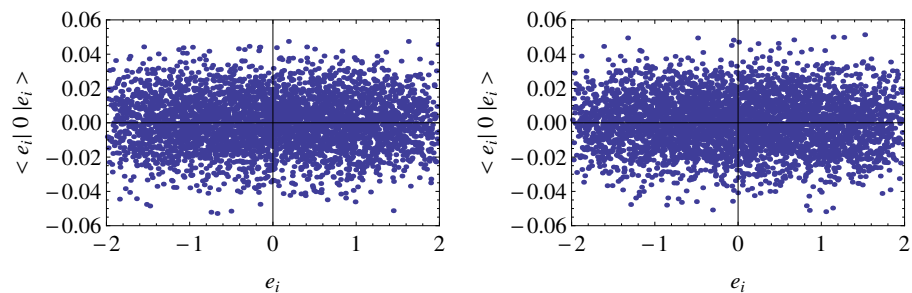


Figure 3.4: Dense random matrices. EEV $\langle E | \mathcal{O} | E \rangle$ vs E . Left: even observable. Right: odd observable.

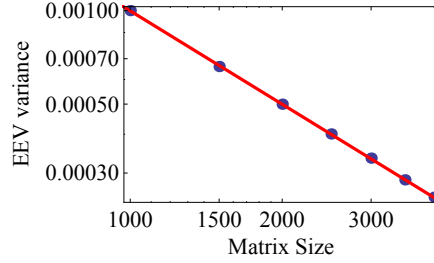


Figure 3.5: Dense random matrices. EEV variance (averaged over the entire spectrum) vs. matrix size. The continuous line is the fit a/x^b with $b = 0.(9)$. The data points for the even and odd observables exactly overlap in this plot.

Now let us consider the full support of the distribution of the EEVs where we define $\delta_{\mathcal{O}}$ as the difference of the maximum and the minimum of the EEVs among all the energy eigenstates $|E\rangle$. Since the distribution is symmetric about zero, we have:

$$\delta_{\mathcal{O}} = 2 \max_E \{\mathcal{O}_{EE}\}. \quad (3.25)$$

To estimate the scaling of this quantity, we again approximate all the overlaps $A_{E,\theta}$ as in Eq. (3.24). Therefore we are led to estimate the maximum of the quantity

$$\mathcal{O}_{EE} \equiv \frac{3}{N} \sum'_{\theta} \mathcal{O}_{\theta},$$

where the prime on the sum indicates that only $1/3$ of the total θ 's are being summed

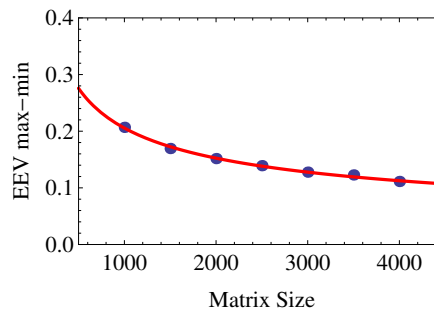


Figure 3.6: Dense random matrices. Max-min EEV vs. matrix size for the range of even observables. The continuous line is the fit $a\sqrt{\frac{\ln N}{N}}$.

3. Quantum quenches

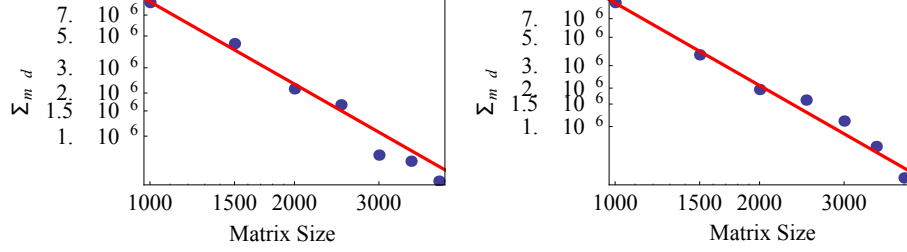


Figure 3.7: Dense random matrices. $\sigma = \sqrt{(\mathcal{O}_{\text{micro}} - \mathcal{O}_{\text{diag}})^2}$ vs. matrix size for initial states laying in the central part of the spectrum $\bar{\epsilon} \approx 0$. The continuous line is the fit a/x^b . Left: even observable $b = 1$.(9); right: odd observable $b = 2$.(1)

over. As before we suppose that the random variables \mathcal{O}_θ are independently distributed according to the intensive semicircle law ($\mathcal{O}_\theta \in [-2, 2]$):

$$\rho(x) \equiv \text{Prob}(\mathcal{O}_\theta = x) = \frac{1}{2\pi} \sqrt{4 - x^2} . \quad (3.26)$$

In this case, from the central limit theorem it follows

$$\text{Prob}(\mathcal{O}_{EE} > x) = \frac{1}{2} \text{Erfc} \left(\sqrt{\frac{\mathcal{N}}{6}} x \right) \simeq e^{-\frac{\mathcal{N}x^2}{6}} , \quad (3.27)$$

Now the probability that $\delta_\mathcal{O}$ is less than a value M is given by

$$\text{Prob}(\delta_\mathcal{O} < M) = \prod_{E=1}^{\mathcal{N}} \text{Prob}(\mathcal{O}_{EE} < M) \simeq \left(1 - e^{-\frac{\mathcal{N}M^2}{6}} \right)^{\mathcal{N}} \simeq 1 - \mathcal{N}e^{-\frac{\mathcal{N}M^2}{6}} .$$

We can find the scaling of the typical value of the maximum by requiring that the probability is large enough

$$\text{Prob}(\delta_\mathcal{O} < M) \simeq \text{const.} \quad \Rightarrow \quad \delta_\mathcal{O} \simeq \sqrt{\frac{\ln \mathcal{N}}{\mathcal{N}}} . \quad (3.28)$$

In Fig. 3.6, one sees the numerical agreement with our heuristic argument.

Finally let's consider the behavior of the difference between the diagonal and the microcanonical ensembles with increasing matrix size. To this end, we analyzed the difference $\sigma = \sqrt{(\mathcal{O}_{\text{micro}} - \mathcal{O}_{\text{diag}})^2}$ of the two ensembles for each initial state $|\psi_0\rangle$. Due to the broad energy distribution of the overlap of the initial states, their intensive

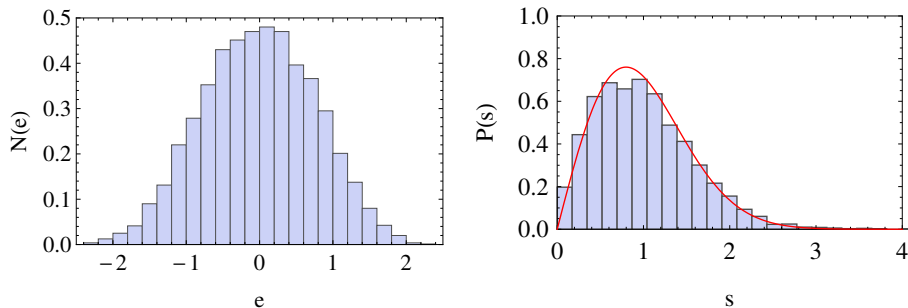


Figure 3.8: Sparse random matrices (with $\mathcal{N}=4000$). Left: density of states, right: level spacing statistics, the continuous line is the Wigner surmise for GOE matrices.

energy $\bar{e} = \langle \psi_0 | H(-h) | \psi_0 \rangle$ lies in a region, $[-0.5, 0.5]$, smaller than the range of the post-quench energies $-2 < e_E < 2$. σ show the same behavior independent of the particular initial state $|\psi_0\rangle$ being considered, as can be argued by the constant PR_2 combined with a structure-less EEV distribution. As all initial states are equivalent, we focus our attention on those initial states belonging to a small energy window around $e = 0$: the result is shown in Fig. 3.7. As can be seen, the difference between micro-canonical and diagonal ensemble rapidly goes to zero as a function of \mathcal{N} .

In conclusion, quenches in dense random matrices are characterized by initial states with large PRs, EEV distributions of the post-quench eigenbasis with no energy dependence and whose variance goes to zero exponentially with increasing system size. In this sense, their thermalization is trivial, as the spread of the micro-diagonal ensemble is governed by a distribution whose support is increasingly localized near zero as system size grows.

3.6 Thermalization in Sparse Random Matrices

We now turn to the more interesting case of thermalization in SME. As we have indicated such matrices describe the Hamiltonians of systems with local interactions. In order to define the ensemble of these matrices, we employed a symmetric mask matrix, \mathcal{M} . This matrix has 1's on the diagonal and in each of its rows we allow it to have on average $\ln \mathcal{N}$ off-diagonal entries equal to 1. All remaining entries of the mask matrix are equal to zero. The upper triangular part of the (symmetric) Hamiltonian is then

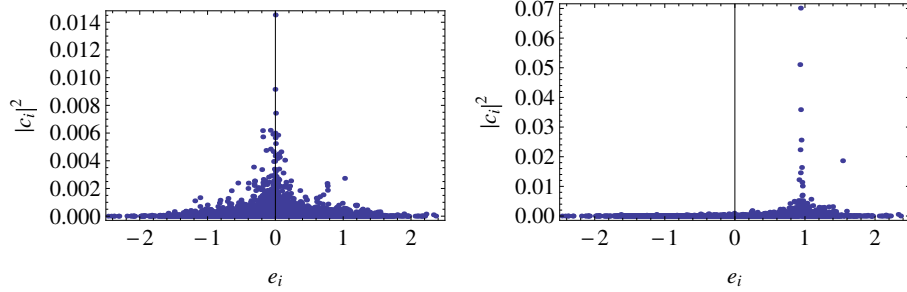


Figure 3.9: Sparse random matrices. Behavior of the overlaps $|c_E|^2$ for a state mid-spectrum (left) and for one in the upper portion of the spectrum (right).

obtained as:

$$H(h)_{i<j} = \begin{cases} d_i \text{ with } d_i \text{ drawn from } \mathcal{N}(0, \ln \mathcal{N}) & \text{if } i = j; \\ o_{ij} \times \mathcal{M}_{ij} \text{ with } o_{ij} \text{ drawn from } \mathcal{N}(0, 1) & \text{if } i < j, \end{cases} \quad (3.29)$$

where $\mathcal{N}(\mu, \sigma^2)$ is a normal distribution with μ mean and σ^2 variance. Then the coefficients in the off-diagonal blocks are multiplied times h to reproduce the structure in Eq. (3.16). The different choice for the variances of the diagonal d_i and off-diagonal elements o_{ij} is motivated by the requirement that the spectrum be extensive. In fact we can compute the variance of the spectrum:

$$\sigma_H^2 \equiv \frac{\text{Tr} H^2}{\mathcal{N}} \simeq 2 \ln \mathcal{N}. \quad (3.30)$$

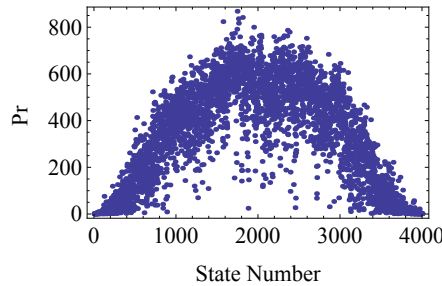


Figure 3.10: Sparse random matrices (with $\mathcal{N} = 4000$). The PR_2 for a specific realization. The ordering of the initial states in this plot is according to their energy relative to the post-quench Hamiltonian, $\langle \psi_0 | H | \psi_0 \rangle$.

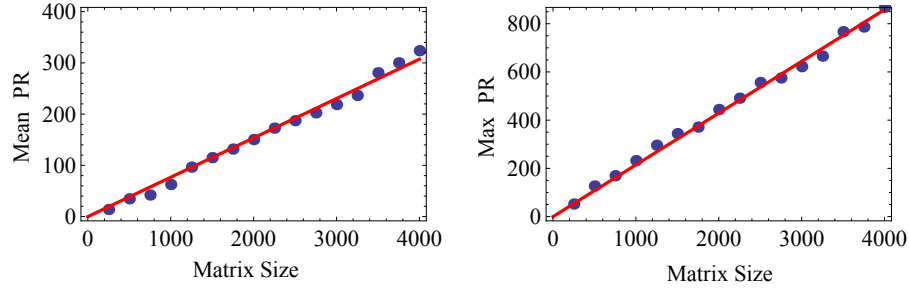


Figure 3.11: Sparse random matrices. PR_2 vs. matrix size. The continuous line is the $y = ax$ fit. Left, average PR_2 on the whole spectrum ($a = 0.0738$). Right, maximum PR_2 ($a = 0.2096$).

In the approximation in which the eigenvalues E are considered independent and normally distributed, one can relate the minimum of the spectrum with the variance, obtaining for the ground-state energy the estimate

$$E_{\text{gs}} = \min_E \{E\} \simeq -\sigma_H \sqrt{2 \ln \mathcal{N}} \simeq -2 \ln \mathcal{N}.$$

The eigenvalues mid-spectrum will be at most a few standard deviations σ_H from the average 0. Thus a typical eigenstate will be such that

$$E^{(0)} - E_{\text{gs}}^{(0)} \propto \ln \mathcal{N}. \quad (3.31)$$

We see then that our choices satisfy the requirement that energy is an extensive quantity.

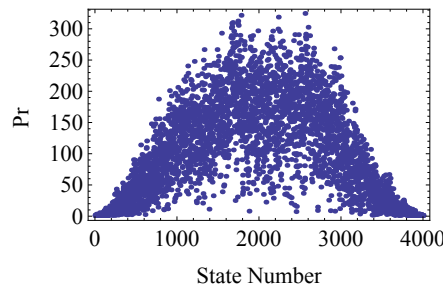


Figure 3.12: Sparse random matrices (with $\mathcal{N} = 4000$). The PR_2 of the post-quench eigenstates w.r.t. the local basis for a specific realization. The ordering of the initial states in this plot is according to their energy eigenvalue.

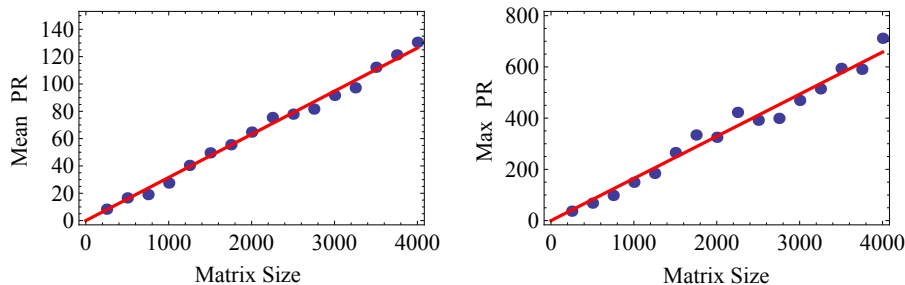


Figure 3.13: Sparse random matrices. PR_2 w.r.t. local basis vs. matrix size. The continuous line is the $y = ax$ fit. Left, average PR_2 on the whole spectrum ($a = 0.0321$). Right, maximum PR_2 ($a = 0.1632$).

We compare these estimates with numerics in Fig. 3.8 where we plot the density of states and the level spacing distribution for one realization of a sparse matrix. The density of states is no longer a semicircle, looking rather more like a bell-shaped distribution. Moreover, notice that, unlike the GOE case where the intensive quantities have a finite distribution in the large \mathcal{N} limit, i.e. Eq. (3.26), in this sparse case the (intensive) standard deviation behaves as $\frac{1}{\sqrt{\ln \mathcal{N}}}$, while the support of the spectrum remains approximately $[-2, 2]$. We also see from the right side of Fig. 3.8 that the level-spacing distribution obeys the Wigner form for a non-integrable model.

To generate the observables we follow a similar procedure, i.e. we employ the same mask \mathcal{M} . The idea behind this choice is that the matrix \mathcal{M} is responsible for the local structure in the Hilbert space and so we keep it for all the physical observables (including the Hamiltonian itself). So we have for the upper triangular part of a symmetric observable

$$\mathcal{O}_{i < j} = \begin{cases} d_i \text{ with } d_i \text{ drawn from } \mathcal{N}(0, 1/\ln \mathcal{N}) & i = j; \\ o_{ij} \times M_{ij} \text{ with } o_{ij} \text{ drawn from } \mathcal{N}(0, 1/(\ln \mathcal{N})^2) & i \neq j. \end{cases}$$

The even and odd parts are then obtained as before by splitting \mathcal{O} into diagonal and off-diagonal blocks.

3.6.1 Numerical results

Unlike the dense case, in sparse random matrices the overlap distributions are peaked around the initial state post-quench intensive energy \bar{e} , as can be seen in two examples

shown in Fig. 3.9.

The PR_2 is no longer constant (as it was for the random dense matrices), but shows behavior dependent on the energy of the initial state, as demonstrated in Fig. 3.10. However there is still scaling of the PR_2 with the matrix size, as can be seen by studying the behavior of the maximum PR_2 vs the matrix size, plotted in Fig. 3.11. In this case the mean and the maximum PR_2 are rather different, due to the presence of states with very small PR_2 .

We see a similar phenomena when we study the PR_2 of the pre-quench and post-quench (they are statistically equivalent) eigenbasis relative to the local basis (that is, the basis of states in which the Hamiltonian matrices, $H(h^<)$ and $H(h^>)$ are expressed). We see in Fig.3.13 that the mean and max PR_2 's here as a function of matrix size, \mathcal{N} , are similar to those in Fig. 3.11.

The equivalence of these two different PRs is not surprising. If we pick an eigenstate of the pre-quench Hamiltonian, $|\psi_0\rangle$, that has a small PR_2 relative to the local basis, it will necessarily be only weakly coupled to the off-diagonal blocks, particularly as the Hamiltonian matrices are sparse. $|\psi_0\rangle$ will then be closely related to some post-quench eigenstate. This implies in turn that $|\psi_0\rangle$ will have a small PR_2 relative to the post-quench eigenbasis. Similarly a pre-quench eigenstate $|\psi_0\rangle$ with a large PR_2 in terms of the local basis will be strongly affected by the quench in the sense that it is unrelated to any eigenstate of the post-quench eigenbasis, and so will have a large PR_2 in terms of this basis. It is this that lies behind the similar shapes of Fig. 3.12 and Fig. 3.10.

The behavior of the PR_2 relative to the local basis (and, by this equivalence, the

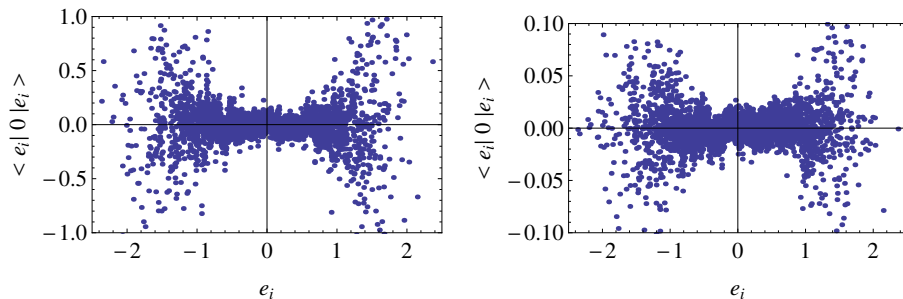


Figure 3.14: Sparse random matrices. EEV $\langle E | \mathcal{O} | E \rangle$ vs e_E . Left: even observable. Right: odd observable

3. Quantum quenches

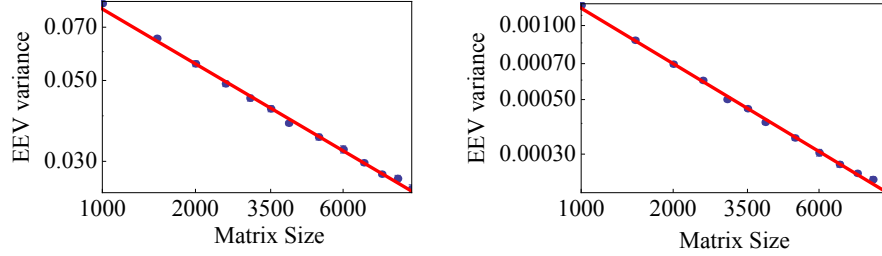


Figure 3.15: Sparse random matrices. EEV variance vs. matrix size for the full spectrum. The continuous lines are the fit a/x^b . Left: even observable $b = 0.5(0)$ Right: odd observable $b = 0.7(5)$.

PR_2 relative to the post-quench eigenbasis) can be understood directly in the framework of AL. Our sparse Hamiltonian can be seen as akin to the dynamics of a non-interacting particle hopping on a Bethe-lattice of fixed connectivity, $\ln \mathcal{N}$, that we introduced in 1.4. Each site has a random potential (the diagonal part of the random Hamiltonian). We already pointed out that for this model the Anderson localization transition occurs with the presence of a *mobility edge* which separates the delocalized states (in the middle of the band) from the localized states (in the tails of the energy spectrum). In our case localization occurs when the PR_2 is $O(1)$, while delocalization is seen for $\text{PR}_2 = O(\mathcal{N})$.

The position, E_m , of the mobility edge can be determined by the following equation, derived along the same lines as [3]

$$2 \ln \mathcal{N} \int_0^\infty \{p'(x - E_m) - p'(E_m - x)\} \ln x dx = 1, \quad (3.32)$$

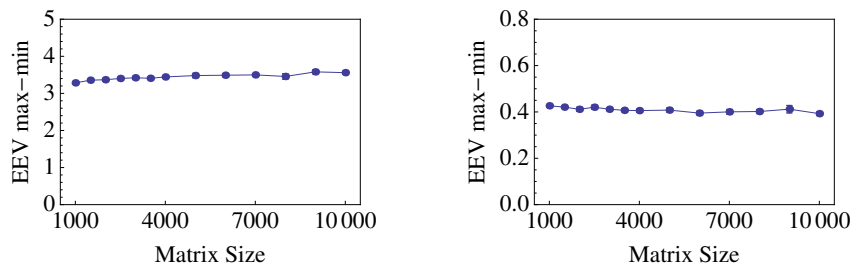


Figure 3.16: Sparse random matrices. Max-min EEV vs matrix size for the full spectrum. Left: even observable. Right: odd observable.

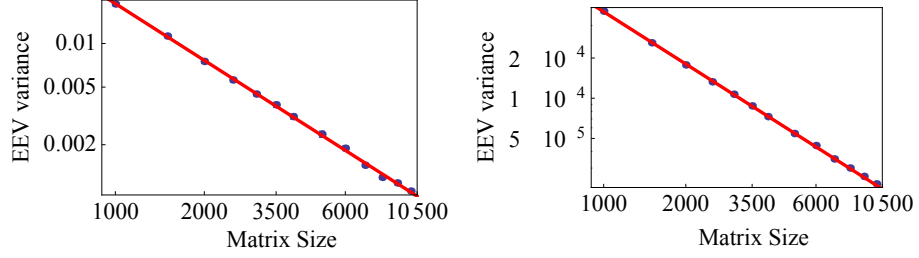


Figure 3.17: Sparse random matrices. EEV variance vs. matrix size for a small energy window around $e = 0$. The continuous line is the fit a/x^b . Left: even observable $b = 1.2(9)$. Right: odd observable $b = 1.2(2)$.

where $p(x)$ is the probability density of the diagonal terms in our Hamiltonian

$$p(x) = \frac{1}{\sqrt{2\pi \ln \mathcal{N}}} \exp\left(-\frac{x^2}{2 \ln \mathcal{N}}\right). \quad (3.33)$$

States with an $|E| > |E_m|$ such that the right hand side of Eq. (3.32) is less than 1 are localized. Otherwise they are delocalized. The integral in Eq. (3.32) can be estimated at the leading order in the large \mathcal{N} limit, and one obtains

$$1 = \exp\left(-\frac{E_m^2}{2 \ln \mathcal{N}}\right) \ln \ln \mathcal{N} \sqrt{\frac{2 \ln \mathcal{N}}{\pi}} \Rightarrow E_m \simeq \pm \sqrt{\ln \mathcal{N} \ln \ln \mathcal{N}}. \quad (3.34)$$

Thus in the large \mathcal{N} limit all the states with a non-zero intensive energy $E/\ln \mathcal{N}$ behave as localized. Nonetheless the majority of the states, as they are concentrated in a

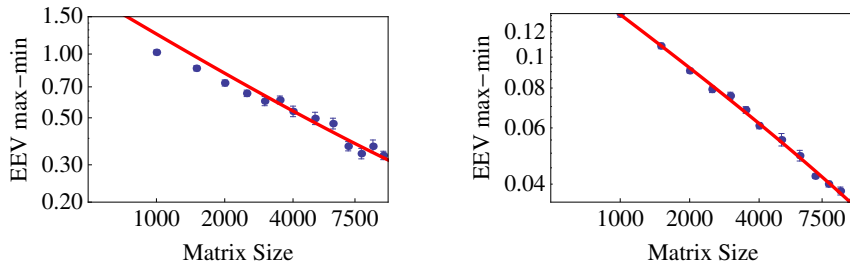


Figure 3.18: Sparse random matrices. Max-min EEV vs. matrix size for a small energy window around $e = 0$ in log-scale. The continuous line is the fit $a/x^b + c$. Left: even observable $e = 0$, $b = 0.6(5)$, $c = 0.06(7)$. Right: odd observable $e = 0$, $b = 0.5(0)$, $c = 0.0(1)$.

window of width σ_H (given in Eq. 3.30) and as $E_m/\sigma_H \gg 1$, will be delocalized with an $\text{PR}_2 = O(\mathcal{N})$.

The localization of states with finite intensive energies has implications for the EEV distribution vs. e_E . As the observables have a matrix structure closely related to that of the Hamiltonians, we expect that localized states to be close to eigenstates of the observables itself, in contrast with Eq. (3.24) in the dense case. On such states, the observables will have expectation values far from their zero average. On the contrary, the delocalized states mid-spectrum will have EEV values closer to the mean of zero. In Fig. 3.14 we see numerical verification of this.

This result marks a strong difference with respect to the case of dense matrices. We also see marked differences between the sparse and dense cases with both the variance and the support of the EEVs distribution of the observable, as shown in Fig. 3.15 and 3.16: while the variance approaches zero as \mathcal{N} grows, the support does not, instead tending to a non-zero constant. Therefore the scaling Eq. (3.28) is no longer applicable, most likely as the overlaps, $A_{i\beta}$, and the eigenvalues of the observable, O_θ , in Eq. (3.23) can no longer be considered as independent.

Since the distribution of the overlap coefficients, c_E , are peaked around the energy $\bar{e} = \langle \psi_0 | H(h) | \psi_0 \rangle$, it is worthwhile to analyze the scaling behavior of the distribution of the EEVs in the vicinity of a specific \bar{e} . Here we choose two different energy windows, one centered around $\bar{e} = 0$, lying exactly mid-spectrum and one around $\bar{e} = 1$. For $\bar{e} = 0$ the variance and the max-min spread as functions of the size \mathcal{N} are plotted in Fig. (3.17) and Fig. (3.18). It is this distribution that is going to determine whether with respect to a particular observable we see thermalization. We again see that the

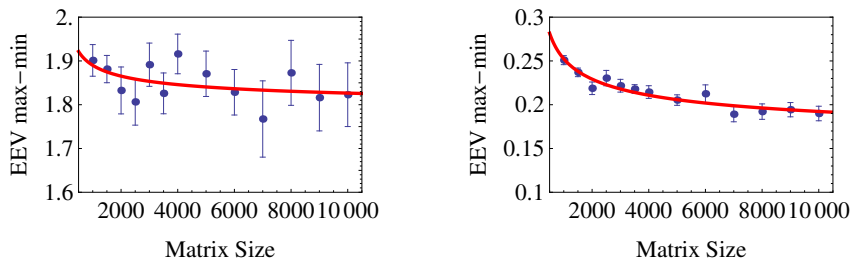


Figure 3.19: Sparse random matrices. Max-min EEV vs. matrix size for a small energy window around $e = 1$. The continuous line is the fit $a/x^b + c$. Left: even observable $e = 1$, $b = 0.3(5)$, $c = 1.(7)$. Right: odd observable $e = 1$, $b = 0.3(3)$, $c = 0.1(4)$.

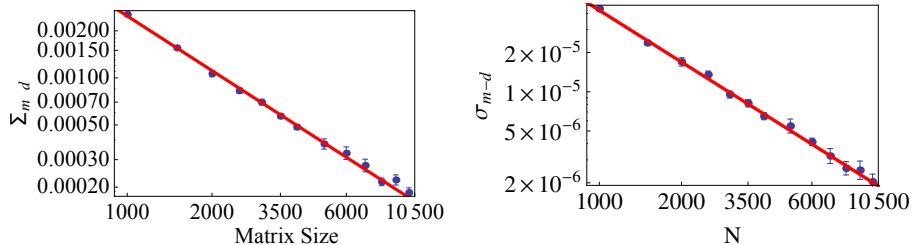


Figure 3.20: Sparse random matrices. $\sigma = \sqrt{(\mathcal{O}_{\text{micro}} - \mathcal{O}_{\text{diag}})^2}$ vs. matrix size for initial states laying in the central part of the spectrum $\bar{e} \approx 0$. The continuous lines are the fits a/x^b . Left: even observable $b = 1.1(5)$. Right: odd observable $b = 1.3(0)$.

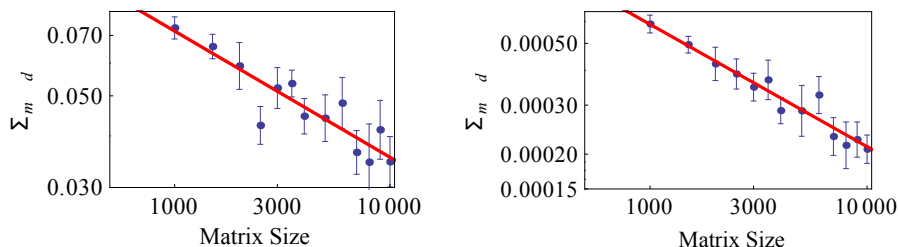


Figure 3.21: Sparse random matrices. $\sigma = \sqrt{(\mathcal{O}_{\text{micro}} - \mathcal{O}_{\text{diag}})^2}$ vs. matrix size for initial states laying in a small window around $e = 1$. The continuous lines are the fits a/x^b . Left: even observable $b = 0.3(1)$. Right: odd observable $b = 0.4(4)$.

variance is going to zero, while in contrast to the full spectrum, the max-min spread seems to tend, asymptotically, to either a very small constant value or to zero. The errors in our numerics are then not small enough to tell us at $\bar{e} = 0$ whether there is a complete absence of rare states. However we can be more definitive for the energy window centered at $\bar{e} = 1$. In this window we see (as evidenced in Fig. 3.19) that the max-min spread of the EEV's in the large \mathcal{N} limit tends to a finite constant for both the even and odd observables.

Our numerical data then suggests that there are rare states where the observable remains far from its average value in each microcanonical energy window corresponding to non-zero intensive energy, differently for what has been observed in the $t - J$ model [102, 110, 111]. In these studies of the t-J model, rare states were argued to be absent for a range of strengths of the next nearest neighbor interaction, V' , and for an energy window centered mid-spectrum. In particular with V' small the t-J model is effectively integrable and rare states were found to be present and with V' large, the

model develops energy bands, also compatible with the existence of rare states. It is for a middle range of V' that rare states were then found to be absent. Our own study sees some agreement with these results. And it is natural to think there would be some agreement at least. Our study of random matrix model should correspond to the $t - J$ model with intermediate values of V' : our matrix models are neither integrable nor do they have any notion of energy bands. In our case, rare states (at least for what we call the odd observable) seem to be vanishing as system size increases exactly in the center of the spectrum. However away from this midpoint of the spectrum, we find that rare states do exist, even in the thermodynamic limit. It would thus be interesting to extend the work of [102, 110, 111] to additional energy windows.

Following [23], we then conclude in the case of sparse matrices that thermalization may depend on the particular nature of the initial state and will not occur when such rare states are given a proportionally large weight in the decomposition of the initial state. We, however, do not find for the particular initial conditions specified by our quench protocol that the rare states are given disproportional weight such that thermalization does not occur. For both energy windows $\bar{e} = 0$ (see Fig. (3.20)) and $\bar{e} = 1$ (Fig. (3.21)), we see that with increasing matrix size the difference between the diagonal and microcanonical ensembles averaged over all initial conditions tends to zero. This implies that the weighting of rare states in our initial states is not preponderant. We do note however that the vanishing of the difference between ensembles decreases considerably more slowly with system size for the energy window, $\bar{e} = 1$, than for $\bar{e} = 0$. We might ascribe this to the presence of rare states at this energy – even though these states do not lead to non-thermalization in the thermodynamic limit, they may

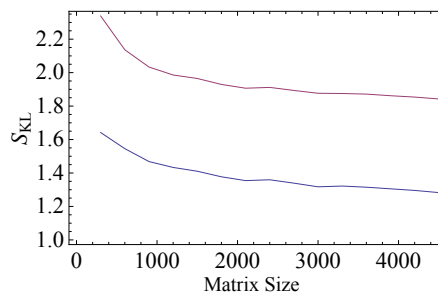


Figure 3.22: Sparse random matrices. Kullback-Leibler entropy vs matrix size for the center of the spectrum for the uniform (squares) and the Gaussian distribution (circles).

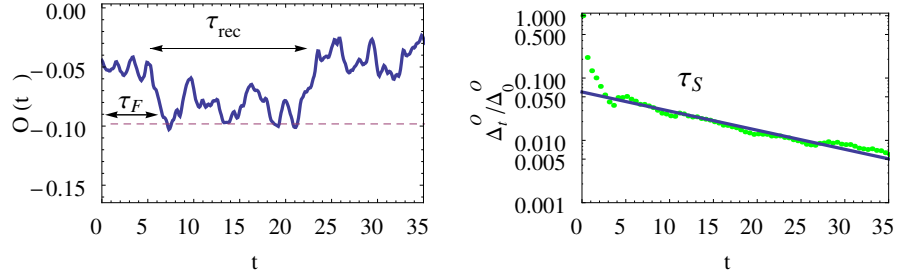


Figure 3.23: Left: time evolution of the observable \mathcal{O}_t versus time t . Right: time evolution of the fluctuations $\Delta_t^{\mathcal{O}}/\Delta_0^{\mathcal{O}}$ versus time t , log-scale on y axis. The straight line is the exponential fit whose slope defines τ_S .

slow the approach to a thermalized state as the system size is increased.

We verify this by computing the Kullback-Leibler entropy. This entropy is an information theoretic tool used to estimate how close two distributions are. It is defined as

$$S_{KL} = \sum_E P(a) \ln \frac{P(a)}{Q(a)}, \quad (3.35)$$

where $P(a)$ is the expected distribution and $Q(a)$ is the distribution to be compared. S_{KL} is zero if the two distributions coincide except for sets of zero measures. In our case we choose $P(a) = |c_E|^2$ and $Q(a)$ to belong to either a uniform or a Gaussian distribution centered about the energy \bar{e} . The range over which $Q(a)$ is defined has been taken such that the variances of Q and P coincides. Fig. 3.22 shows the average KL-entropy vs. matrix size for the central part of the spectrum which indicates in both cases a slow decay as the system size is increased. The slow approach of the distribution $P(a)$ to a distribution $Q(a)$ that is both smooth and symmetric about \bar{e} suggests that rare states are not weighted in a peculiar way, thus permitting thermalization.

In conclusion, for sparse random matrices our numerical data is compatible with the existence of rare states. However, the initial states selected by the quench protocol do not seem to have large overlaps with these rare states and so we typically find thermalization as the end result of our quench process.

3.7 Time Scales of Thermalization

The sparse random ensemble, inasmuch as it mimics some characteristic properties of thermalization in systems with local Hamiltonians, is the right framework to address the study of the thermalization time. Interest in this quantity can be traced back to the seminal paper by Von Neumann [92] regarding the quantum ergodic theorem (QET). The statement made in Von Neumann's paper is that, under suitable assumptions (the Hamiltonian has no resonances - meaning that the energy level differences are non degenerate), any state $|\psi_0\rangle$ in the energy shell $[e - \Delta, e + \Delta]$, will thermalize for most choices of the observable and most times t , i.e.

$$\mathcal{O}_t = \langle \psi_0(t) | \mathcal{O} | \psi_0(t) \rangle = \text{Tr} \mathcal{O} \rho_{\text{mc}} \quad \text{for almost all } t, \mathcal{O} .$$

To make the notion of (macroscopic) observable and “most” used here precise would require the development of an involved technical apparatus and so instead we refer the reader to the existing literature [54, 92]. Nonetheless we can say there are important differences between this quantum thermalization and the classical notion of ergodicity where a time-average is involved. It is therefore of interest to give a precise estimate of the time needed for thermalization. There have been different approaches which have tried to clarify this question [26, 76, 114, 132]. In Fig. 3.23, we examine the typical behavior of a realization of a random observable, \mathcal{O}_t . It decays towards the average value given by the diagonal ensemble:

$$\mathcal{O}_\infty = \text{Tr} \mathcal{O} \rho_{\text{diag}} ,$$

and we define the time τ_F as the first time at which \mathcal{O}_t meets \mathcal{O}_∞ . We stress here, that even if this quantity has not a direct physical interpretation, it can be considered as a lower bound for the thermalization time. The time evolution of the observable however keeps fluctuating around the average, due to finite system size, with it coming close to its initial value after a time, τ_{rec} , the recurrence time. To quantify these fluctuations we define

$$\Delta_t^\mathcal{O} \equiv \frac{1}{t} \int_0^t (\mathcal{O}_\tau - \mathcal{O}_\infty)^2 d\tau \xrightarrow{t \rightarrow \infty} \sum_{E, E'} c_E^2 c_{E'}^2 O_{EE'}^2 \equiv \Delta_\infty^\mathcal{O} ,$$

where we have assumed the absence of energy degeneracies and resonances. The quantity $\Delta_t^{\mathcal{O}}$ can be considered as the variance in the time interval $[0, t]$ of the observable and its behavior is plotted in Fig. 3.23: relaxation to the infinite time value is found as expected. We can fit this curve supposing an exponential relaxation, e^{-t/τ_S} , defining in this way another time scale, τ_S , the time interval needed for the relaxation of the fluctuations. Notice that this quantity is the one closer to the Von Neumann formulation: indeed, from the Chebyshev inequality, one has a bound on the fraction, μ/t , of times where the observable has an expectation value far from its average

$$\frac{\mu(\tau \in [0, t] \text{ and } |\mathcal{O}_\tau - \mathcal{O}_\infty| > a)}{t} < \frac{\Delta_t^{\mathcal{O}}}{a^2}.$$

As in the thermodynamic limit $\Delta_\infty^{\mathcal{O}} \rightarrow 0$, this fraction must also go to zero in the long time limit. In Fig. 3.24, we see the comparison between the two timescales τ_S and τ_F versus the system size. From this plot one can see clearly that τ_S is a long time-scale, with a behavior proportional to \mathcal{N} , i.e. the size of the Hilbert space. Notice that this can also be interpreted as the minimum spectral gap and at the leading order in \mathcal{N} :

$$\min_{E \neq E'} |E - E_{E'}| \propto \frac{1}{\mathcal{N}}.$$

In contrast, τ_F is characterized by a much slower scaling with the size of the system and is therefore a fast time-scale. Although it is not easy to extract the precise scaling

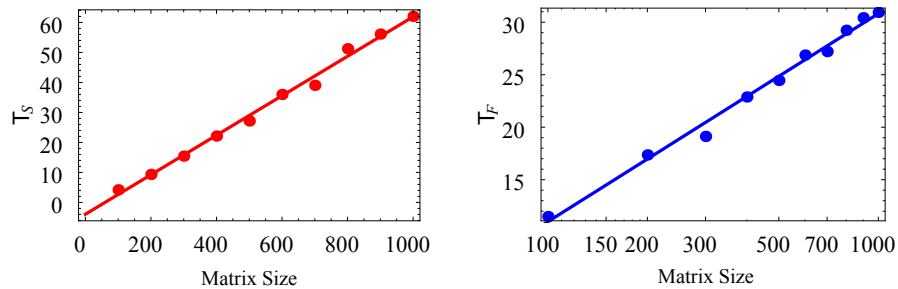


Figure 3.24: Scaling with the matrix size of the two time scale τ_S (left) with a linear fit $(-3.94 + 0.066\mathcal{N})$ and τ_F (right) with a logarithmic fit $(-28.61 + 8.60 \ln \mathcal{N})$.

law from the available data, we have fit this data with the form

$$\tau_F(\mathcal{N}) = a \ln \mathcal{N} \ ,$$

and so taking the scaling of this time scale to go as the volume. In contrast, the time scale for dense matrices was recently argued to go as the *inverse* of the volume[26].

3.8 Conclusions

In this chapter we have addressed the issues of thermalization and the Eigenstate Thermalization Hypothesis in the framework of random matrices, aiming to identify certain statistical properties of quantum extended systems subjected to a quench process. For this purpose we focused our attention on Z_2 breaking quantum Hamiltonians, among the simplest theoretical quench protocols. In an attempt to encode in our analysis the property of locality, we have considered the ensemble of sparse random matrices and we have compared the data coming from this ensemble with similar data extracted from the ensemble of dense random matrices. We have found reliable evidence of different behavior in the two ensembles. These differences show up both in the PR_2 of the quench states and in the distribution of the expectation values of the observables on post-quench energy eigenstates. In particular, while in the dense random matrix ensemble both the variance and the support of the observables vanish with increasing system size N , the sparse random matrix ensemble sees instead strong indications that the variance of EEVs goes to zero while the support remains finite as $N \rightarrow \infty$. The different behavior of the two ensembles can be traced back to the different density of states exhibited by the two sets of matrices: while in the dense matrices all states are delocalized in the Hilbert space, with almost equal overlap on all energy eigenstates, in the sparse matrices there are instead both delocalized and localized states. Localized states give rise to rare values of the expectation values of the observables, i.e. values which differ from the typical ones sampled by the micro-canonical ensemble. If properly weighted, such localized states may give rise to a breaking of thermalization. In the absence of such weighting, as seems to be the case in the initial conditions chosen by our quench protocol, one instead observes relaxation to the thermal value of the local observables.

3. Quantum quenches

In the framework of sparse random matrices, we have also provided numerical estimates of the different time scales of thermalization. We have found that it is possible to identify two time scales: a fast one τ_F and a slow one τ_S , and that they depend differently upon the size of the system.

Chapter 4

Final remarks

In this work of thesis, we delineated a path in between two important topics such as the characterization of the steady state in closed quantum systems and the existence of a phase transition in disordered and interacting quantum systems. We tried to show that important connections, between the two, exist and that it is fundamental to investigate the ergodicity of the wave function inside the Hilbert space. In chapter 2, we presented our work trying to characterize the two phases in the MBL transition. We showed how indicators coming from the AL approach, can be conveniently reformulated in the many-body cases providing good indication for the position of the critical points. The comparison with the single particle case allowed us to identify some important similarities and differences. The localized phase looks “less localized” and the real transition appears as a change of scaling in the wave-function distributions, corresponding to the breaking of ergodicity, instead that by concrete localization in the many-body Hilbert space. This suggested a profitable identification with a Bethe-lattice for large connectivity that remains an open topic for future investigations, both numerical and analytical. Moreover, once the Richardson model has been recognized as toy model for the localized phase, it can be used to compute almost exactly important indicators as the anomalous dimensions, in order to investigate the presence of multi-fractality in this problem. In chapter 3, we studied the problem of thermalization in closed quantum systems. Instead of focusing on a specific models, we tried to understand what happens in “typical” cases. To really define typicality in this framework, we elaborated on the main features that characterize the long time dynamics of a quantum physical system and how they affect the long time behavior. This allowed

us to define an interesting ensemble of random matrixes, close friend of the random energy model on the Bethe lattice, already known to the spin glass community. The resulting class of models gave strong indications of the existence of rare states, thus providing an example for a particular mechanism of thermalization, related to a weak version of the ETH, that had been recently conjectured. These numerical results lack of an analytical confirm that could be important in the future. We are also interested in the definition of an ensemble of random Hamiltonian that reproduces the features of integrable models. Indeed, it is still open the debate regarding the thermalization or the lack thereof in integrable models. Due to the existence of a set of conserved charges, one could expect that their dynamics is strongly constrained and hardly reaches a thermal steady state. However, a clear answer is difficult in the general case, both for the difficulties in the exact computations of long time expectation values and for the lack of universality of any specific example. Therefore, it would be important to be able to give an answer for the “typical” integrable case. This is part of our current research.

We stress once more that many-body localized systems represent an example of interacting, non-integrable systems, that do not reach any thermal equilibrium. So a general understanding of this transition would represent a decisive result for both these important questions.

References

- [1] R. Abou-Chacra and DJ Thouless. Self-consistent theory of localization. ii. localization near the band edges. *Journal of Physics C: Solid State Physics*, 7: 65, 1974. 21
- [2] R Abou-Chacra, D J Thouless, and P W Anderson. A selfconsistent theory of localization. *Journal of Physics C: Solid State Physics*, 6(10):1734, 1973. URL <http://stacks.iop.org/0022-3719/6/i=10/a=009>. 21, 23
- [3] R. Abou-Chacra, DJ Thouless, and PW Anderson. A selfconsistent theory of localization. *Journal of Physics C: Solid State Physics*, 6:1734, 1973. 49, 50, 83
- [4] E. Abrahams. *50 Years of Anderson Localization*. International journal of modern physics : B, condensed matter physics, statistical physics, applied physics. World Scientific, 2010. ISBN 9789814299077. URL http://books.google.it/books?id=_KoSwxcw7WQC. 21
- [5] E. Abrahams, PW Anderson, DC Licciardello, and TV Ramakrishnan. Scaling theory of localization: Absence of quantum diffusion in two dimensions. *Physical Review Letters*, 42(10):673–676, 1979. 25
- [6] D. Aharonov, W. Van Dam, J. Kempe, Z. Landau, S. Lloyd, and O. Regev. Adiabatic quantum computation is equivalent to standard quantum computation. In *Foundations of Computer Science, 2004. Proceedings. 45th Annual IEEE Symposium on*, pages 42–51. IEEE, 2004. 33

REFERENCES

- [7] D. Aharonov, D. Gottesman, S. Irani, and J. Kempe. The power of quantum systems on a line. *Communications in Mathematical Physics*, 287(1):41–65, 2009. 33
- [8] B. Altshuler, H. Krovi, and J. Roland. Anderson localization casts clouds over adiabatic quantum optimization. *Arxiv preprint arxiv:0912.0746*, 2009. 28, 42
- [9] B.L. Altshuler, Y. Gefen, A. Kamenev, and L.S. Levitov. Quasiparticle lifetime in a finite system: A nonperturbative approach. *Physical review letters*, 78(14):2803–2806, 1997. 49
- [10] Boris Altshuler, Hari Krovi, and Jrmie Roland. Anderson localization makes adiabatic quantum optimization fail. *Proceedings of the National Academy of Sciences*, 107(28):12446–12450, 2010. doi: 10.1073/pnas.1002116107. URL <http://www.pnas.org/content/107/28/12446.abstract>. 28, 29, 36
- [11] P. W. Anderson. Absence of Diffusion in Certain Random Lattices. *Physical Review Online Archive (Prola)*, 109(5):1492–1505, March 1958. doi: 10.1103/PhysRev.109.1492. URL <http://dx.doi.org/10.1103/PhysRev.109.1492>. 1, 5, 13, 18, 28
- [12] B. Apolloni, C. Carvalho, and D. de Falco. Quantum stochastic optimization. *Stochastic Processes and their Applications*, 33(2):233–244, 1989. 33
- [13] J. H. Bardarson, F. Pollmann, and J. E. Moore. Unbounded growth of entanglement in models of many-body localization. *ArXiv e-prints*, February 2012. 40
- [14] E. Barouch, B.M. McCoy, and M. Dresden. Statistical mechanics of the xy model. i. *Physical Review A*, 2:1075–1092, 1970. 64
- [15] DM Basko, IL Aleiner, and BL Altshuler. Metal-insulator transition in a weakly interacting many-electron system with localized single-particle states. *Annals of physics*, 321(5):1126–1205, 2006. ISSN 0003-4916. 3, 28
- [16] DM Basko, IL Aleiner, and BL Altshuler. On the problem of many-body localization. *Arxiv preprint cond-mat/0602510*, 2006. 3, 28, 49

REFERENCES

- [17] DM Basko, IL Aleiner, and BL Altshuler. Possible experimental manifestations of the many-body localization. *Physical Review B*, 76(5):052203, 2007. [v](#), [3](#)
- [18] MV Berry. Regular and irregular semiclassical wavefunctions. *Journal of Physics A: Mathematical and General*, 10:2083, 1977. [64](#)
- [19] HA Bethe. Statistical theory of superlattices. *Proceedings of the Royal Society of London. Series A, Mathematical and Physical Sciences*, 150(871):552–575, 1935. [21](#)
- [20] Z. Bian, F. Chudak, W.G. Macready, L. Clark, and F. Gaitan. Experimental determination of ramsey numbers with quantum annealing. *Arxiv preprint arXiv:1201.1842*, 2012. [34](#)
- [21] J. Billy, V. Josse, Z. Zuo, A. Bernard, B. Hambrecht, P. Lugan, D. Clément, L. Sanchez-Palencia, P. Bouyer, and A. Aspect. Direct observation of anderson localization of matter waves in a controlled disorder. *Nature*, 453(7197):891–894, 2008. [1](#)
- [22] G. Biroli, R. Monasson, and M. Weigt. A variational description of the ground state structure in random satisfiability problems. *The European Physical Journal B-Condensed Matter and Complex Systems*, 14(3):551–568, 2000. [36](#)
- [23] G. Biroli, C. Kollath, and A. Laeuchli. Effect of rare fluctuations on the thermalization of isolated quantum systems. *Arxiv preprint arXiv:0907.3731*, 2009. [66](#), [69](#), [70](#), [87](#)
- [24] G. Biroli, G. Semerjian, and M. Tarzia. Anderson model on bethe lattices: density of states, localization properties and isolated eigenvalue. *Arxiv preprint arXiv:1005.0342*, 2010. [vi](#), [24](#)
- [25] I. Bloch, J. Dalibard, and W. Zwerger. Many-body physics with ultracold gases. *Reviews of Modern Physics*, 80(3):885, 2008. [1](#)
- [26] F.G.S.L. Brandão, P. Ćwikliński, M. Horodecki, P. Horodecki, J. Korbicz, and M. Mozrzykas. Convergence to equilibrium under a random hamiltonian. *Arxiv preprint arXiv:1108.2985*, 2011. [89](#), [91](#)

REFERENCES

- [27] G. P. Brandino, A. De Luca, R. M. Konik, and G. Mussardo. Quench dynamics in randomly generated extended quantum models. *Phys. Rev. B*, 85:214435, Jun 2012. doi: 10.1103/PhysRevB.85.214435. URL <http://link.aps.org/doi/10.1103/PhysRevB.85.214435>. 4
- [28] J. Brooke, D. Bitko, G. Aeppli, et al. Quantum annealing of a disordered magnet. *Science*, 284(5415):779–781, 1999. 33, 34
- [29] F. Buccheri, A. De Luca, and A. Scardicchio. Structure of typical states of a disordered richardson model and many-body localization. *Physical Review B*, 84(9):094203, 2011. 4, 49
- [30] P. Calabrese and J. Cardy. Time dependence of correlation functions following a quantum quench. *Physical review letters*, 96(13):136801, 2006. 64
- [31] P. Calabrese, F.H.L. Essler, and M. Fagotti. Quantum quench in the transverse-field ising chain. *Physical Review Letters*, 106(22):227203, 2011. 64
- [32] IA Campbell, JM Flesselles, R. Jullien, and R. Botet. Random walks on a hypercube and spin glass relaxation. *Journal of Physics C: Solid State Physics*, 20:L47, 1987. 59
- [33] R. Carmona, A. Klein, and F. Martinelli. Anderson localization for bernoulli and other singular potentials. *Communications in Mathematical Physics*, 108(1):41–66, 1987. 25
- [34] J.S. Caux and J. Mossel. Remarks on the notion of quantum integrability. *J. Stat. Mech.*, page P02023, 2011. 52, 58
- [35] MA Cazalilla. Effect of suddenly turning on interactions in the luttinger model. *Physical review letters*, 97(15):156403, 2006. 64
- [36] C. Cohen-Tannoudji, J. DuPont-Roc, and G. Grynberg. *Atom-Photon Interactions: Basic Processes and Applications*. Wiley Science Paperback Series. Wiley, 1998. ISBN 9780471293361. URL <http://books.google.it/books?id=QY15QgAACAAJ>. 9

REFERENCES

- [37] C. De Grandi, V. Gritsev, and A. Polkovnikov. Quench dynamics near a quantum critical point. *Physical Review B*, 81(1):012303, 2010. [64](#)
- [38] A. De Luca and F. Franchini. Approaching critical points through entanglement: why take one, when you can take them all? *Arxiv preprint arXiv:1205.6426*, 2012. [4](#)
- [39] A. De Luca and A. Scardicchio. Many body localization, ergodicity breaking and the distribution of the wave-function coefficients. *Arxiv preprint arXiv:1206.2342*, 2012. [4](#)
- [40] HJ De Vega. Families of commuting transfer matrices and integrable models with disorder. *Nuclear Physics B*, 240(4):495–513, 1984. [51](#)
- [41] JM Deutsch. Quantum statistical mechanics in a closed system. *Physical Review A*, 43(4):2046, 1991. [64](#), [69](#)
- [42] F. Dominguez, C. Esebbag, and J. Dukelsky. Solving the richardshhttp://dx.doi.org/10.on equations close to the critical points. *Journal of Physics A*, 39(37):10, 2006. [54](#)
- [43] J. Dukelsky, S. Pittel, and G. Sierra. Colloquium: Exactly solvable Richardson-Gaudin models for many-body quantum systems. *Reviews of Modern Physics*, 76(3):643–662, 2004. ISSN 1539-0756. [51](#)
- [44] M. Eckstein and M. Kollar. Nonthermal steady states after an interaction quench in the falicov-kimball model. *Physical review letters*, 100(12):120404, 2008. [65](#)
- [45] M. Eckstein, M. Kollar, and P. Werner. Thermalization after an interaction quench in the hubbard model. *Physical review letters*, 103(5):56403, 2009. [65](#)
- [46] E. Farhi, J. Goldstone, S. Gutmann, and M. Sipser. Quantum computation by adiabatic evolution. *Arxiv preprint quant-ph/0001106*, 2000. [33](#)
- [47] E. Farhi, J. Goldstone, S. Gutmann, J. Lapan, A. Lundgren, and D. Preda. A quantum adiabatic evolution algorithm applied to random instances of an np-complete problem. *Science*, 292(5516):472–475, 2001. [28](#), [33](#), [42](#)

REFERENCES

- [48] A. Faribault, P. Calabrese, and J.S. Caux. Bethe ansatz approach to quench dynamics in the Richardson model. *Journal of Mathematical Physics*, 50:095212, 2009. [54](#)
- [49] A. Faribault, O. El Araby, C. Strater, and V. Gritsev. Gaudin models solver based on the bethe ansatz/ordinary differential equations correspondence. *Phys. Rev. B*, 83:235124, 2011. [55](#)
- [50] G. Feher and E. A. Gere. Electron spin resonance experiments on donors in silicon. ii. electron spin relaxation effects. *Phys. Rev.*, 114:1245–1256, Jun 1959. doi: 10.1103/PhysRev.114.1245. URL <http://link.aps.org/doi/10.1103/PhysRev.114.1245>. [5](#)
- [51] AB Finnila, MA Gomez, C. Sebenik, C. Stenson, and JD Doll. Quantum annealing: a new method for minimizing multidimensional functions. *Chemical physics letters*, 219(5):343–348, 1994. [33](#)
- [52] D. Fioretto and G. Mussardo. Quantum quenches in integrable field theories. *New Journal of Physics*, 12:055015, 2010. [64](#)
- [53] T. Giamarchi and HJ Schulz. Anderson localization and interactions in one-dimensional metals. *Physical Review B*, 37(1):325, 1988. [42](#)
- [54] S. Goldstein, J.L. Lebowitz, R. Tumulka, and N. Zanghi. Long-time behavior of macroscopic quantum systems. *The European Physical Journal H*, 35(2): 173–200, 2010. [63](#), [89](#)
- [55] M. Greiner, O. Mandel, T. Esslinger, T.W. Hänsch, I. Bloch, et al. Quantum phase transition from a superfluid to a mott insulator in a gas of ultracold atoms. *Nature*, 415(6867):39–44, 2002. [62](#)
- [56] F. Haake. *Quantum signatures of chaos*, volume 54. Springer Verlag, 2001. [73](#)
- [57] A.K. Hartmann and H. Rieger. *Optimization Algorithms in Physics*. Wiley-VCH, 2002. ISBN 9783527403073. [28](#)

REFERENCES

- [58] S. Hofferberth, I. Lesanovsky, B. Fischer, T. Schumm, and J. Schmiedmayer. Non-equilibrium coherence dynamics in one-dimensional bose gases. *Nature*, 449(7160):324–327, 2007. [62](#)
- [59] W. Hunziker and IM Sigal. The quantum n-body problem. *Journal of Mathematical Physics*, 41:3448, 2000. [25](#)
- [60] A. Iucci and MA Cazalilla. Quantum quench dynamics of the luttinger model. *Physical Review A*, 80(6):063619, 2009. [64](#)
- [61] D.S. Johnson and M.R. Garey. Computers and intractability: A guide to the theory of np-completeness. *Freeman&Co, San Francisco*, 1979. [31](#)
- [62] T. Kadowaki and H. Nishimori. Quantum annealing in the transverse ising model. *Arxiv preprint cond-mat/9804280*, 1998. [33](#)
- [63] R.M. Karp. Reducibility among combinatorial problems. *50 Years of Integer Programming 1958-2008*, pages 219–241, 2010. [31](#)
- [64] T. Kinoshita, T. Wenger, and D.S. Weiss. A quantum newton’s cradle. *Nature*, 440(7086):900–903, 2006. [v](#), [2](#), [62](#)
- [65] S. Kirkpatrick, C.D. Gelatt Jr, and M.P. Vecchi. Optimization by simulated annealing. *science*, 220(4598):671–680, 1983. [33](#)
- [66] S. Knysh and V. Smelyanskiy. On the relevance of avoided crossings away from quantum critical point to the complexity of quantum adiabatic algorithm. *Arxiv preprint arXiv:1005.3011*, 2010. [28](#)
- [67] M. Kollar and M. Eckstein. Relaxation of a one-dimensional mott insulator after an interaction quench. *Physical Review A*, 78(1):013626, 2008. [65](#)
- [68] C. Kollath, A.M. Läuchli, and E. Altman. Quench dynamics and nonequilibrium phase diagram of the bose-hubbard model. *Physical review letters*, 98(18):180601, 2007. [64](#)
- [69] A. Legendijk, B. Van Tiggelen, and D.S. Wiersma. Fifty years of anderson localization. *Phys. Today*, 62(8):24–29, 2009. [27](#)

REFERENCES

- [70] LD Landau, EM Lifshitz, and Q.M. Non. Quantum mechanics (non-relativistic theory), volume 3 of. *Course of Theoretical Physics*, 1965. [34](#)
- [71] C. Laumann, A. Scardicchio, and SL Sondhi. Cavity method for quantum spin glasses on the bethe lattice. *Physical Review B*, 78(13):134424, 2008. [21](#)
- [72] E.H. Lieb and W. Liniger. Exact analysis of an interacting bose gas. i. the general solution and the ground state. *Physical Review*, 130(4):1605, 1963. [v](#), [2](#)
- [73] J. Links, H.-Q. Zhou, R. McKenzie, and M. Gould. Algebraic bethe ansatz method for the exact calculation of energy spectra and form factors: applications to models of bose–einstein condensates and metallic nanograins. *J. Phys. A*, 36: R63, 2003. [53](#)
- [74] P. Lloyd. Exactly solvable model of electronic states in a three-dimensional disordered hamiltonian: non-existence of localized states. *Journal of Physics C: Solid State Physics*, 2:1717, 1969. [9](#)
- [75] S.R. Manmana, S. Wessel, R.M. Noack, and A. Muramatsu. Strongly correlated fermions after a quantum quench. *Physical review letters*, 98(21):210405, 2007. [65](#)
- [76] L. Masanes, A.J. Roncaglia, and A. Acin. The complexity of energy eigenstates as a mechanism for equilibration. *Arxiv preprint arXiv:1108.0374*, 2011. [89](#)
- [77] P. Mazur. Non-ergodicity of phase functions in certain systems. *Physica*, 43: 533–545, 1969. [58](#)
- [78] ML Mehta. Random matrices 2nd edn (new york: Academic). 1991. [65](#)
- [79] A. Messiah. Quantum mechanics, vol. ii. *English Edition*(North Holland: Amster, 1962. [34](#)
- [80] M. Mézard and G. Parisi. The bethe lattice spin glass revisited. *The European Physical Journal B-Condensed Matter and Complex Systems*, 20(2):217–233, 2001. [23](#)

REFERENCES

- [81] M. Mezard, G. Parisi, and M.A. Virasoro. *Spin glass theory and beyond*, volume 9. World scientific Singapore, 1987. 21
- [82] A. D. Mirlin. Statistics of energy levels and eigenfunctions in disordered systems. *Physics Reports*, 326:259–382, March 2000. doi: 10.1016/S0370-1573(99)00091-5. 46
- [83] A D Mirlin and Y V Fyodorov. The statistics of eigenvector components of random band matrices: analytical results. *Journal of Physics A: Mathematical and General*, 26(12):L551, 1993. URL <http://stacks.iop.org/0305-4470/26/i=12/a=012>. 46
- [84] A D Mirlin and Y V Fyodorov. Statistical properties of eigenfunctions of random quasi 1d one-particle hamiltonians. *International Journal of Modern Physics B*, 8:3795–3842, 1994. doi: 10.1142/S0217979294001640. 46
- [85] Alexander D. Mirlin and Yan V. Fyodorov. Distribution of local densities of states, order parameter function, and critical behavior near the anderson transition. *Phys. Rev. Lett.*, 72:526–529, Jan 1994. doi: 10.1103/PhysRevLett.72.526. URL <http://link.aps.org/doi/10.1103/PhysRevLett.72.526>. 46, 49
- [86] C. Monthus and T. Garel. Anderson transition on the cayley tree as a traveling wave critical point for various probability distributions. *Journal of Physics A: Mathematical and Theoretical*, 42:075002, 2009. 23
- [87] J. Mossel and J.S. Caux. Relaxation dynamics in the gapped xxz spin-1/2 chain. *New Journal of Physics*, 12:055028, 2010. 64
- [88] NF Mott. Conduction in non-crystalline materials. *Philosophical Magazine*, 19 (160):835–852, 1969. 28
- [89] N.F. Mott and E.A. Davis. *Electronic processes in non-crystalline materials*. Oxford Univ Pr, 2012. 28
- [90] NF Mott and WD Twose. The theory of impurity conduction. *Advances in Physics*, 10(38):107–163, 1961. 25

REFERENCES

- [91] G. Mussardo. *Statistical field theory: an introduction to exactly solved models in statistical physics*. Oxford University Press, USA, 2009. [50](#)
- [92] J. Neumann. Beweis des ergodensatzes und desh-theorems in der neuen mechanik. *Zeitschrift für Physik A Hadrons and Nuclei*, 57(1):30–70, 1929. [63](#), [89](#)
- [93] J. Neumann. Beweis des ergodensatzes und desh-theorems in der neuen mechanik. *Zeitschrift für Physik A Hadrons and Nuclei*, 57(1):30–70, 1929. [42](#)
- [94] H. Nishimori. *Statistical Physics of Spin Glasses and Information Processing: An Introduction*. International Series of Monographs on Physics. Oxford University Press, 2001. ISBN 9780198509400. [28](#)
- [95] G. Ortiz, R. Somma, J. Dukelsky, and S. Rombouts. Exactly-solvable models derived from a generalized Gaudin algebra. *Nuclear Physics B*, 707(3):421–457, 2005. ISSN 0550-3213. [51](#)
- [96] Arijeet Pal and David A. Huse. Many-body localization phase transition. *Phys. Rev. B*, 82(17):174411, Nov 2010. doi: 10.1103/PhysRevB.82.174411. [vii](#), [40](#), [41](#), [44](#), [56](#)
- [97] C.E. Porter. *Statistical Theories of Spectra: Fluctuations*. Perspectives in physics. Academic Press, 1965. ISBN 9780125623568. [46](#)
- [98] J. Raymond, A. Sportiello, and L. Zdeborová. Phase diagram of the 1-in-3 satisfiability problem. *Physical Review E*, 76(1):011101, 2007. [36](#)
- [99] RW Richardson. A restricted class of exact eigenstates of the pairing-force Hamiltonian. *Physics Letters*, 3(6):277–279, 1963. [51](#)
- [100] RW Richardson and N. Sherman. Exact eigenstates of the pairing-force Hamiltonian. *Nuclear Physics*, 52:221–238, 1964. ISSN 0029-5582. [51](#)
- [101] M. Rigol. Breakdown of thermalization in finite one-dimensional systems. *Physical review letters*, 103(10):100403, 2009. [64](#)

REFERENCES

- [102] M. Rigol and L.F. Santos. Quantum chaos and thermalization in gapped systems. *Physical Review A*, 82(1):011604, 2010. [66](#), [86](#), [87](#)
- [103] M. Rigol, V. Dunjko, V. Yurovsky, and M. Olshanii. Relaxation in a completely integrable many-body quantum system: An ab initio study of the dynamics of the highly excited states of 1d lattice hard-core bosons. *Physical review letters*, 98(5):50405, 2007. [64](#)
- [104] M. Rigol, V. Dunjko, and M. Olshanii. Thermalization and its mechanism for generic isolated quantum systems. *Nature*, 452(7189):854–858, 2008. [64](#), [69](#)
- [105] M. Rigol, V. Dunjko, and M. Olshanii. Thermalization and its mechanism for generic isolated quantum systems. *Nature*, 481:224, January 2012. doi: 10.1038/nature10773. [42](#)
- [106] G. Roati, C. DErrico, L. Fallani, M. Fattori, C. Fort, M. Zaccanti, G. Modugno, M. Modugno, and M. Inguscio. Anderson localization of a non-interacting bose–einstein condensate. *Nature*, 453(7197):895–898, 2008. [1](#)
- [107] D. Rossini, A. Silva, G. Mussardo, and G.E. Santoro. Effective thermal dynamics following a quantum quench in a spin chain. *Physical review letters*, 102(12):127204, 2009. [64](#)
- [108] D. Rossini, S. Suzuki, G. Mussardo, G.E. Santoro, and A. Silva. Long time dynamics following a quench in an integrable quantum spin chain: Local versus nonlocal operators and effective thermal behavior. *Physical Review B*, 82(14):144302, 2010. [64](#)
- [109] LE Sadler, JM Higbie, SR Leslie, M. Vengalattore, and DM Stamper-Kurn. Spontaneous symmetry breaking in a quenched ferromagnetic spinor bose–einstein condensate. *Nature*, 443(7109):312–315, 2006. [62](#)
- [110] Lea F. Santos and Marcos Rigol. Onset of quantum chaos in one-dimensional bosonic and fermionic systems and its relation to thermalization. *Phys. Rev. E*, 81(3):036206, Mar 2010. doi: 10.1103/PhysRevE.81.036206. [66](#), [86](#), [87](#)

REFERENCES

- [111] L.F. Santos and M. Rigol. Localization and the effects of symmetries in the thermalization properties of one-dimensional quantum systems. *Physical Review E*, 82(3):031130, 2010. 66, 86, 87
- [112] L. Sapienza, H. Thyrestrup, S. Stobbe, P.D. Garcia, S. Smolka, and P. Lodahl. Cavity quantum electrodynamics with anderson-localized modes. *Science*, 327(5971):1352–1355, 2010. v, 6
- [113] K. Sengupta, S. Powell, and S. Sachdev. Quench dynamics across quantum critical points. *Physical Review A*, 69(5):053616, 2004. 64
- [114] A.J. Short and T.C. Farrelly. Quantum equilibration in finite time. *New Journal of Physics*, 14:013063, 2012. 89
- [115] G. Sierra, J. M. Roman, and J. Dukelsky. The elementary excitations of the bcs model in the canonical ensemble. *IJMPA*, 19:381, 2004. 54
- [116] M. Srednicki. The approach to thermal equilibrium in quantized chaotic systems. *Journal of Physics A: Mathematical and General*, 32:1163, 1999. 64, 69
- [117] Mark Srednicki. Chaos and quantum thermalization. *Phys. Rev. E*, 50:888–901, Aug 1994. doi: 10.1103/PhysRevE.50.888. URL <http://link.aps.org/doi/10.1103/PhysRevE.50.888>. 42, 64, 69
- [118] Mark Srednicki. The approach to thermal equilibrium in quantized chaotic systems. *Journal of Physics A: Mathematical and General*, 32(7):1163, 1999. 42
- [119] M. Steffen, W. Van Dam, T. Hogg, G. Breyta, and I. Chuang. Experimental implementation of an adiabatic quantum optimization algorithm. *Physical review letters*, 90(6):67903, 2003. 34
- [120] M. Suzuki. Ergodicity, constants of motion, and bounds for susceptibilities. *Physica*, 50:277–291, 1971. 58
- [121] G. Szego. *Orthogonal polynomials*. Amer Mathematical Society, 1939. ISBN 0821810235. 54

REFERENCES

- [122] DJ Thouless. Anderson's theory of localized states. *Journal of Physics C: Solid State Physics*, 3:1559, 1970. [18](#), [20](#)
- [123] W. Van Dam, M. Mosca, and U. Vazirani. How powerful is adiabatic quantum computation? In *Foundations of Computer Science, 2001. Proceedings. 42nd IEEE Symposium on*, pages 279–287. IEEE, 2001. [33](#)
- [124] L.C. Venuti and P. Zanardi. Universality in the equilibration of quantum systems after a small quench. *Physical Review A*, 81(3):032113, 2010. [62](#)
- [125] L. Viola and W.G. Brown. Generalized entanglement as a framework for complex quantum systems: purity versus delocalization measures. *Journal of Physics A: Mathematical and Theoretical*, 40:8109, 2007. [56](#)
- [126] J. Von Neuman and E. Wigner. Über merkwürdige diskrete eigenwerte. über das verhalten von eigenwerten bei adiabatischen prozessen. *Zhurnal Physik*, 30:467–470, 1929. [35](#)
- [127] R. Vosk and E. Altman. Many-body localization in one dimension as a dynamical renormalization group fixed point. *Arxiv preprint arXiv:1205.0026*, 2012. [52](#)
- [128] M. Žnidarič, T. Prosen, and P. Prelovšek. Many-body localization in the Heisenberg XXZ magnet in a random field. *Physical Review B*, 77(6):64426, 2008. ISSN 1550-235X. [40](#)
- [129] K. M. Watson. Multiple scattering by quantum-mechanical systems. *Phys. Rev.*, 105:1388–1398, Feb 1957. doi: 10.1103/PhysRev.105.1388. URL <http://link.aps.org/doi/10.1103/PhysRev.105.1388>. [15](#)
- [130] C.N. Weiler, T.W. Neely, D.R. Scherer, A.S. Bradley, M.J. Davis, and B.P. Anderson. Spontaneous vortices in the formation of bose–einstein condensates. *Nature*, 455(7215):948–951, 2008. [62](#)
- [131] AP Young, S. Knysh, and VN Smelyanskiy. First-order phase transition in the quantum adiabatic algorithm. *Physical review letters*, 104(2):20502, 2010. [28](#), [42](#)

REFERENCES

- [132] M. Žnidarič et al. Subsystem dynamics under random hamiltonian evolution. *Journal of Physics A: Mathematical and Theoretical*, 45(12):125204, 2012. [89](#)